NASA TN D-1957

TECHNICAL NOTE

D-1957

LOW-SPEED INVESTIGATION OF THE EFFECTS OF WING SWEEP ON THE AERODYNAMIC CHARACTERISTICS OF PARAWINGS HAVING EQUAL-LENGTH LEADING EDGES AND KEEL

By Rodger L. Naeseth and Thomas G. Gainer

Langley Research Center
Langley Station, Hampton, Va.

NATIONAL AERONAUTICS AND SPACE ADMINISTRATION
WASHINGTON

August 1963

NATIONAL AERONAUTICS AND SPACE ADMINISTRATION

TECHNICAL NOTE D-1957

LOW-SPEED INVESTIGATION OF THE EFFECTS OF WING SWEEP ON THE AERODYNAMIC CHARACTERISTICS OF PARAWINGS HAVING EQUAL-LENGTH LEADING EDGES AND KEEL

By Rodger L. Naeseth and Thomas G. Gainer

SUMMARY

An investigation has been made in the Langley 300-MPH 7- by 10-foot tunnel to determine the aerodynamic characteristics of a related series of parawings in which wing sweep was the primary variable. The leading-edge sweep angles varied from 40° to 75° and the three basic parawings had flat-planform sweep angles of 35°, 45°, and 55°. The canopies of the wings were made of fabric. Tests were made at an airspeed of 38.6 mph and a Reynolds number of approximately 1.5×10^6. The maximum angle-of-attack range was from 14° to 53° for the wings having a canopy of 35° flat-planform sweep. A limited investigation of lateral characteristics was made for sideslip angles from approximately -5° to 16° for two angles of attack, and lateral stability derivatives were obtained for some configurations through an angle-of-attack range. Forces and moments acting on the wing and apex hinge moments were measured.

The highest value of maximum lift-drag ratio was obtained with the 40° swept wing having a 35° flat-planform sweep. The maximum lift-drag ratio of this wing was closely approached by the 50° swept wing having a 45° flat-planform sweep. Maximum lift-drag ratios obtained with a given canopy decreased appreciably with increasing sweep angle. A brief study of the effects of canopy attachment location on lift-drag ratios indicated that the most favorable attachment location was at the top of the leading edges and keel. Increasing the size of the leading edges and keel from a diameter of 1.5 percent to 7 percent of the keel length indicated that the maximum lift-drag ratio was reduced from a value of 5.3 to 3.7. A maximum lift coefficient, based on flat-planform area, of approximately 1.15 was obtained for the three canopies tested when the wing sweep was 5° greater than the flat-planform sweep.

Pitching-moment characteristics for assumed complete parawing and payload configurations with the center of gravity appreciably below the keel indicated that longitudinal trim could be obtained over a lift-coefficient range from 0.40 to maximum lift by a center-of-gravity shift of 9 percent of the keel length. The variations of apex hinge moments with wing sweep and angle of attack indicated that a wing with some restraint at the apex to balance shroud-line moments would inflate to a rather full lobe shape and would tend to fly at a high sweep angle

in high-speed flight and would tend to open and operate at a lower sweep angle for low-speed flight at high angles of attack.

INTRODUCTION

The National Aeronautics and Space Administration is currently conducting research investigations of the aerodynamic and flight characteristics of lightweight, flexible parawings which have a wide range of potential applications. Published information relating to the use of parawings for the recovery of space payloads may be found in references 1 to 9. Research on other applications such as the use of a parawing as a high-lift device for airplanes and for low-speed powered vehicles are reported in references 10 to 12. Because the parawing concept is fairly new, a good deal of the past work has been concentrated on obtaining just enough information to demonstrate the feasibility of a particular application rather than on obtaining general design information. However, in reference 13 the range of parawing aerodynamic and performance characteristics is indicated and the use of theory in parawing design is illustrated.

The present investigation was undertaken as an initial step in providing design information. Inasmuch as emphasis was placed on the recovery of space vehicles and rocket boosters, the design consideration of stowage of a parawing having rigid leading edges and keel on a rocket booster led to the use of equal lengths for these members.

Wing weight is also important in parawing recovery applications for space vehicles, and consideration of this factor had a significant influence on the model variations and the coefficients measured. In a flexible wing in flight the design sweep is attained by a proper balance of forces on the canopy, restraints in the canopy support structure, and cables supporting the payload. These considerations led to the study of wing planforms in which the wing sweep was varied over a large range for a fixed canopy surface area. The longitudinal and lateral aerodynamic characteristics and the apex hinge moments obtained can be used to determine minimum-weight wing planforms for given design conditions.

The present investigation of parawings having leading edges and keel of equal length was made on models for which the sweep angle of the leading edges could be varied from 40° to 75°. Three different fabric canopies having flat-planform sweep angles of 35°, 45°, and 55° were tested. Static longitudinal aerodynamic characteristics were determined through an angle-of-attack range which varied appreciably with both flat-planform sweep and leading-edge sweep because the lowest angle of attack for which data could be obtained was limited by the canopy unloading with attendant luffing. The maximum angle-of-attack range extended from approximately 14° to 53°. A range of trailing-edge boltrope settings was investigated on one model. (Boltrope shortening, essentially a shortening of the trailing edge, is sometimes used to control fabric motions.) Other effects investigated included deflection of the leading edges with respect to the keel when viewed from the side, increasing the diameter of the leading edges and keel, and a study of canopy attachment location on the large-diameter leading-edge configuration.

A limited investigation of lateral stability characteristics was made on some of the configurations. Tests were conducted over an angle-of-sideslip range that generally extended from -5° to 16° for a low and a moderate angle of attack. Some lateral stability derivatives over the angle-of-attack range were also determined from tests at sideslip angles of $\pm 5^{\circ}$ to indicate effects of wing sweep, leading-edge deflection, and canopy attachment on these derivatives.

All the test results of this investigation were obtained with the wing keel attached to a six-component balance and the data therefore are directly applicable only to the wing-alone characteristics. The wing leading edges were fixed relative to the keel by a spreader bar, and apex moments were obtained from a strain-gage balance in the spreader bar.

Tests were made in the Langley 300-MPH 7- by 10-foot tunnel at an airspeed of 38.6 miles per hour. The Reynolds number of the tests was 1.5×10^6, based on the model keel length.

SYMBOLS

The data obtained in this investigation are referred to the system of axes shown in figure 1. Pitching-, rolling-, and yawing-moment coefficients are referred to a moment center located on the center line of the keel at a longitudinal position 50 percent of the keel length. Apex hinge moments are referred to the wing-apex joint as shown in figure 1. All coefficients are based on the flat-planform area of the wing; the reference length used in determination of pitching-moment coefficients was the keel length and the reference length used in determination of rolling-moment and yawing-moment coefficients was the flat-planform span.

A aspect ratio, $\frac{b^2}{S_o}$

b wing span, ft

C_D drag coefficient, $\frac{\text{Drag}}{qS_o}$

$C_{h,h}$ leading-edge hinge-moment coefficient measured in plane formed by leading edges (see fig. 1), $\frac{\text{Horizontal hinge moment}}{qS_o l_k}$

$C_{h,v}$ leading-edge hinge-moment coefficient measured in a vertical plane (see fig. 1), $\frac{\text{Vertical hinge moment}}{qS_o l_k}$

C_L lift coefficient, $\frac{\text{Lift}}{qS_o}$

C_l rolling-moment coefficient, $\frac{\text{Rolling moment}}{qS_o b_o}$

C_m pitching-moment coefficient, $\frac{\text{Pitching moment}}{qS_o l_k}$

C_{m_o} value of pitching-moment coefficient at $C_L = 0$

C_n yawing-moment coefficient, $\frac{\text{Yawing moment}}{qS_o b_o}$

C_Y side-force coefficient, $\frac{\text{Side force}}{qS_o}$

C_{L_α} lift-curve slope, per deg

C_{l_β} effective-dihedral parameter, $\frac{\partial C_l}{\partial \beta}$, per deg

C_{n_β} static directional-stability parameter, $\frac{\partial C_n}{\partial \beta}$, per deg

C_{Y_β} side-force parameter, $\frac{\partial C_Y}{\partial \beta}$, per deg

L/D lift-drag ratio, $\frac{C_L}{C_D}$

l_k keel length, ft

q free-stream dynamic pressure, lb/sq ft

S reference area, sq ft

x distance of assumed center of gravity from wing apex, measured along keel, ft

z vertical distance of assumed center of gravity below wing keel, ft

α angle of attack of wing keel, deg

β angle of sideslip of model, deg

Λ leading-edge sweep angle, deg

δ wing leading-edge deflection angle with respect to keel when viewed from side (positive when leading edge is deflected below keel), deg

Subscripts:

max maximum

o refers to flat-planform condition

MODEL DESCRIPTION

The general arrangement of the models tested is shown in figures 2 and 3 and tabulated geometric characteristics of the various configurations tested are given in table I. Details of keel and leading-edge modifications made to one model are shown in figure 3 and photographs showing the model with flat-planform sweep of 45° installed in the tunrel are presented in figure 4.

TABLE I.- GEOMETRIC CHARACTERISTICS OF MODELS

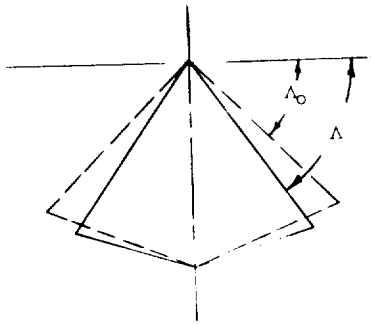

Λ, deg	Λ_o = 35° model		Λ_o = 45° model		Λ_o = 55° model	
	b, ft	A	b, ft	A	b, ft	A
35	*6.825	*3.276				
40	6.383	2.868				
45	5.891	2.020	*5.891	*2.828		
50	5.358	1.636	5.358	2.340		
55	4.783	1.220	4.783	1.864	*4.783	*2.296
60	4.167	.824	4.167	1.016	4.167	1.744
65			3.525	.662	3.525	1.248
70					2.850	.816
75					2.158	.468

*Flat-planform characteristics.

The leading edges of the model frame were made of 3/4-inch-diameter steel tube having an 0.058-inch wall thickness and the spreader bar and keel were made of 3/4-inch-diameter solid steel bar (fig. 2). A strain-gage balance was attached to the spreader bar and the left wing leading edge as shown in figure 2 in order to obtain apex-hinge-moment data. The apex fitting for the wing (see detail fig. 2) was hinged to allow freedom of the leading edges from moment restraint. The apex hinge moments were accordingly determined from the forces normal to and parallel to the axis of the strain-gage balance in the spreader bar.

The canopies for the model were made of rip-stop parachute nylon which was made nonporous by bonding 1-mil aluminized Mylar to the nylon fabric. The canopies tested in most of the investigation were made with pockets for the leading edges and keel. This method of fabric attachment caused the canopy to have an effective attachment point near the center line of the leading edges and keel. The three basic canopy patterns which were tested had flat-planform sweep angles of 35°, 45°, and 55°. Inasmuch as these patterns had equal-length leading edges and keel, the canopy area is defined by the relationship $S_o = l_k^2 \cos \Lambda_o$. The flat-planform reference areas of the three canopies were 14.22 square feet, 12.28 square feet, and 9.96 square feet for the 35°, 45°, and 55° sweep angles, respectively.

The leading-edge sweep angle of the model was held fixed during the tests by a spreader bar located at the 60-percent-keel station, perpendicular to the keel. The minimum test sweep angle was always 5° greater than the flat-planform sweep for each of the canopies tested; therefore, the range of test sweep angles with each flat-planform model was different.

The basic data of this investigation were obtained with no boltrope in the wing trailing edge and, as a result, there was appreciable trailing-edge luffing on all configurations at low angles of attack. The use of a boltrope in the hem sewn at the wing trailing edge has been found to alleviate this trailing-edge luffing, and some tests were made to study the effects of various boltrope lengths on the measured aerodynamic characteristics. The boltrope length is usually defined by the boltrope shortening and is expressed as the amount the boltrope length is shortened in terms of percent of the flat-planform trailing-edge length. Tests were made with 0-percent (boltrope length equal to the canopy trailing-edge length), 0.6-percent, 1.2-percent, 2.4-percent, and 3.6-percent boltrope shortening. The appearance of the trailing edge with various amounts of boltrope shortening is shown in the photographs of figure 5.

Tests were also made in which the models were modified in attempts to reduce the rolling moment due to sideslip at high lift. For these tests, the leading edges were deflected below the keel by placing a spacer between the keel and spreader bar as shown in figure 3(b). Tests were made with leading-edge deflection angles δ of 0°, 5.8°, 6.7°, and 11.5°.

An inflated-tube wing configuration was simulated by attaching 3.5-inch-diameter ($0.07l_k$-diameter) balsa cylinders over the existing steel leading edges and keel, and by filling in the apex region with a rounded balsa fairing as shown in figure 3(a). Three vertical positions of these balsa cylinders were investigated in connection with a study of the effects of fabric attachment location shown also in figure 3(a). No hinge moments were obtained on this wing because the clearance at the nose joint could not be maintained. The flat-planform area and span of the model with $0.07l_k$ leading-edge diameter were 13.24 square feet and 6.054 feet, respectively. The vertical reference center was at the center line of the supporting tubes for all three leading-edge positions. (See fig 3(a).)

Tests of a basic configuration were repeated with each set of tests made to investigate a particular variable because the geometry of the models changed somewhat over the extended period of testing because of fabric stretch, for example. Pitching moments were most sensitive to changes and it was considered desirable to repeat the basic condition in order to obtain more accurately the particular incremental effects being investigated.

TESTS AND CORRECTIONS

The tests were made in the Langley 300-MPH 7- by 10-foot tunnel at a dynamic pressure of 3.8 pounds per square foot, which corresponds to an airspeed of approximately 38.6 miles per hour. The Reynolds number of the tests was approximately 1.5×10^6, based on the model keel length of 4.167 feet.

Aerodynamic characteristics in pitch were obtained at an angle of sideslip of 0° through an angle-of-attack range that extended from the lowest value of about 14° to approximately 53°. The lowest test angle of attack generally was different for each wing configuration inasmuch as the lower angle limit was determined by the occurrence of canopy luffing. Lateral stability derivatives were obtained from tests through the angle-of-attack range at sideslip angles of $\pm 5^\circ$ for some of the model configurations. A few tests were also made to obtain the aerodynamic characteristics in sideslip by varying the sideslip from approximately -5° to 16° at constant angles of attack.

Jet-boundary corrections to the angle of attack and drag coefficients as determined from the charts of reference 14 have been added to the data. Blockage corrections to account for the constriction effects of the model and its wake in the tunnel have been applied to the test data by the method of reference 15.

PRESENTATION OF RESULTS

Results of the present parawing investigation are presented in the figures outlined as follows:

RESULTS AND DISCUSSION

The present investigation of parawing design variables was conducted on model configurations having equal-length leading edges and keel. Wing leading-edge sweepback was the primary variable investigated. As the leading-edge sweep was varied for a given flat-planform sweep, other important geometric parameters such as wing aspect ratio, twist, camber, span, and projected planform area varied. These other factors must be considered in an assessment of wing planforms and in selection of a wing configuration for a particular application. Inasmuch as the separate effects of the several factors that varied with wing sweep cannot readily be determined from the experimental results, for sake of convenience, reference will be made to effects of wing sweep because it was the primary variable.

Longitudinal Characteristics

Effects of wing sweep on lift and drag characteristics.- The occurrence of canopy luffing limited the minimum lift coefficient at which data could be obtained and this lift coefficient was generally between 0.1 and 0.3. The angle of attack at which the minimum test lift coefficient was obtained varied greatly with wing-sweep angle (fig. 6). The lowest test angle of attack of approximately 14° was obtained with wing configurations having the least canopy curvature (wings having a 5° increment in sweep from the flat-planform sweep). Increasing the wing sweep for a given flat-planform canopy sweep increased the geometric twist (washout at the tips) and required a higher angle of attack to generate the minimum lift needed to load the canopy.

The variation of lift-curve slope with wing sweep (fig. 11) showed the expected loss with increasing sweep and was in fair agreement with theory for

conventional wing planforms of the same aspect ratio and sweep (ref. 16). The maximum lift coefficient obtained for the three different canopies (also shown in fig. 11) was approximately 1.15 when the wing sweep was 5° greater than the flat-planform sweep. Increasing the sweep caused a large reduction in maximum lift coefficient; however, most of this loss can be attributed to use of the flat-planform reference area rather than the projected area.

The highest value of maximum lift-drag ratio obtained in this investigation was 5.4 (fig. 12) and was obtained with the 40° swept wing having a 35° flat-planform sweep. The 50° swept wing with a 45° flat-planform sweep had a maximum lift-drag ratio that was only slightly lower (5.35). A maximum lift-drag ratio of 6.2 was obtained for this 50° swept wing in the investigation reported in reference 13 and the lower value obtained in the present study is attributed to differences in the canopy attachment details at the leading edge. Increasing the wing sweep for a given canopy caused significant reductions in maximum lift-drag ratio as would be expected from both the increase in sweep and twist (ref. 13), and from the decrease in aspect ratio.

Effects of boltrope shortening.- Shortening the length of the boltrope in the wing trailing edge reduced luffing of the wing canopy in the low-lift coefficient range and provided significant increases in lift coefficient at a given angle of attack and in maximum lift coefficient. These values were approximately proportional to the amount of boltrope shortening (fig. 7). Shortening the length of the boltrope caused proportional negative increments in pitching moments, with very little effect on longitudinal stability. The values of C_{m_o}, found by extrapolating the linear part of the pitching-moment curves to $C_L = 0$, become more negative with increasing boltrope shortening. As pointed out in reference 12, C_{m_o} has an important effect with regard to the stick-force gradients for aircraft-type applications of parawings and a positive value is, of course, desirable. Changes in boltrope length had little effect on maximum lift-drag ratios; however, there was some increase indicated in going from the loose boltrope to the attached boltrope with no shortening (fig. 7).

Effects of canopy attachment location.- The effects of canopy attachment location were investigated on the configuration having leading-edge and keel diameters of $0.07l_k$. The longitudinal aerodynamic characteristics obtained are presented in figure 10. Attachment of the wing canopy to the bottom of the leading edges and keel increased the lift coefficient at low angles of attack but gave a somewhat lower value of maximum lift coefficient and generally lower lift-drag ratios than the basic center attachment of the fabric. An opposite effect of attachment location was indicated when the canopy was attached to the top of the leading edges and keel, and the increase in both maximum lift coefficient and lift-drag ratios was very pronounced. These results indicate therefore that from the standpoint of both maximum lift coefficient and lift-drag ratios, the most favorable canopy attachment location is at the top of the leading edges and keel. These appreciable effects of canopy attachment location were probably augmented by the large-diameter leading edges used in this study, and the incremental effects observed might not be directly applicable to smaller diameter leading edges. However, a comparison of the results of figure 6(b) and the test results of reference 13, referred to previously, substantiate the fact that some gains in

maximum lift-drag ratio are to be expected for the model with the relatively small leading-edge diameter of $0.015l_k$.

There were no large effects of moving the canopy attachment location from the center line to the top of the leading edges and keel on longitudinal stability at low lift, but as can be seen by extending the pitching-moment curves to zero lift, there was a negative increment in C_{m_o} in going from the center to the top attachment. The bottom attachment, on the other hand, significantly increased the longitudinal stability and provided an appreciable positive pitching-moment coefficient at zero lift.

Effects of leading-edge size.- The largest effect of leading-edge size, as expected, was on the value of maximum lift-drag ratio. For the center attachment location of the canopy, the maximum lift-drag ratio of the basic model with the $0.015l_k$-diameter leading edges was about 5.3 (fig. 6(b)) and decreased to a value of about 3.7 (fig. 10(a)) with the $0.07l_k$-diameter leading edges. It is apparent therefore from these results that if performance considerations are of primary importance, the diameter of the leading edges should be minimized as far as possible. In this regard, it is believed that the size of the keel was only of secondary importance.

Effects of center-of-gravity location.- Pitching-moment results for many of the basic wing configurations tested indicated that for the moment reference selected, the wing had either neutral stability or were unstable below the angle of attack for maximum lift. Furthermore, most of these configurations would have appreciable negative value of pitching moment at zero lift. In order to obtain trim and have positive longitudinal stability at trim, the pitching moment at zero lift should be positive. These desired conditions of stability and trim can be achieved on a parawing configuration by locating the payload an appreciable distance below the wing, and longitudinal control may be obtained by fore-and-aft movement of the center of gravity with respect to the wing.

Pitching-moment data for three wings have been transferred to a vertical location of the center of gravity that was 75 percent of the keel length below the wing keel in order to illustrate the longitudinal travel of the center of gravity required to trim from a lift coefficient of 0.40 to the maximum lift coefficient. The data of figure 13 indicate that this range of trimmed lift coefficients can be obtained with a center-of-gravity shift of about 9 percent of the keel length for wings having sweep angles 5° greater than the flat-planform sweep.

Apex Hinge Moments

Effects of wing sweep.- The apex hinge-moment coefficients in the horizontal plane $C_{h,h}$ were positive (moment tending to increase the wing sweep) for wing planforms which had wing-sweep angles 5° greater than the flat-planform sweep. (See fig. 6.) These hinge-moment coefficients decreased appreciably with both increasing wing sweep and with flat-planform sweep. The values of $C_{h,h}$ increased with angle of attack for wings having wing-sweep angles 5° greater than the flat-planform sweep, were relatively invariant with angle of attack for a

10° sweep increment, and generally decreased with increasing angle of attack and became negative for wings having a sweep increment from the flat-planform sweep of 15° or greater. These results indicate that a parawing with some restraint at the apex to balance shroud-line moments would inflate to a rather full lobe shape and would tend to fly at a high-sweep angle for high-speed flight and would tend to open and operate at a lower sweep for low-speed flight at high angles of attack. This observation has been substantiated by free-glide tests of a number of parawing models.

The apex hinge-moment coefficients in the vertical plane $C_{h,v}$ were negative (moment tending to raise the leading edges) for all wing configurations and angles of attack of this investigation. These moments were greatest for wings having sweep angles 5° greater than the flat-planform sweep and generally increased with increasing angle of attack for all the wing configurations tested.

Effects of boltrope shortening and leading-edge deflection.- Increasing the amount of boltrope shortening caused a corresponding increase in the magnitude of both $C_{h,h}$ and $C_{h,v}$. (See fig. 7.) The increments in apex hinge-moment coefficients were on the average about 0.06 through the angle-of-attack range for a change in boltrope from 0 percent (loose) to 3.6 percent.

Deflection of the wing leading edge had a relatively small effect on $C_{h,h}$ (fig. 9); however, $C_{h,v}$ was increased (negatively) by a downward deflection of the leading edges, as might be expected.

Lateral Characteristics

The scope of the investigation of static lateral characteristics was limited in comparison to the study of longitudinal characteristics and only a few configurations were investigated to provide some indications of the type of lateral characteristics to be expected on parawings.

Effects of wing sweep.- Lateral stability derivatives obtained on wings having a 45° flat-planform sweep (fig. 18) indicated that, in general, at low angles of attack, the static directional-stability parameter C_{n_β} increased and the effective-dihedral parameter $\left(-C_{l_\beta}\right)$ decreased with increasing sweep angle. At high angles of attack there was little consistent effect of sweep on the rolling moment due to sideslip. The directional stability at all sweep angles tested was positive in the low angle-of-attack range but directional instability was indicated at higher angles of attack. Attention should be called to the fact that, as with the pitching moments, these results are for the wing alone, and the derivatives presented would have to be transferred to a center-of-gravity location considerably below the wing in order to represent the wing characteristics of a complete configuration. In addition, the inertia characteristics of such a configuration are probably very different from those of conventional aircraft, particularly with regard to the inclination of the principal axes. These characteristics are of sufficient importance that they must be considered in assessing the possible existence of a directional divergence.

Effects of leading-edge deflection.- Deflection of the wing leading edges had the intended effect of providing positive increments in rolling moment due to sideslip throughout most of the angle-of-attack range (fig. 19). There was also some increase in directional stability at low angles of attack and at high angles.

SUMMARY OF RESULTS

Based on low-speed wind-tunnel tests of a series of parawing planforms in which wing sweep was the primary variable, the following results were obtained:

1. The highest value of maximum lift-drag ratio was obtained with the 40° swept wing having a 35° flat-planform sweep. The maximum lift-drag ratio of this wing was closely approached by the 50° swept wing having a 45° flat-planform sweep. Maximum lift-drag ratios obtained with a given canopy decreased appreciably with increasing sweep angle.

2. A brief study of the effects of canopy attachment location on lift-drag ratios indicated that the most favorable attachment location was at the top of the leading edges and keel.

3. An investigation of the effects of increasing the size of the leading edges and keel from a diameter of 1.5 percent to 7 percent of the keel length indicated that the maximum lift-drag ratio was reduced from a value of 5.3 to 3.7.

4. A maximum lift coefficient, based on flat-planform area, of approximately 1.15 was obtained for the three canopies tested when the wing sweep was 5° greater than the flat-planform sweep.

5. Pitching-moment characteristics for assumed complete parawing and payload configurations with the center of gravity appreciably below the keel indicated that longitudinal trim could be obtained over a lift-coefficient range from 0.40 to the maximum lift coefficient by a center-of-gravity shift of 9 percent of the keel length.

6. The variation of apex hinge moments with wing sweep and angle of attack indicated that a wing with some restraint at the apex to balance shroud-line moments would inflate to a rather full lobe shape and would tend to fly at a high sweep angle in high-speed flight and would tend to open and operate at a lower sweep angle for low-speed flight at high angles of attack.

Langley Research Center,
National Aeronautics and Space Administration,
Langley Station, Hampton, Va., June 17, 1963.

REFERENCES

1. Rogallo, Francis M., Lowry, John G., Croom, Delwin R., and Taylor, Robert T.: Preliminary Investigation of a Paraglider. NASA TN D-443, 1960.

2. Taylor, Robert T.: Wind-Tunnel Investigation of Paraglider Models at Supersonic Speeds. NASA TN D-985, 1961.

3. Penland, Jim A.: A Study of the Aerodynamic Characteristics of a Fixed Geometry Paraglider Configuration and Three Canopies With Simulated Variable Canopy Inflation at a Mach Number of 6.6. NASA TN D-1022, 1962.

4. Hatch, Howard G., Jr., and McGowan, William A.: An Analytical Investigation of the Loads, Temperatures, and Ranges Obtained During the Recovery of Rocket Boosters by Means of a Parawing. NASA TN D-1003, 1962.

5. Sleeman, William C., Jr., and Johnson, Joseph L., Jr.: Parawing Aerodynamics. Astronautics and Aerospace Eng., vol. 1, no. 5, June 1963, pp. 49-55.

6. Fournier, Paul G., and Bell, B. Ann: Low Subsonic Pressure Distributions on Three Rigid Wings Simulating Paragliders With Varied Canopy Curvature and Leading-Edge Sweep. NASA TN D-983, 1961.

7. Fournier, Paul G., and Bell, B. Ann: Transonic Pressure Distributions on Three Rigid Wings Simulating Paragliders With Varied Canopy Curvature and Leading-Edge Sweep. NASA TN D-1009, 1962.

8. Fournier, Paul G.: Pressure Distributions on Three Rigid Wings Simulating Parawings With Varied Canopy Curvature and Leading-Edge Sweep at Mach Numbers From 2.29 to 4.65. NASA TN D-1618, 1963.

9. Sleeman, William C., Jr.: Low-Speed Investigation of Cable Tension and Aerodynamic Characteristics of a Parawing and Spacecraft Combination. NASA TN D-1937, 1963.

10. Naeseth, Rodger L.: An Exploratory Study of a Parawing as a High-Lift Device for Aircraft. NASA TN D-629, 1960.

11. Hewes, Donald E.: Free-Flight Investigation of Radio-Controlled Models With Parawings. NASA TN D-927, 1961.

12. Johnson, Joseph L., Jr.: Low-Speed Wind-Tunnel Investigation to Determine the Flight Characteristics of a Model of a Parawing Utility Vehicle. NASA TN D-1255, 1962.

13. Polhamus, Edward C., and Naeseth, Rodger L.: Experimental and Theoretical Studies of the Effects of Camber and Twist on the Aerodynamic Characteristics of Parawings Having Nominal Aspect Ratios of 3 and 6. NASA TN D-972, 1963.

14. Gillis, Clarence L., Polhamus, Edward C., and Gray, Joseph L., Jr.: Charts for Determining Jet-Boundary Corrections for Complete Models in 7- by 10-Foot Closed Rectangular Wind Tunnels. NACA WR L-123, 1945. (Formerly NACA ARR L5G31.)

15. Herriot, John G.: Blockage Corrections for Three-Dimensional-Flow Closed-Throat Wind Tunnels, With Consideration of the Effect of Compressibility. NACA Rep. 995, 1950. (Supersedes NACA RM A7B28.)

16. Lowry, John G., and Polhamus, Edward C.: A Method for Predicting Lift Increments Due to Flap Deflection at Low Angles of Attack in Incompressible Flow. NACA TN 3911, 1957.

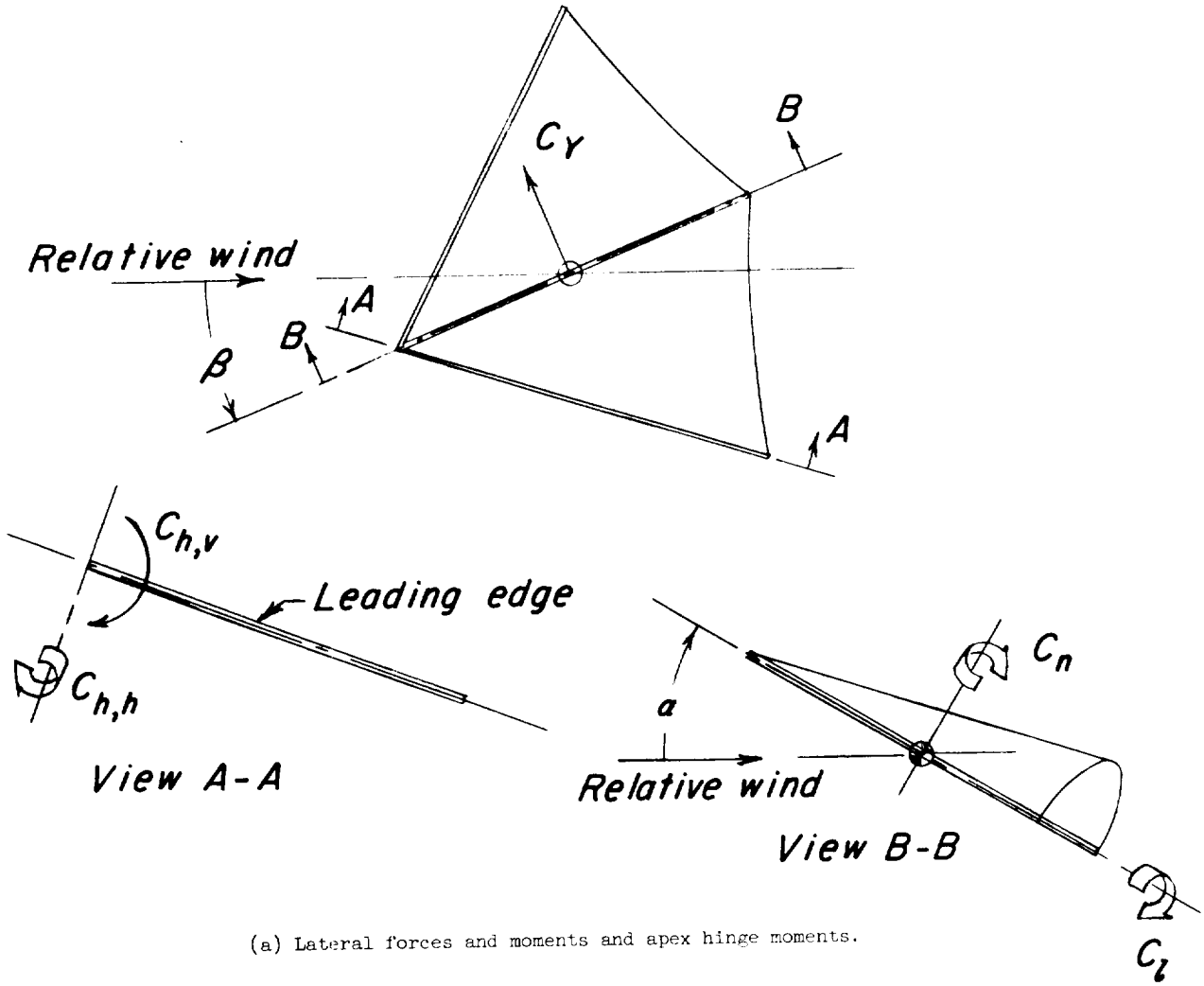

(a) Lateral forces and moments and apex hinge moments.

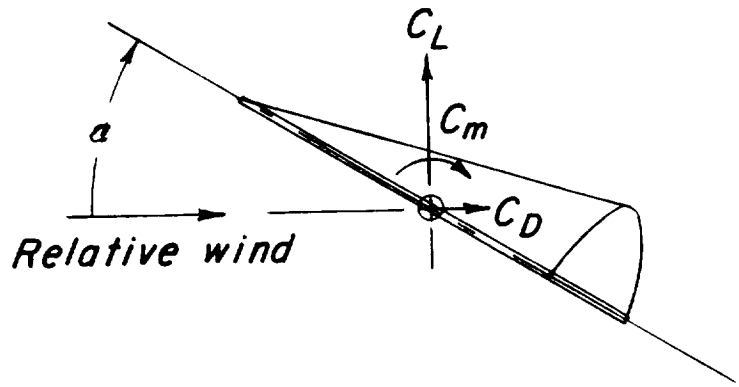

(b) Longitudinal forces and moments.

Figure 1.- Axes systems and convention used to define positive sense of forces, moments, and angles.

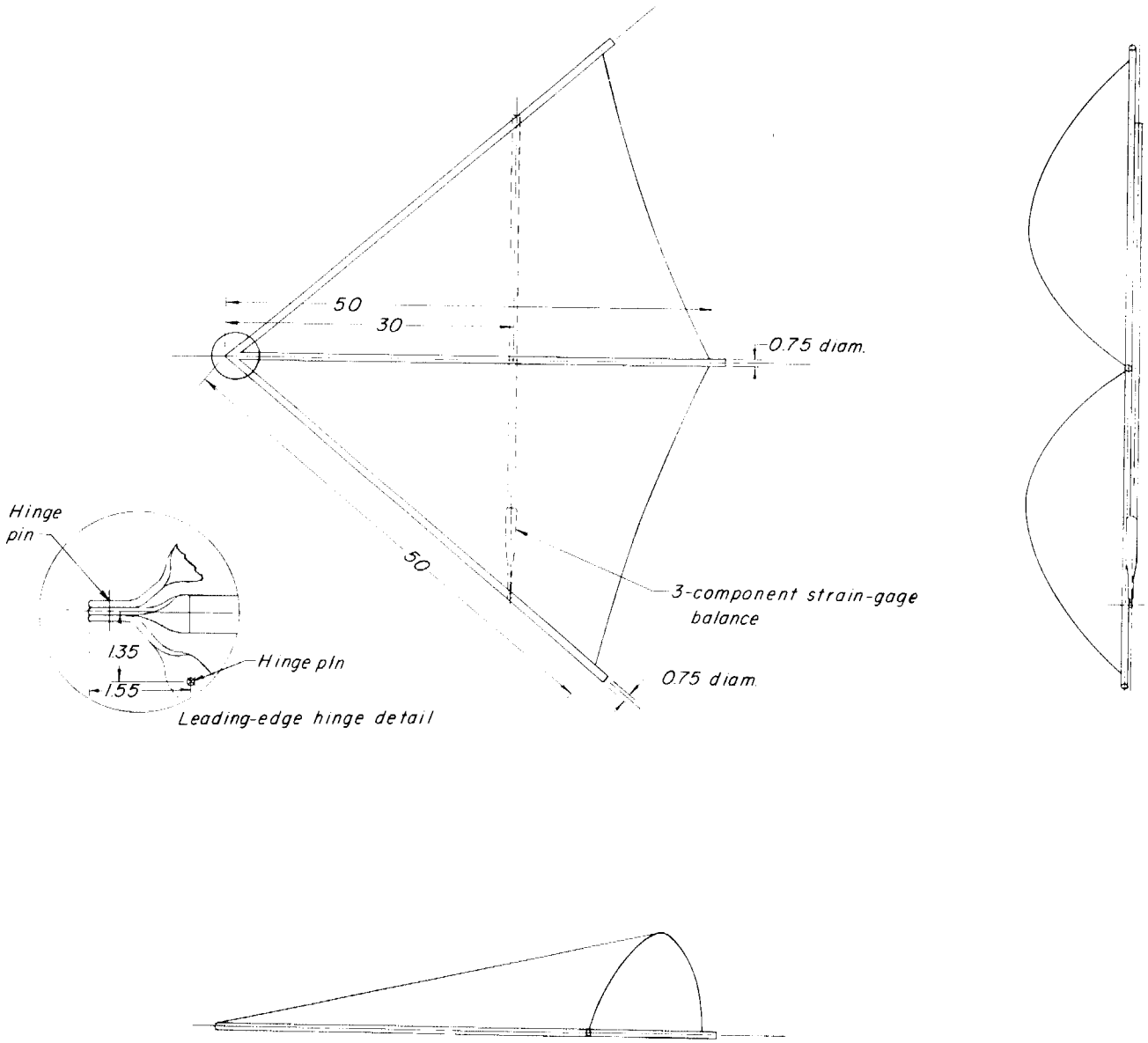

Figure 2.- General arrangement of models. (All linear dimensions are in inches.)

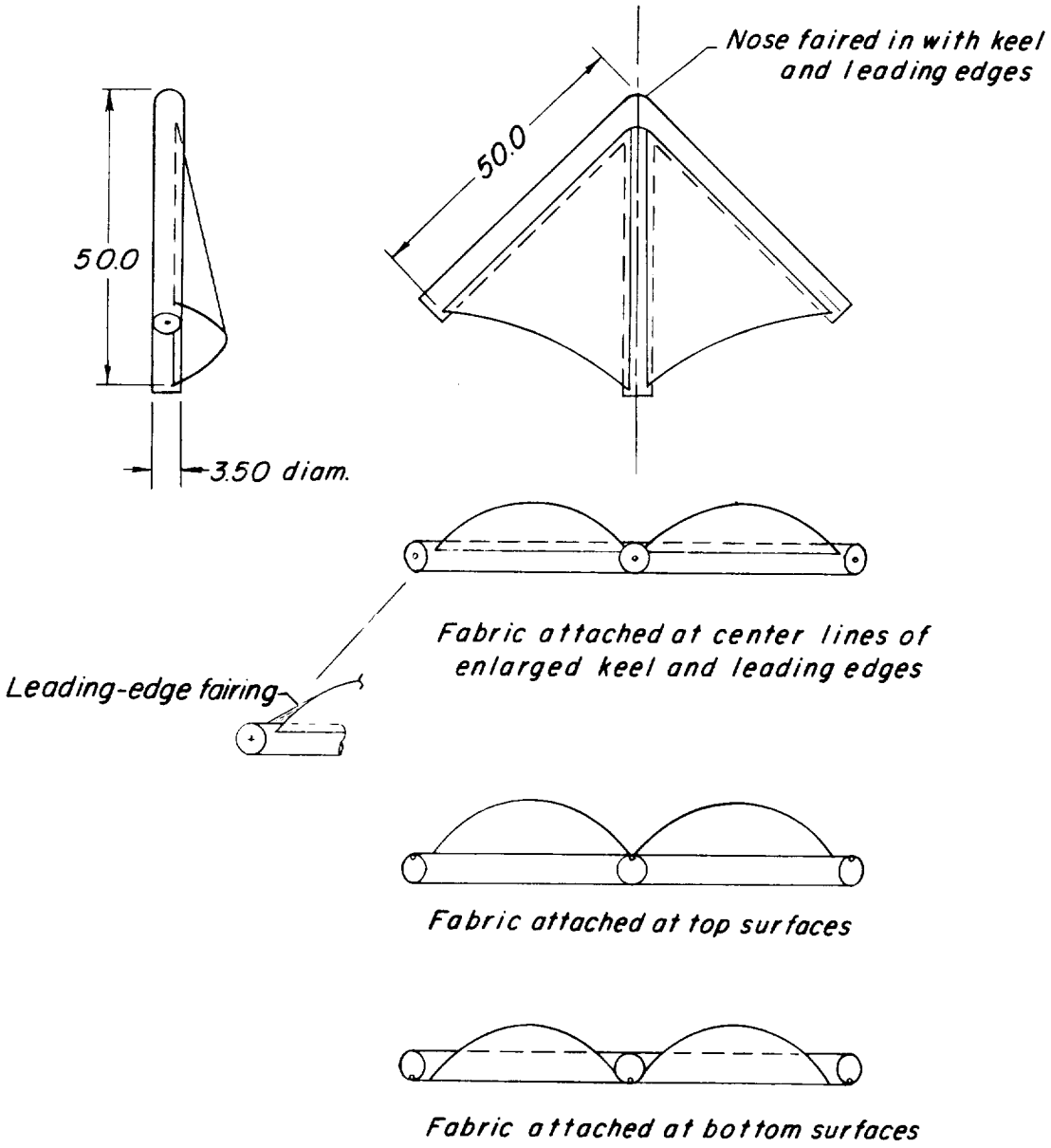

(a) Configurations with $0.07l_k$-diameter keel and leading edges.

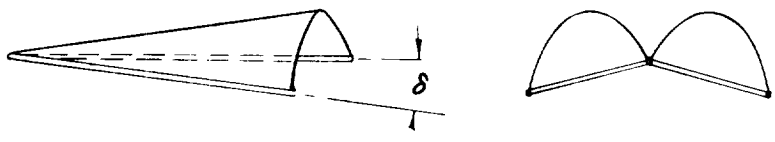

(b) Leading-edge deflection.

Figure 3.- Details of keel and leading-edge modifications.

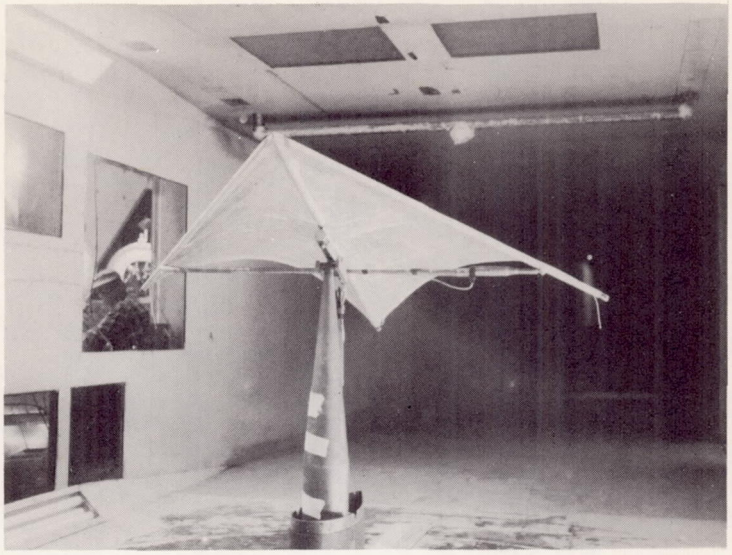

(a) Front view.

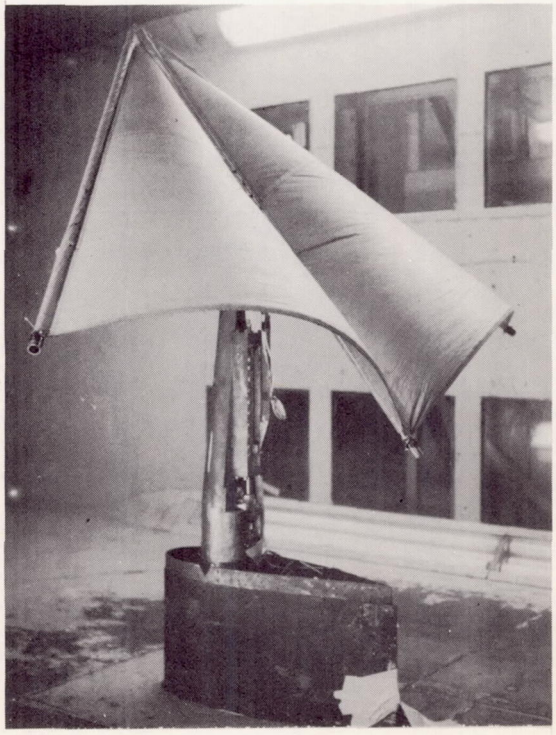

(b) Three-quarter rear view. L-63-3197

Figure 4.- Photographs of $\Lambda_o = 45^\circ$ basic parawing model in Langley 300-MPH 7- by 10-foot tunnel.

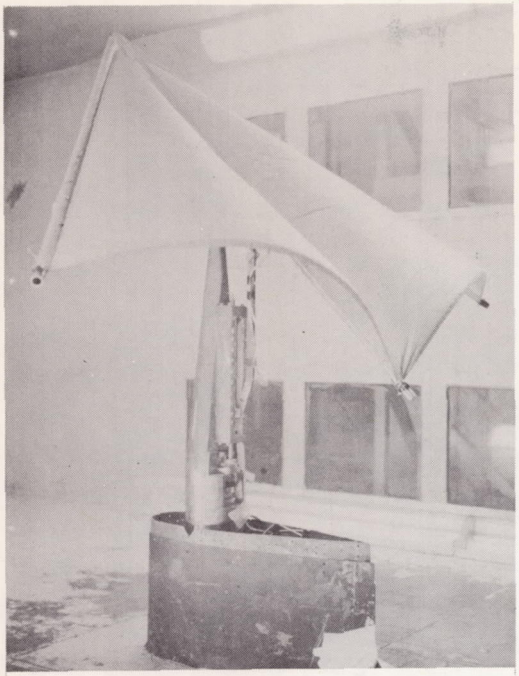

(a) 0.6-percent shortening.

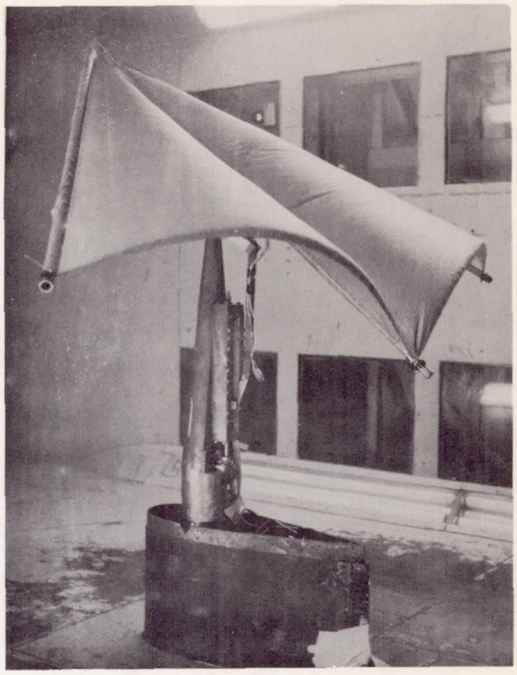

(b) 1.2-percent shortening.

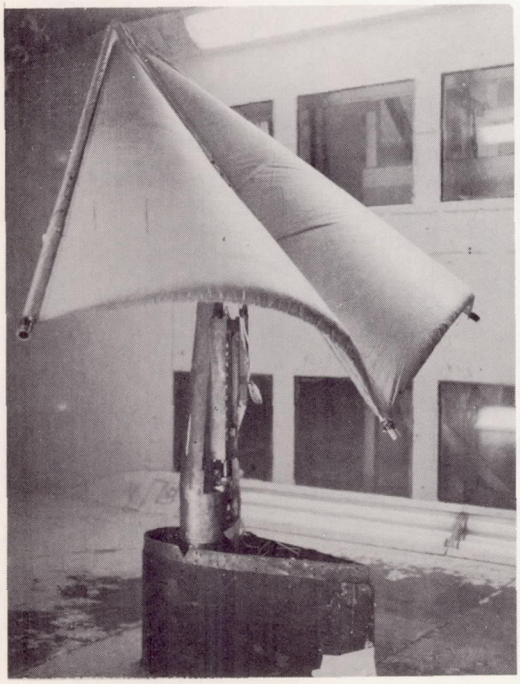

(c) 2.4-percent shortening.

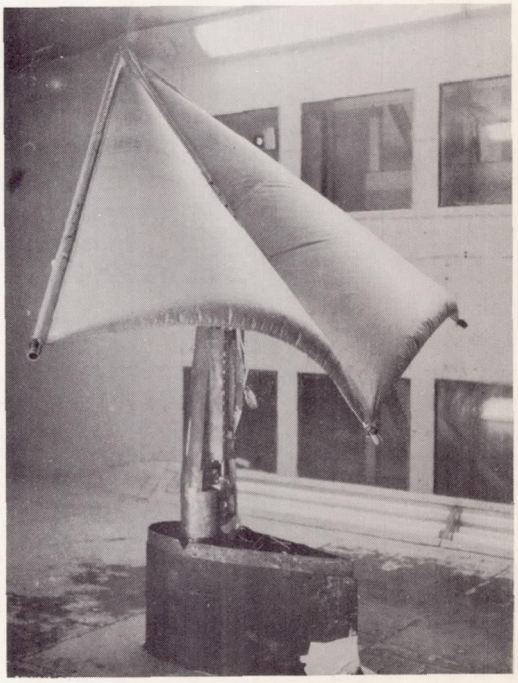

L-63-3198

(d) 3.6-percent shortening.

Figure 5.- Effects of boltrope shortening on trailing-edge shape. $\Lambda_o = 45^o$ model; $\Lambda = 50^o$.

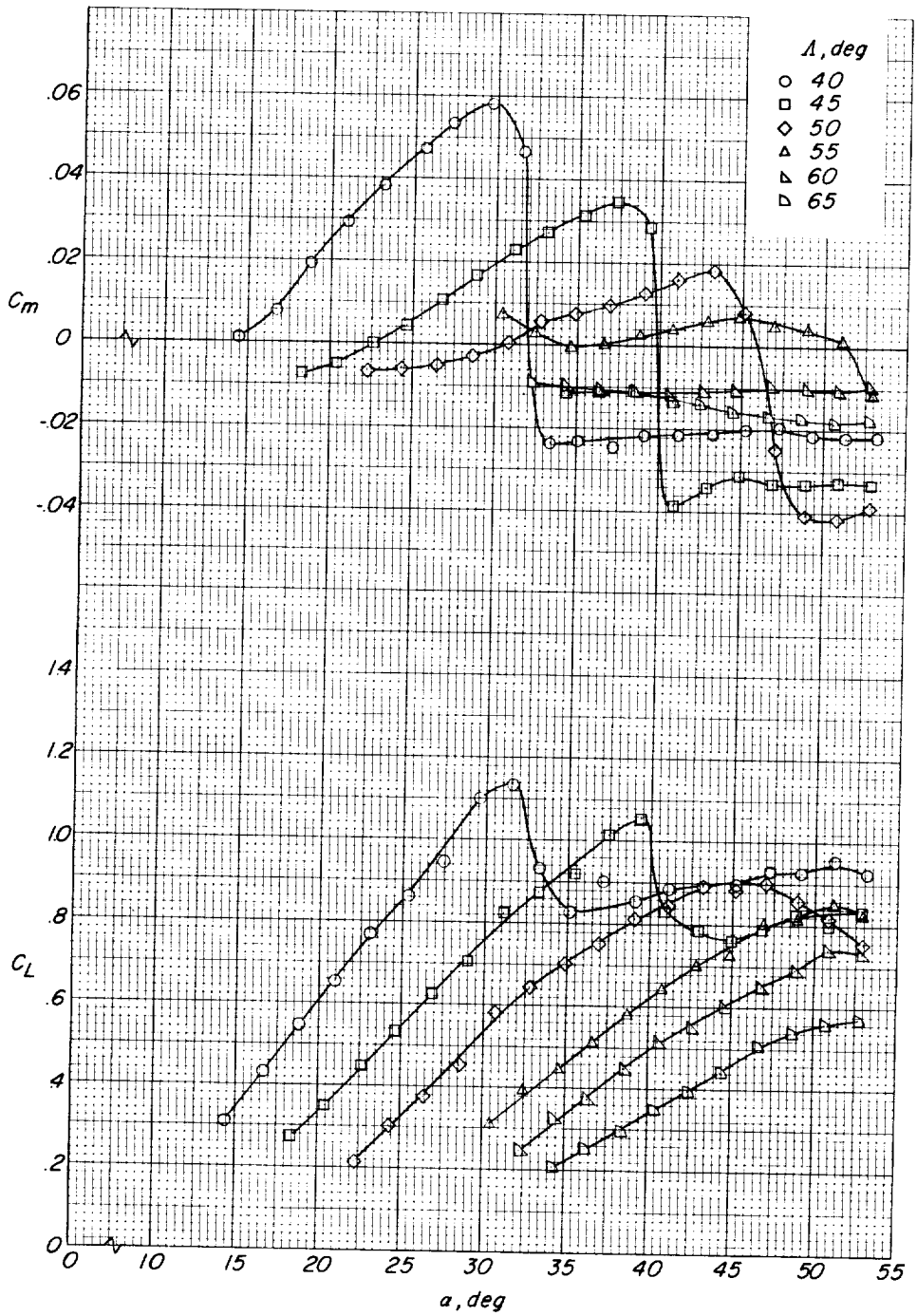

(a) $\Lambda_0 = 35^\circ$ model.

Figure 6.- Effects of changes in wing leading-edge sweep angle on the longitudinal characteristics of the models with flat-planform leading-edge sweeps of 35°, 45°, and 55°.

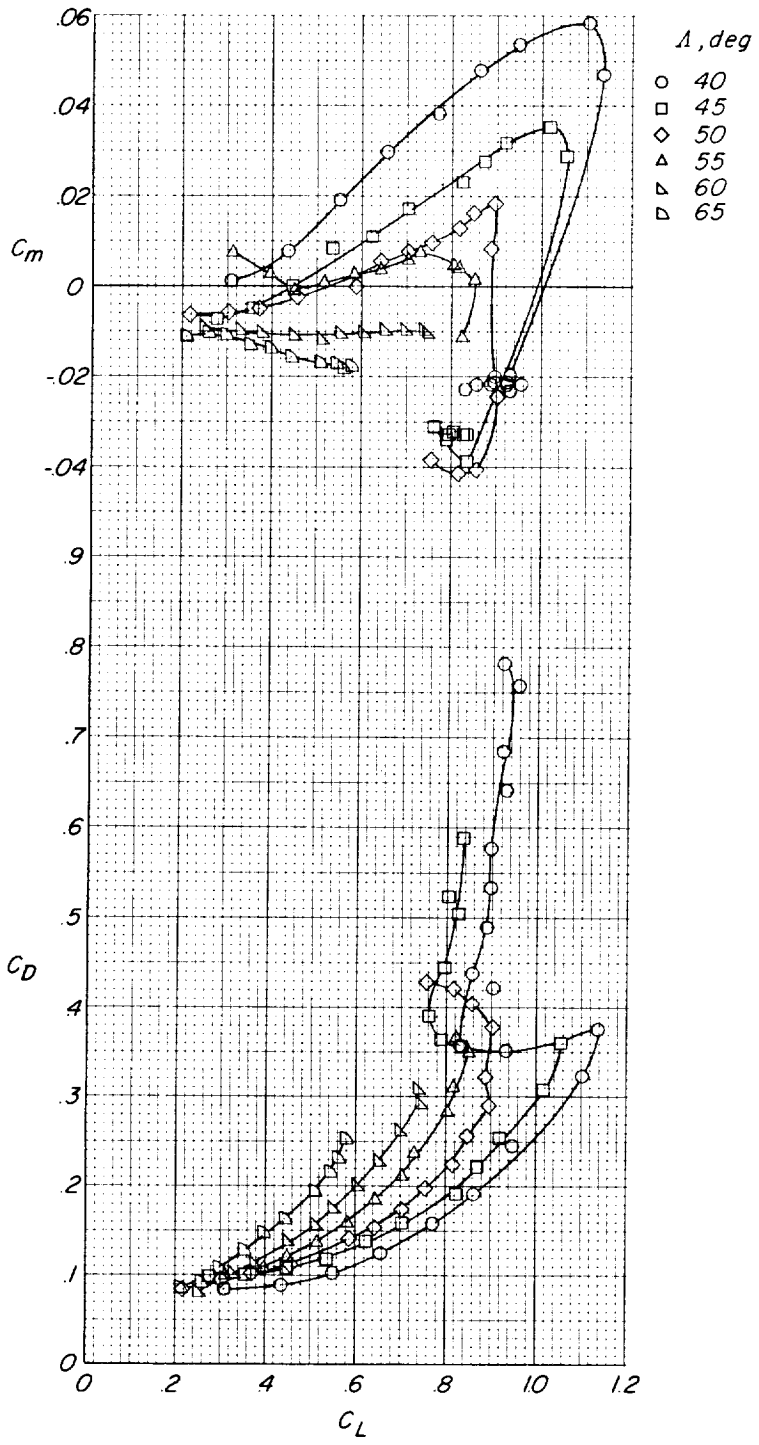

(a) $\Lambda_0 = 35^\circ$ model. Continued.

Figure 6.- Continued.

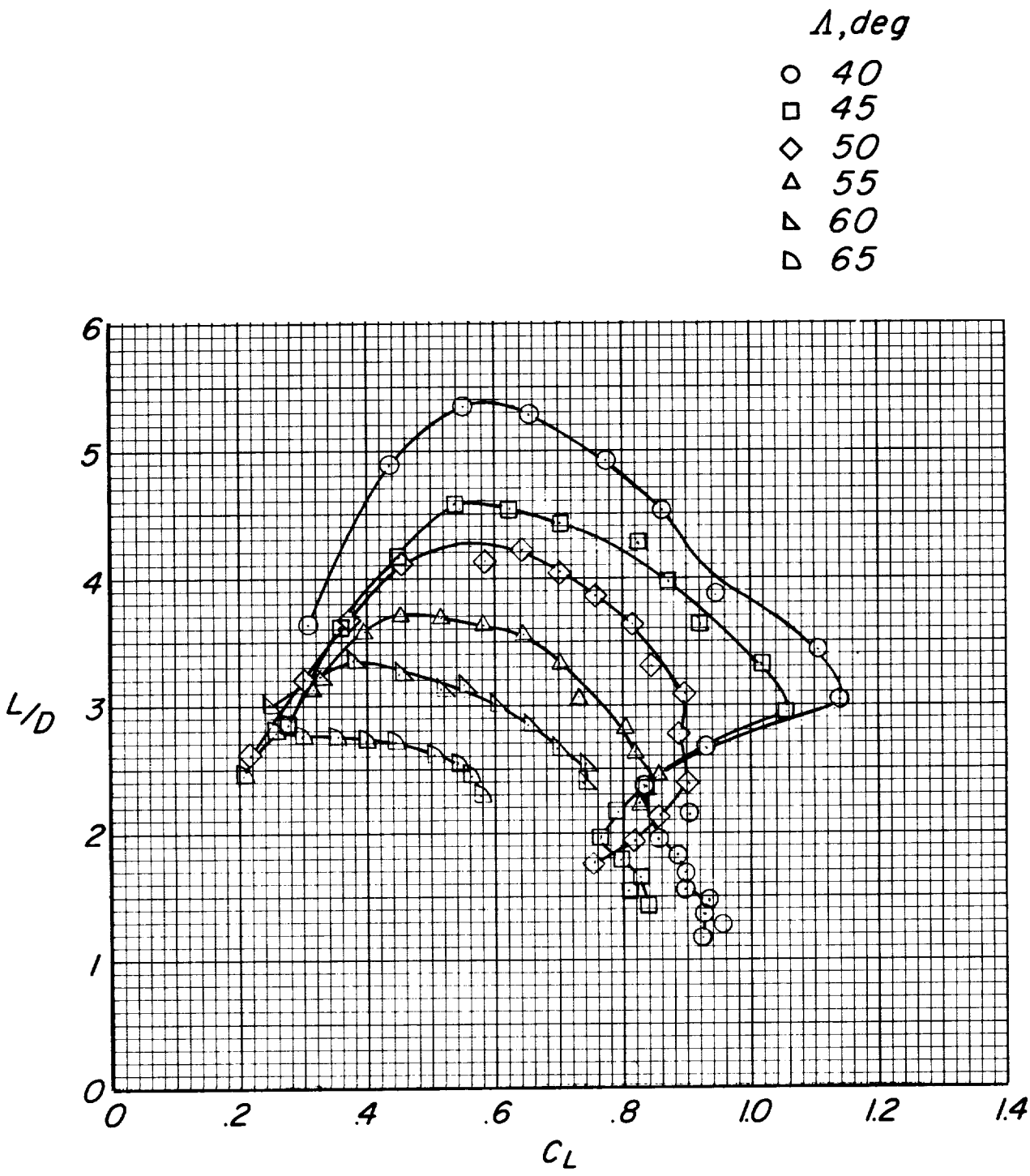

(a) $\Lambda_o = 35^\circ$ model. Continued.

Figure 6.- Continued.

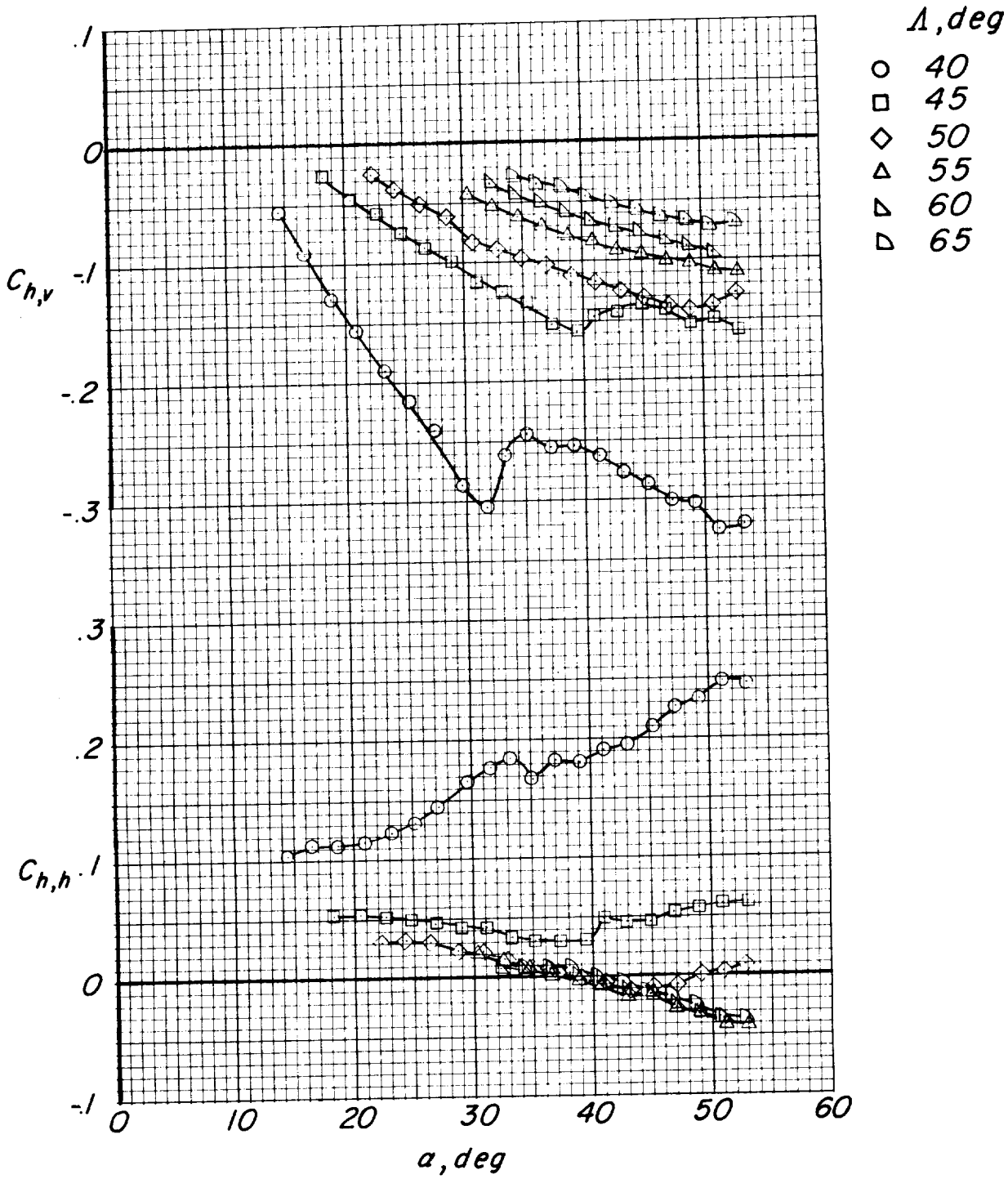

(a) $\Lambda_o = 35^o$ model. Concluded.

Figure 6.- Continued.

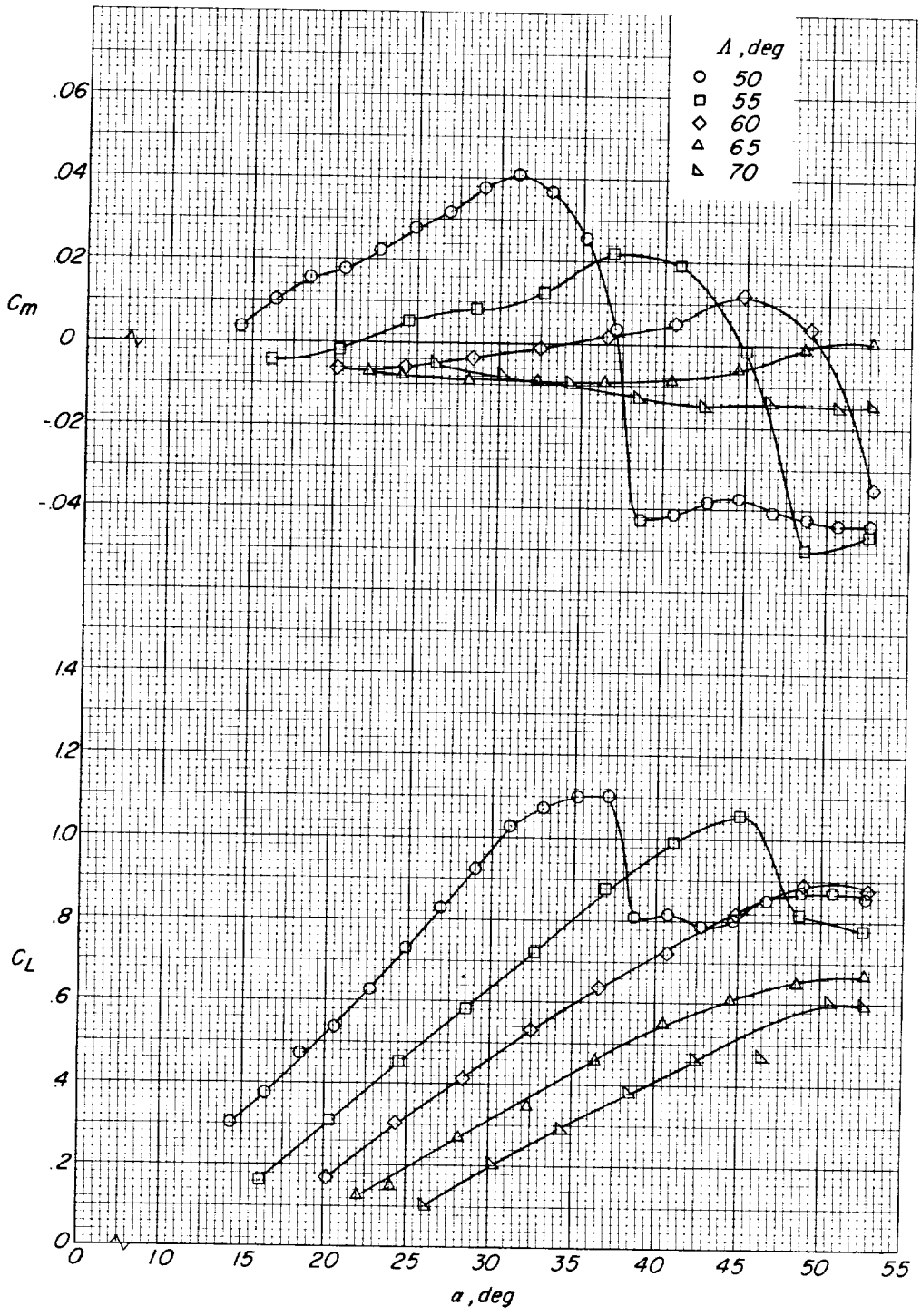

(b) $\Lambda_o = 45^\circ$ model.

Figure 6.- Continued.

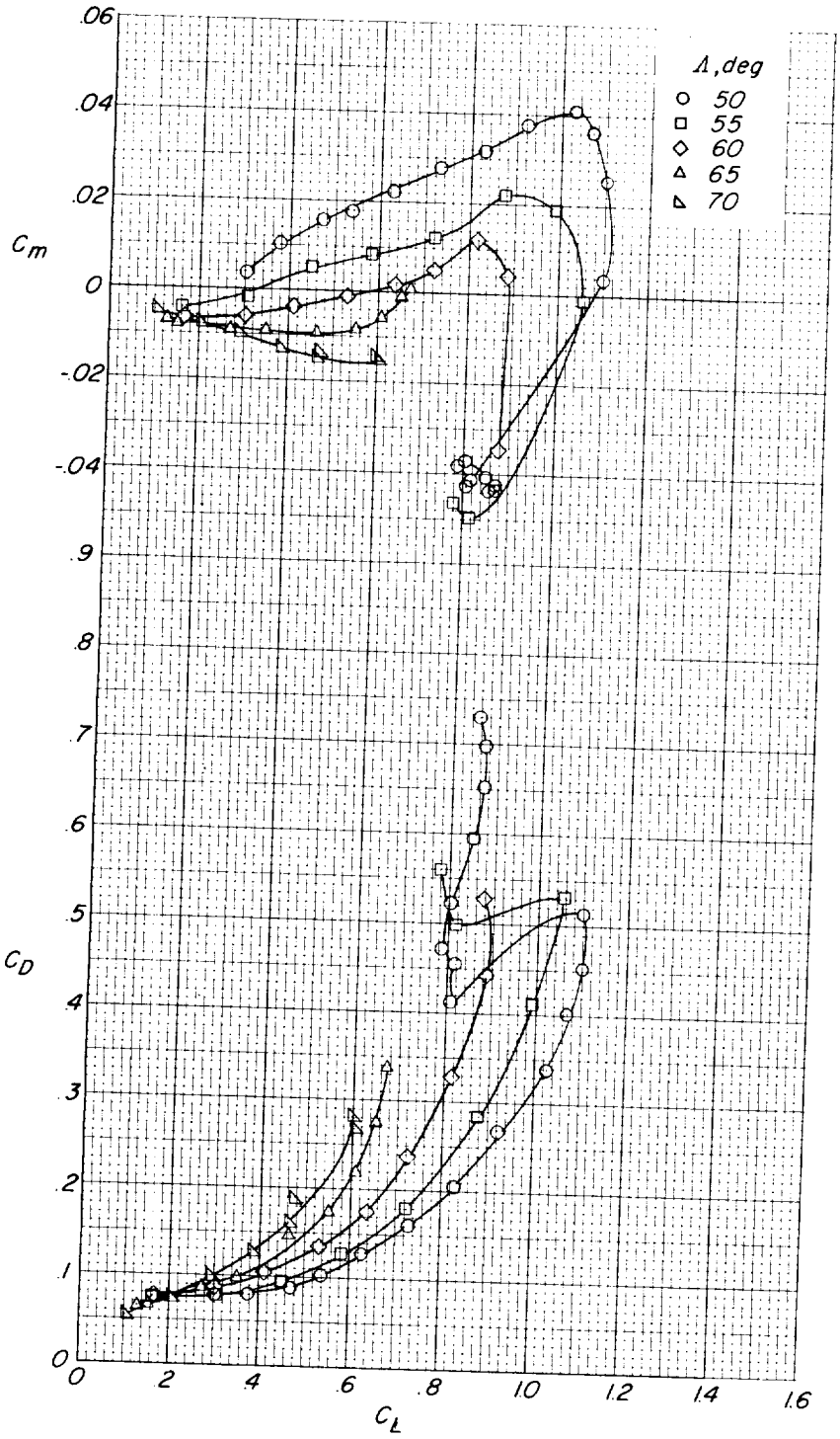

(b) $\Lambda_o = 45^\circ$ model. Continued.

Figure 6.- Continued.

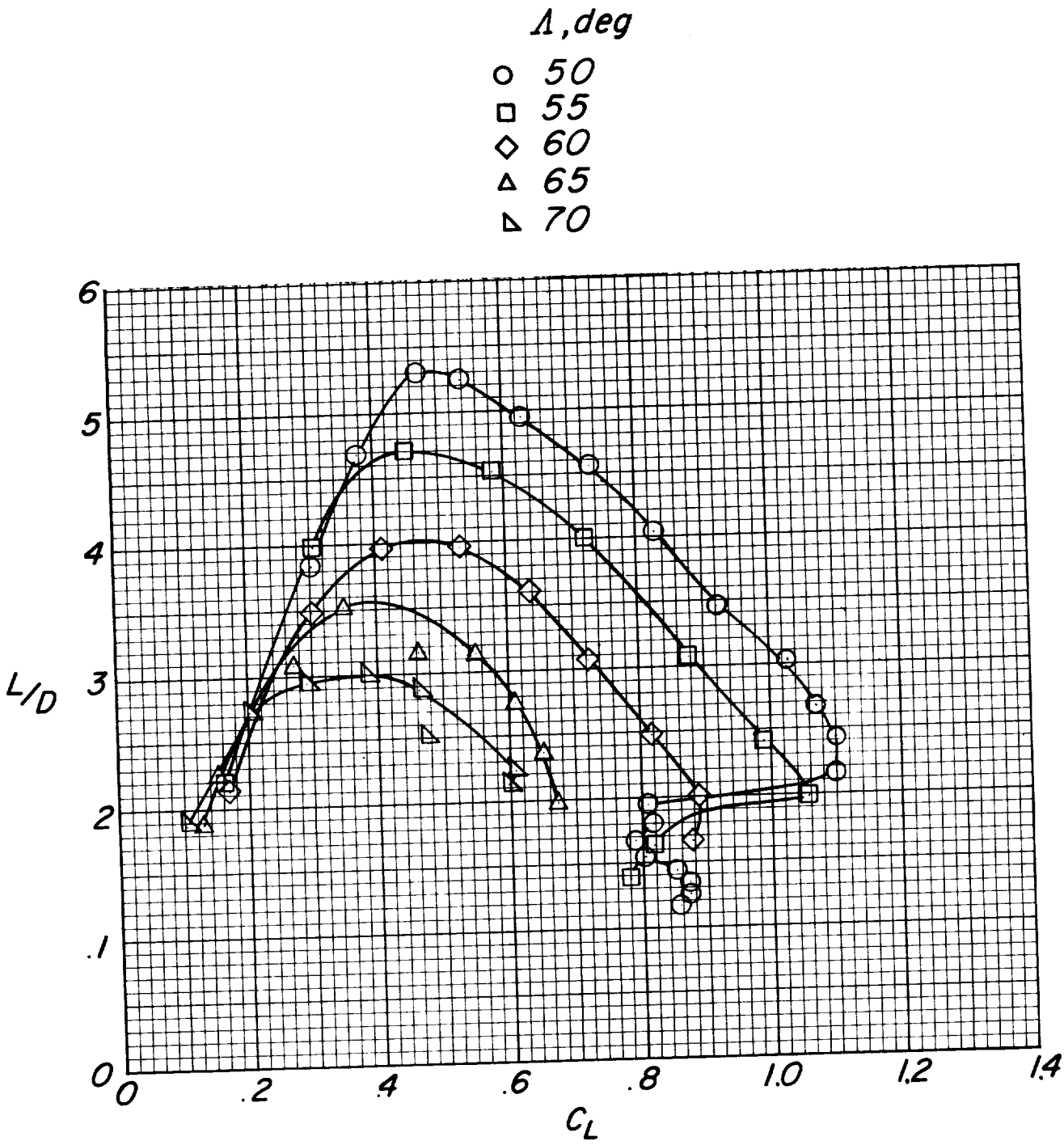

(b) $\Lambda_o = 45^o$ model. Continued.

Figure 6.- Continued.

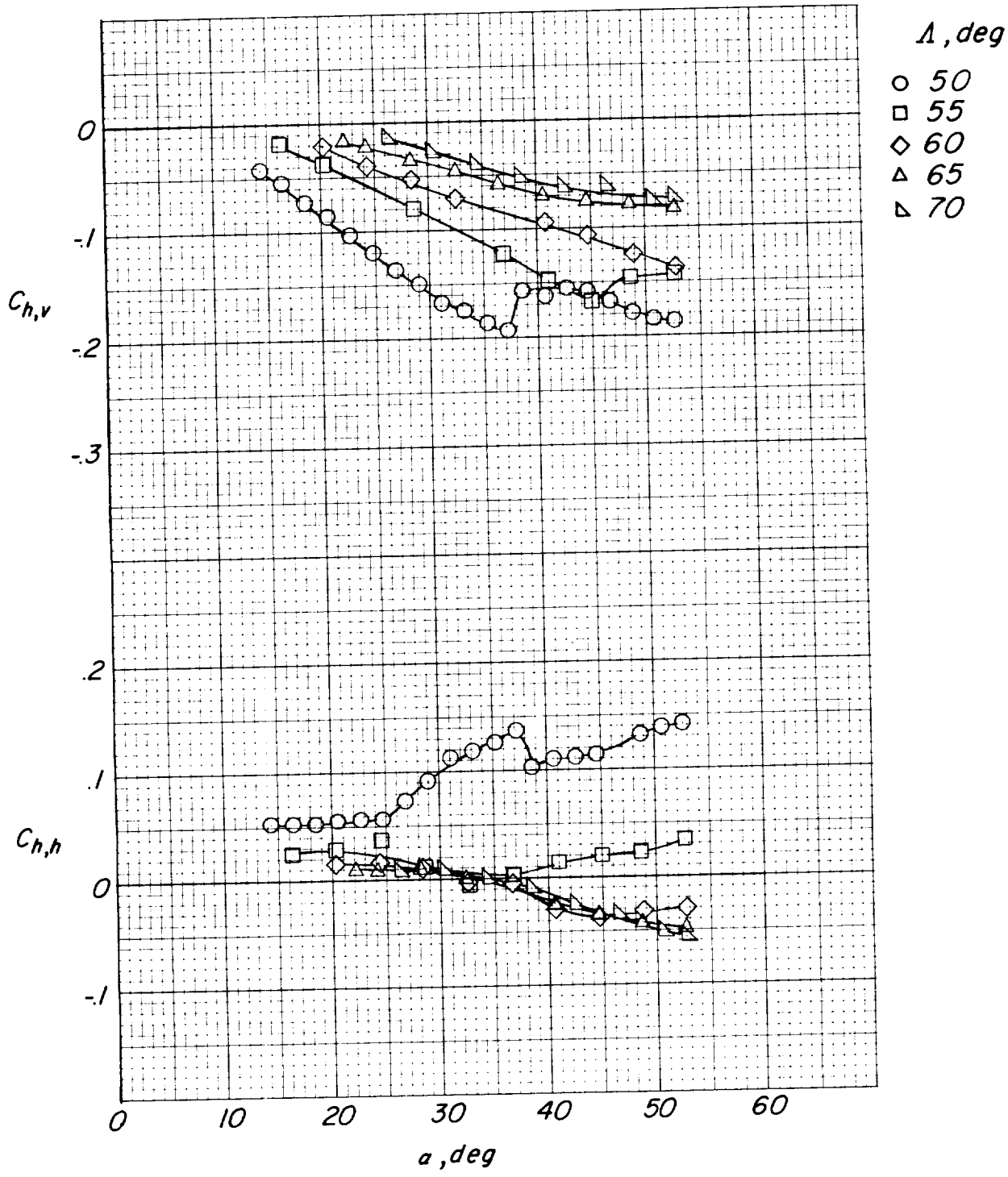

(b) $\Lambda_o = 45^\circ$ model. Concluded.

Figure 6.- Continued.

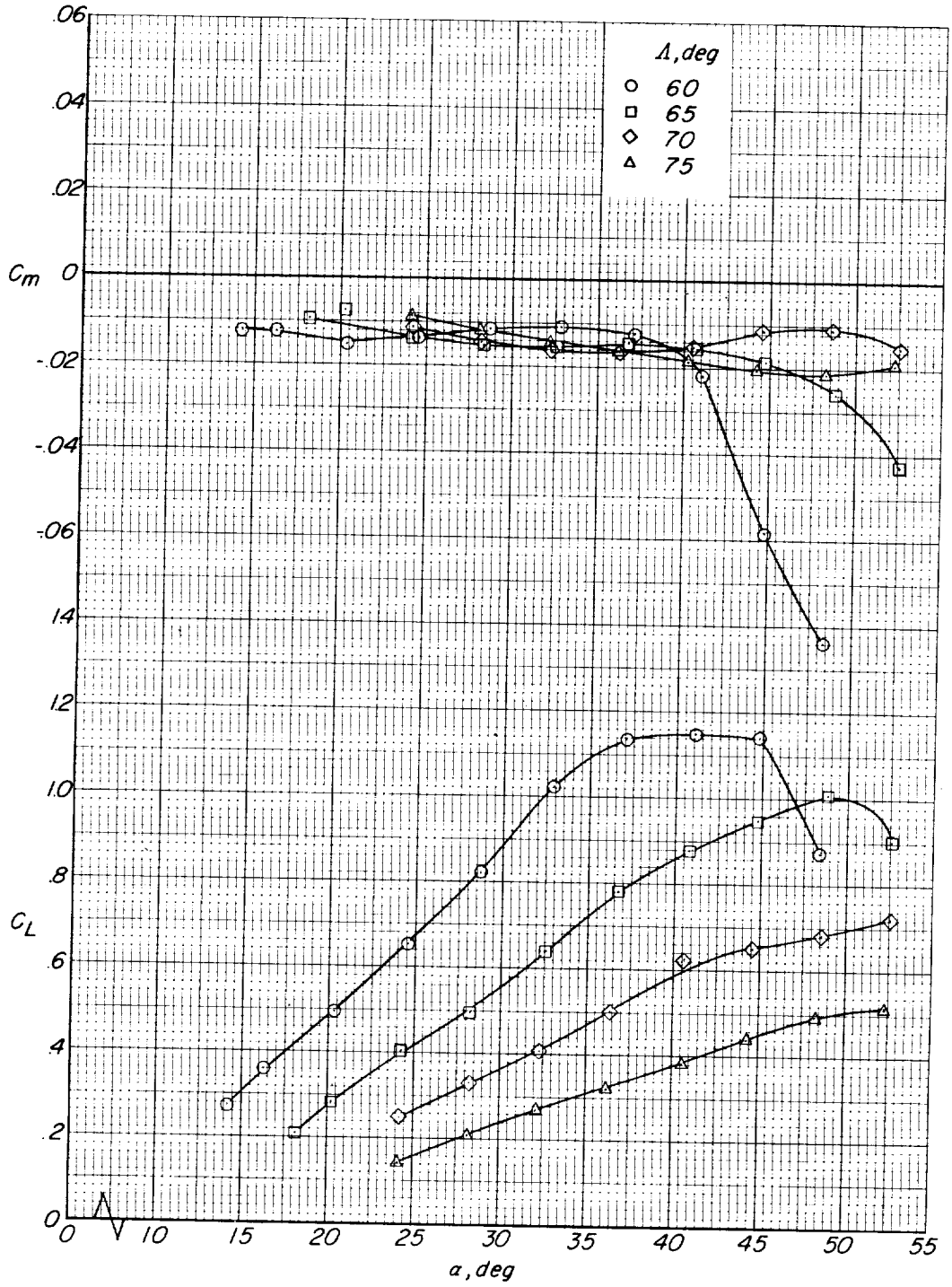

(c) $\Lambda_o = 55^\circ$ model.

Figure 6.- Continued.

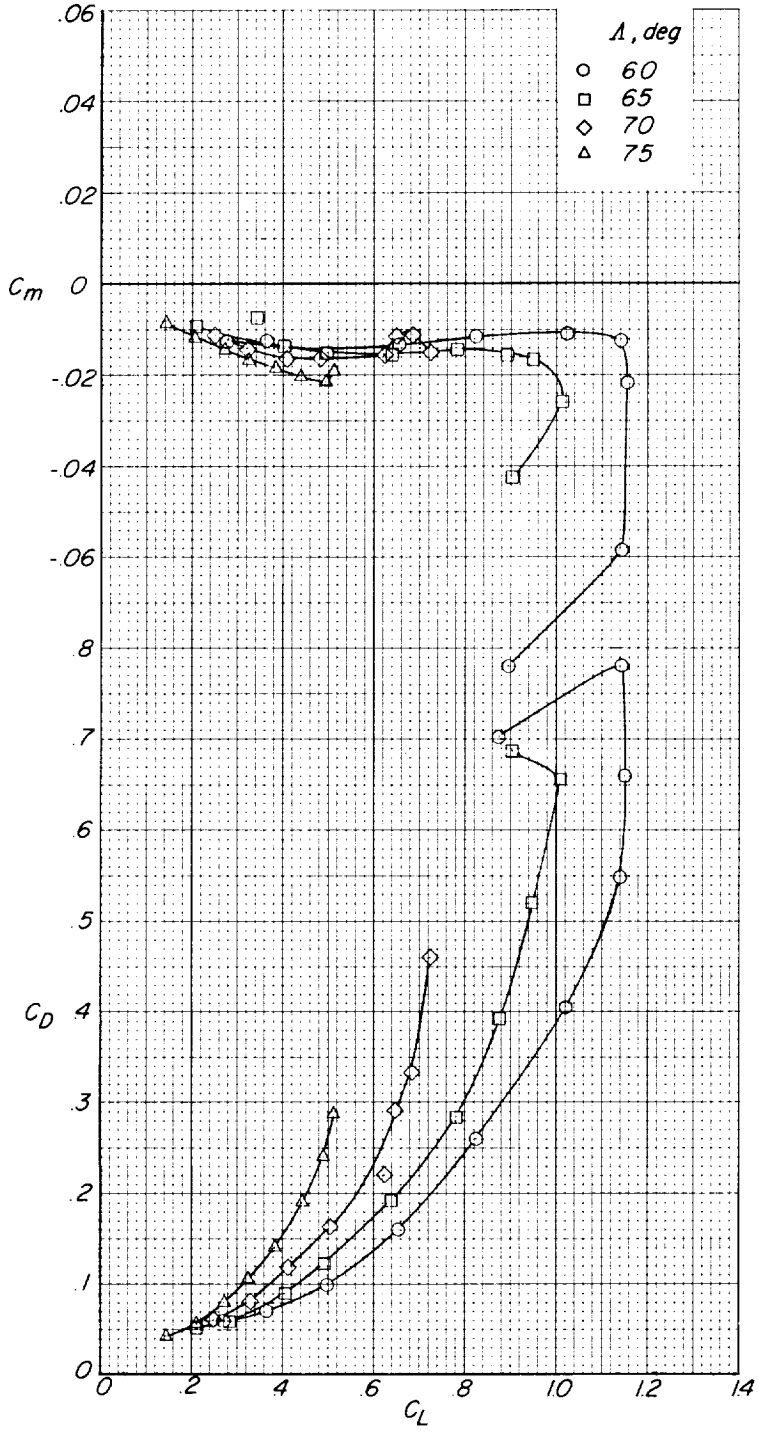

(c) $\Lambda_o = 55^\circ$ model. Continued.

Figure 6.- Continued.

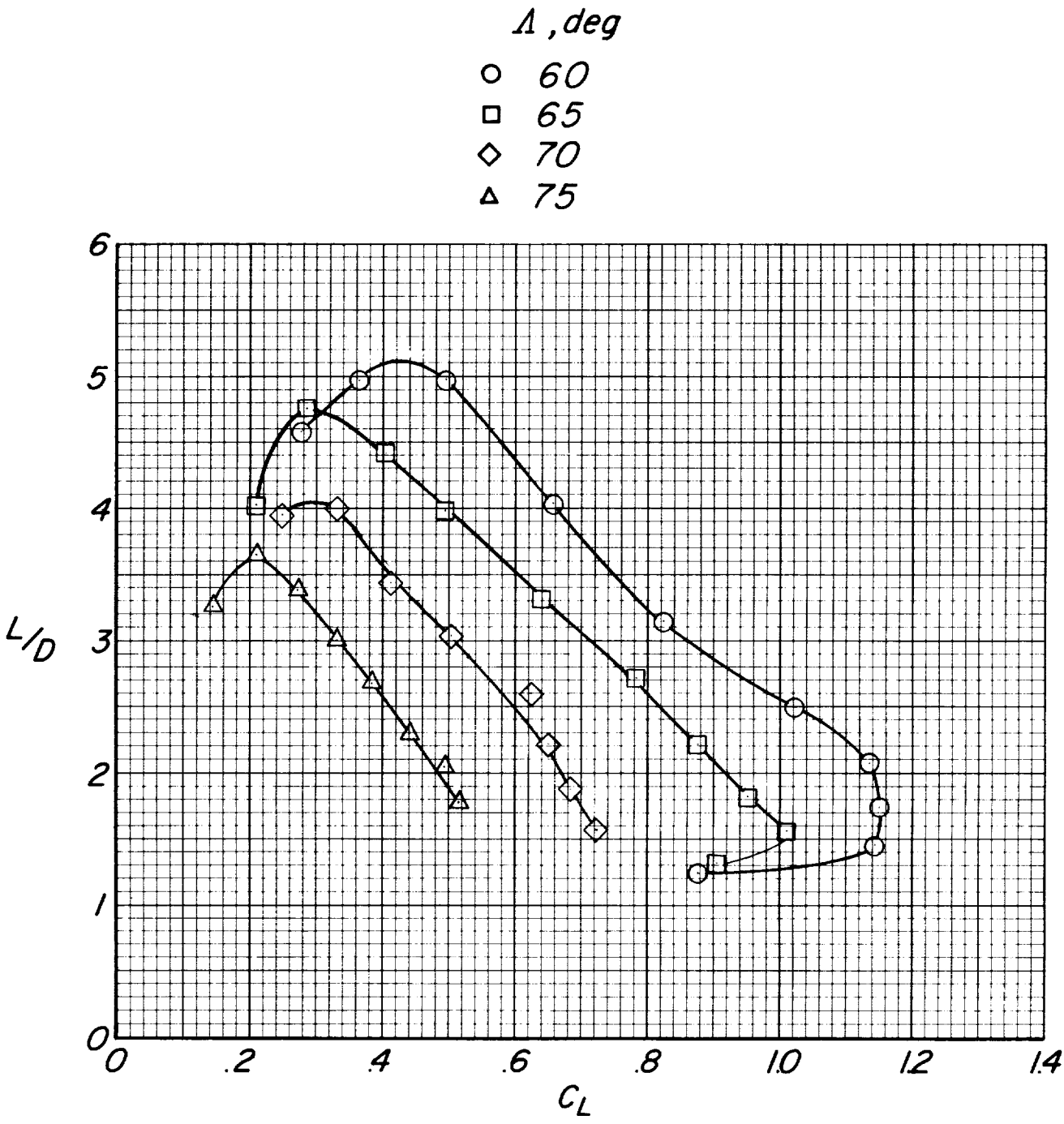

(c) $\Lambda_0 = 55^\circ$ model. Continued.

Figure 6.- Continued.

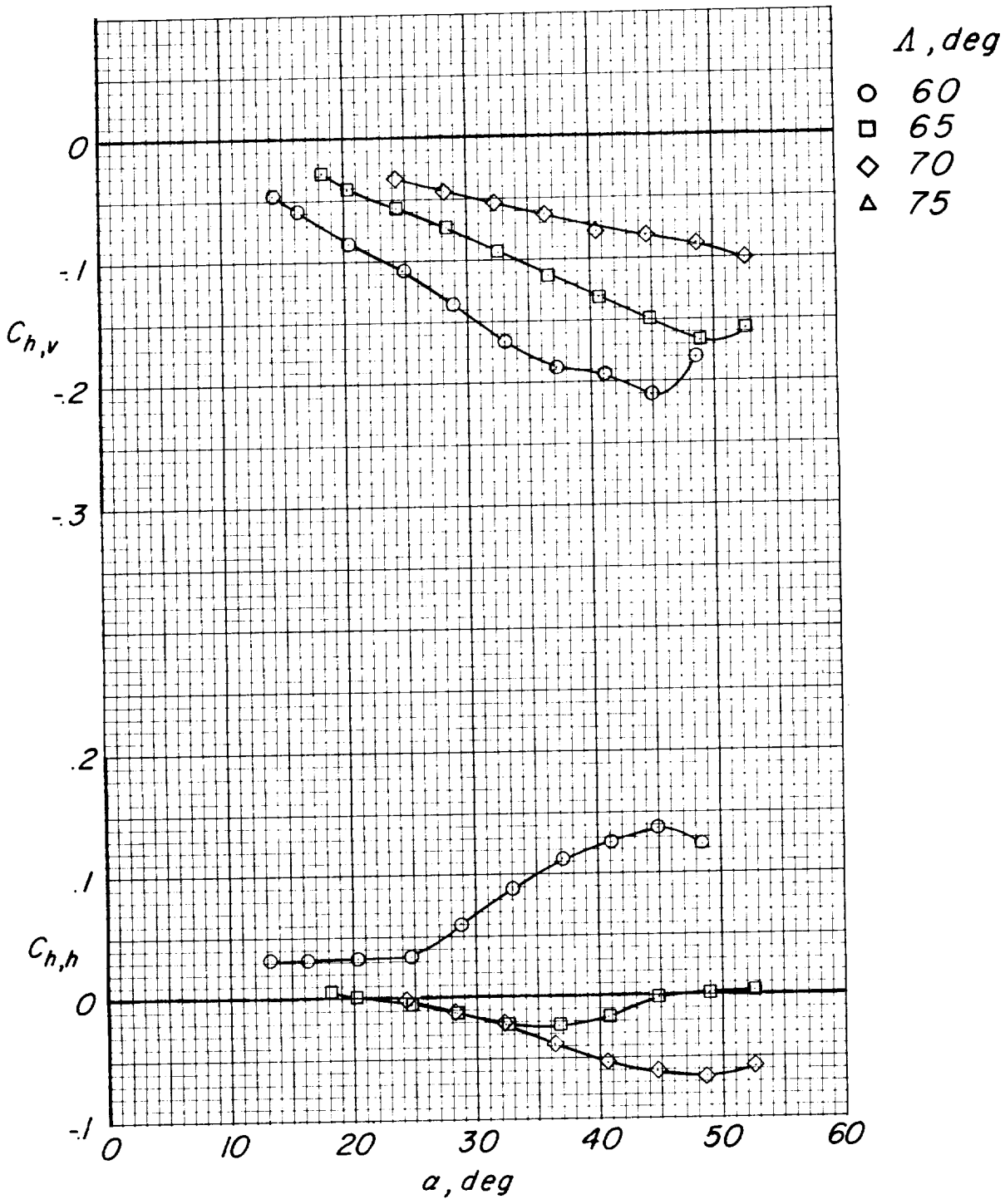

(c) $\Lambda_o = 55^\circ$ model. Concluded.

Figure 6.- Concluded.

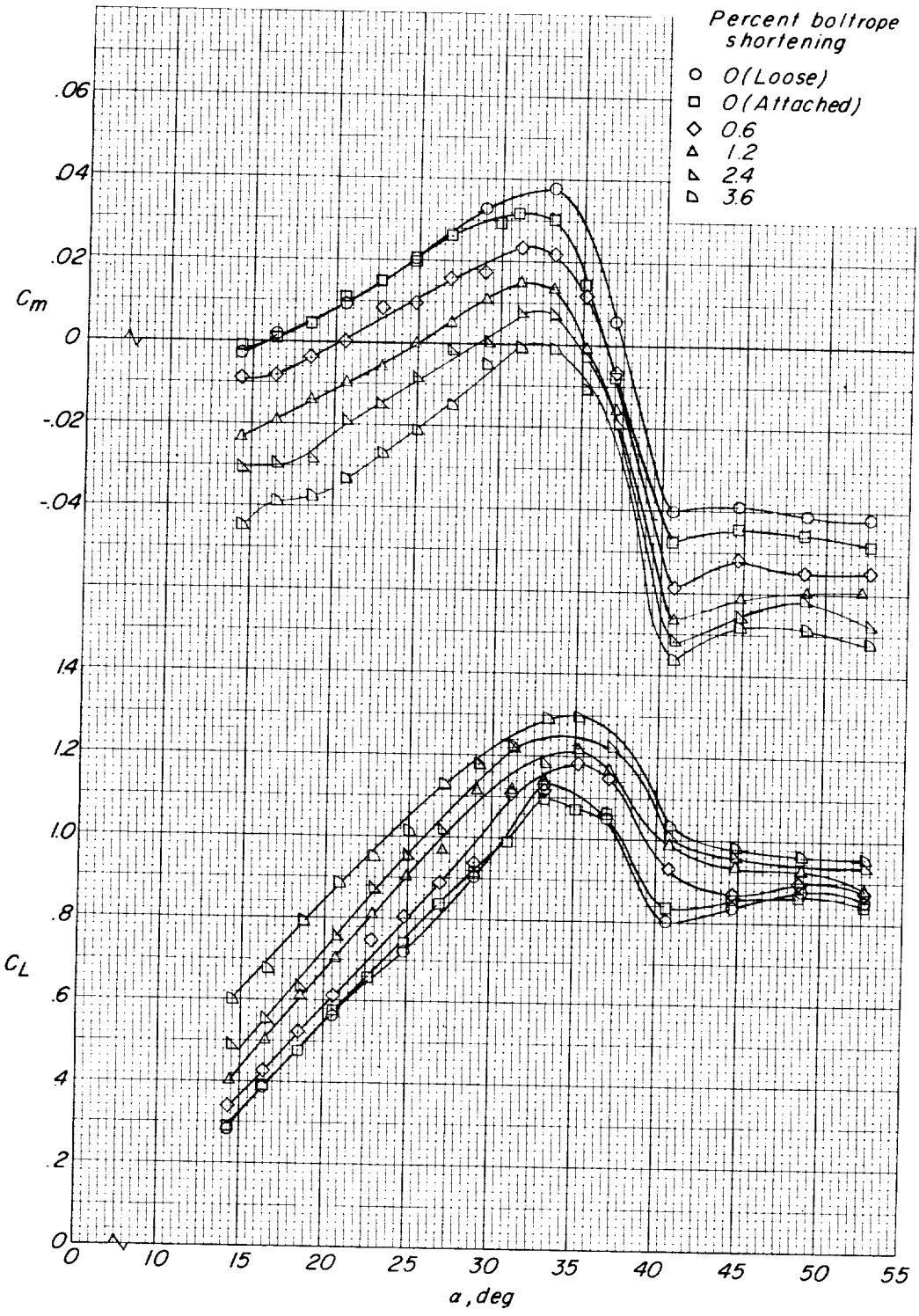

Figure 7.- Effects of boltrope shortening on the longitudinal characteristics of the $\Lambda_o = 45^\circ$ model. $\Lambda = 50^\circ$.

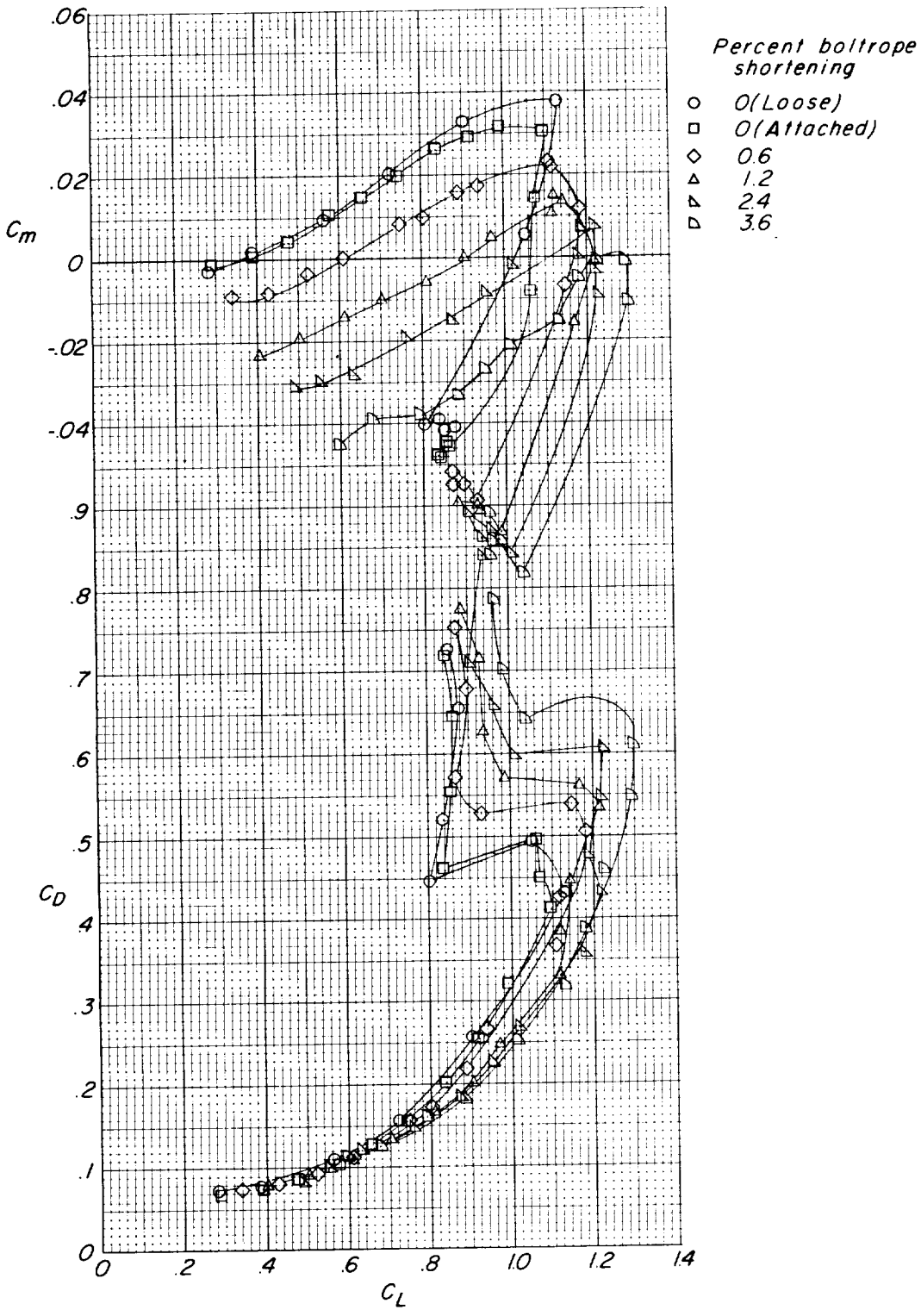

Figure 7.- Continued.

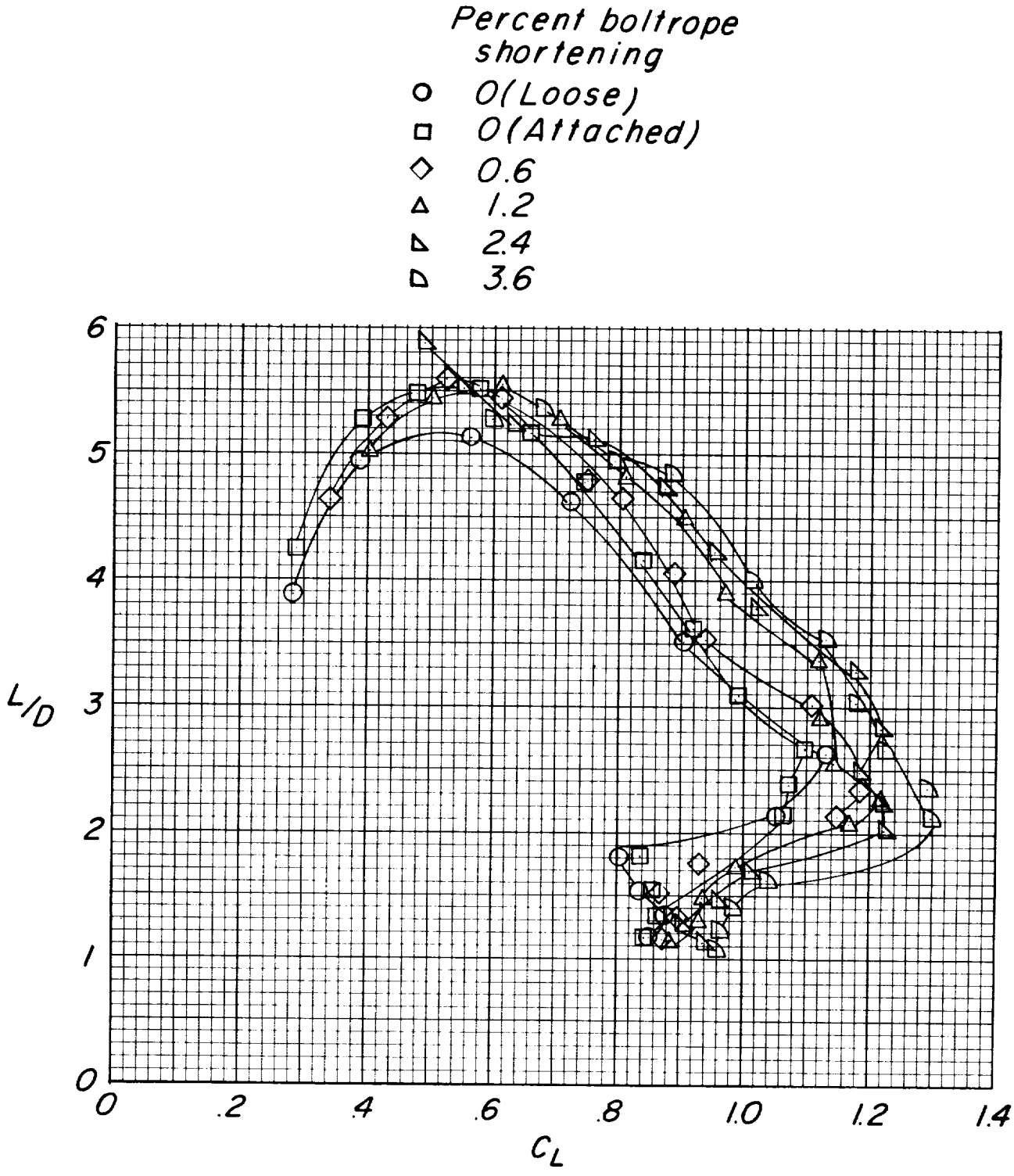

Figure 7.- Continued.

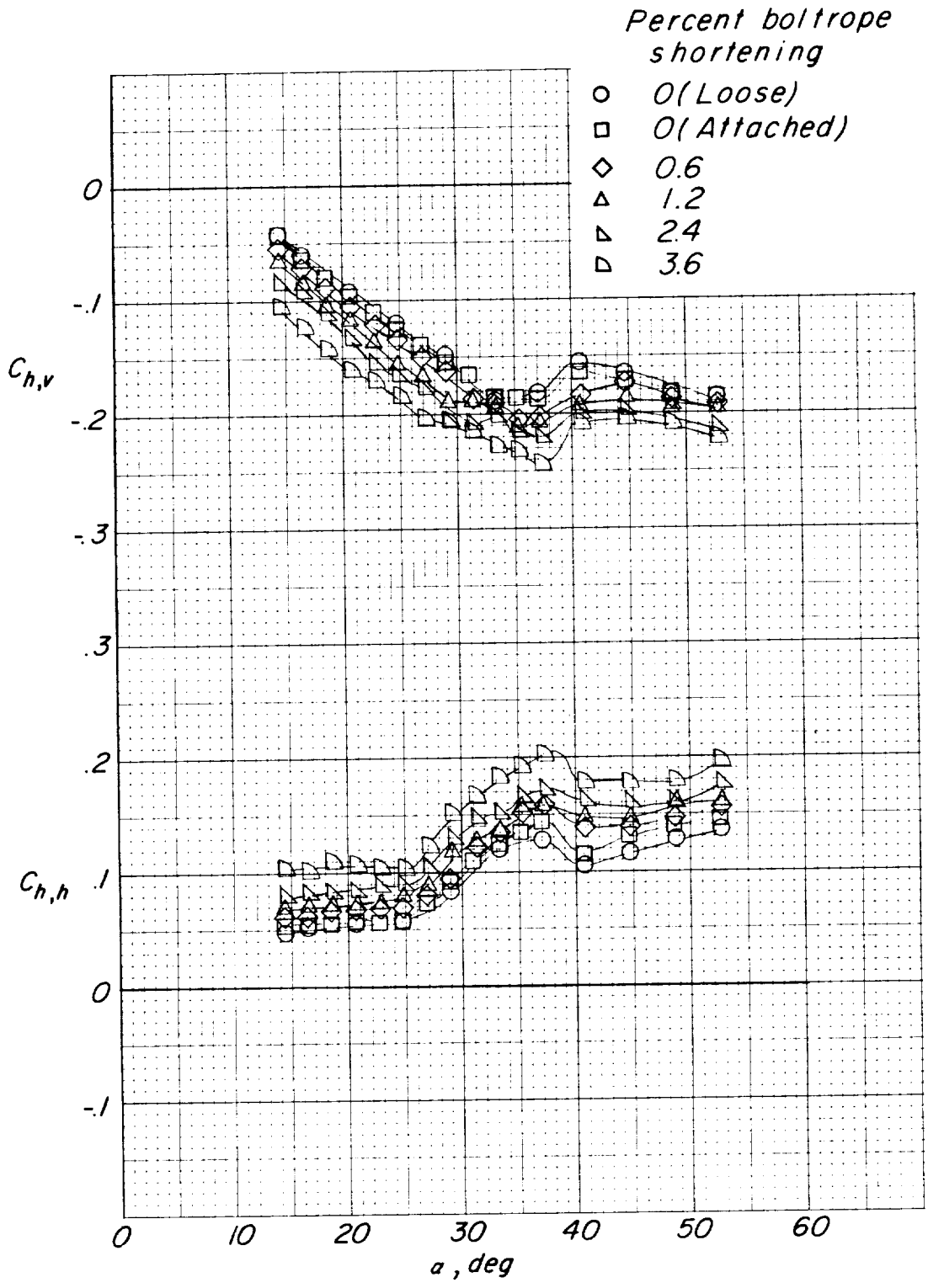

Figure 7.- Concluded.

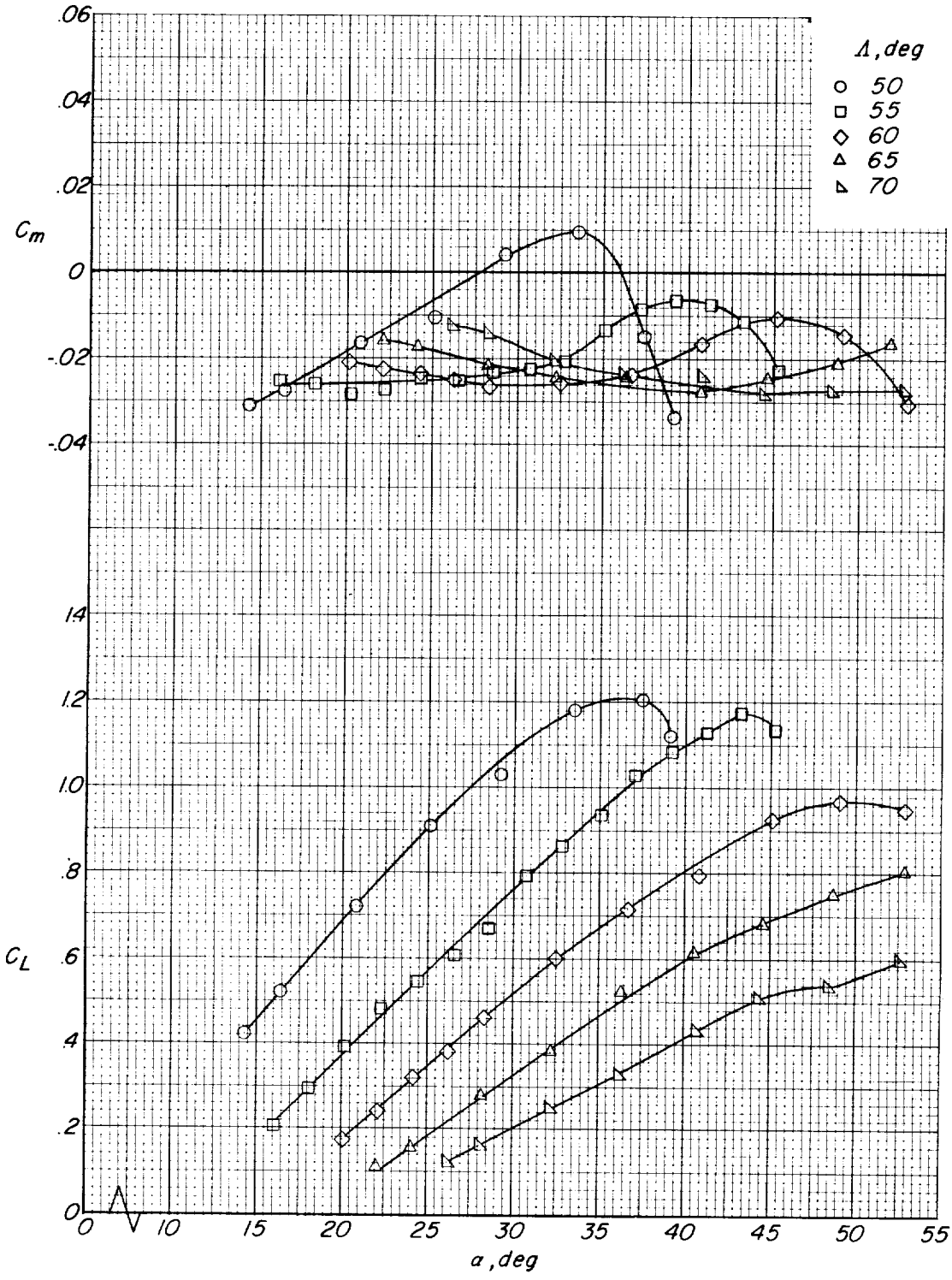

Figure 8.- Effects of changes in wing leading-edge sweep on the longitudinal characteristics of the $\Lambda_O = 45^\circ$ model. 1.2-percent boltrope shortening.

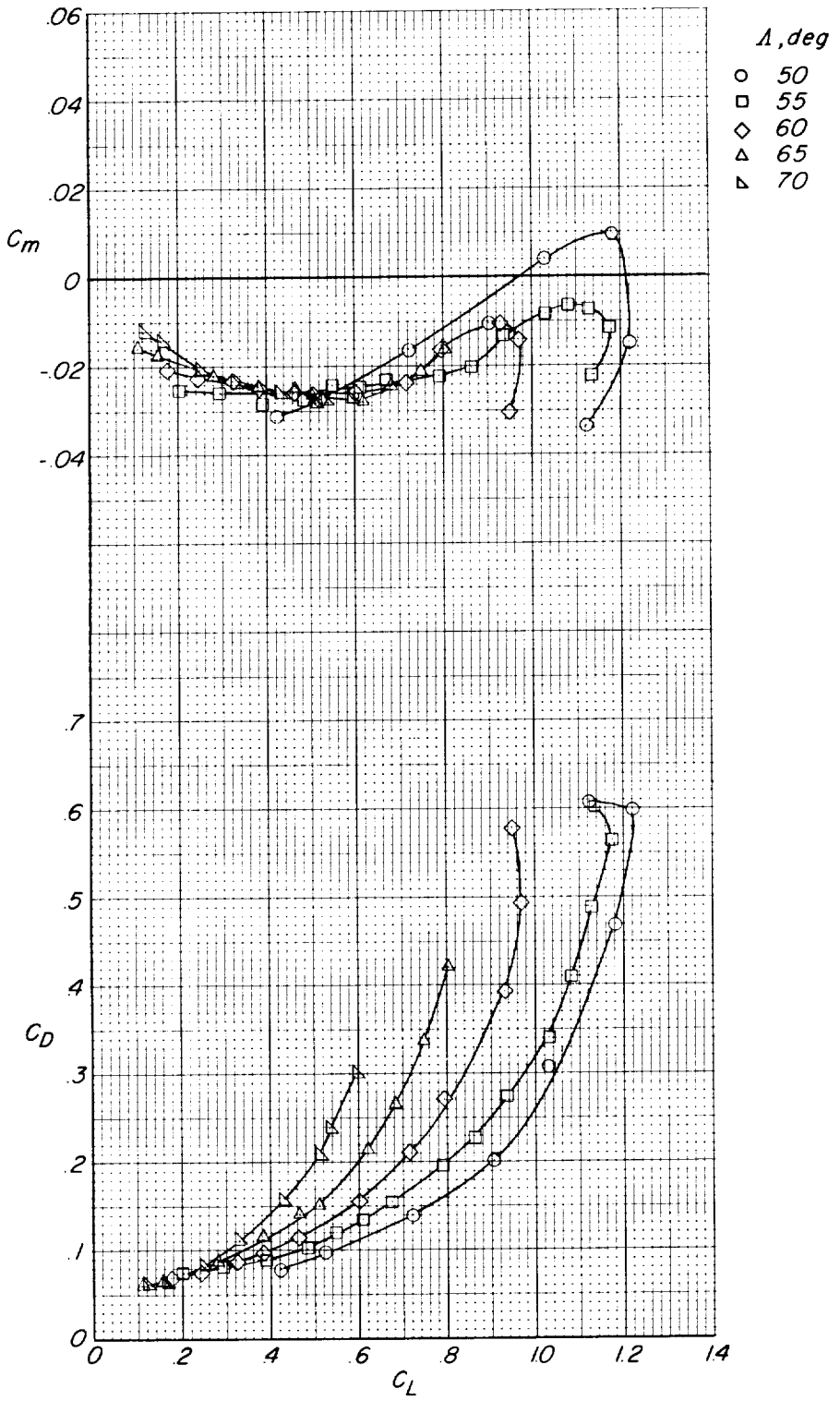

Figure 8.- Continued.

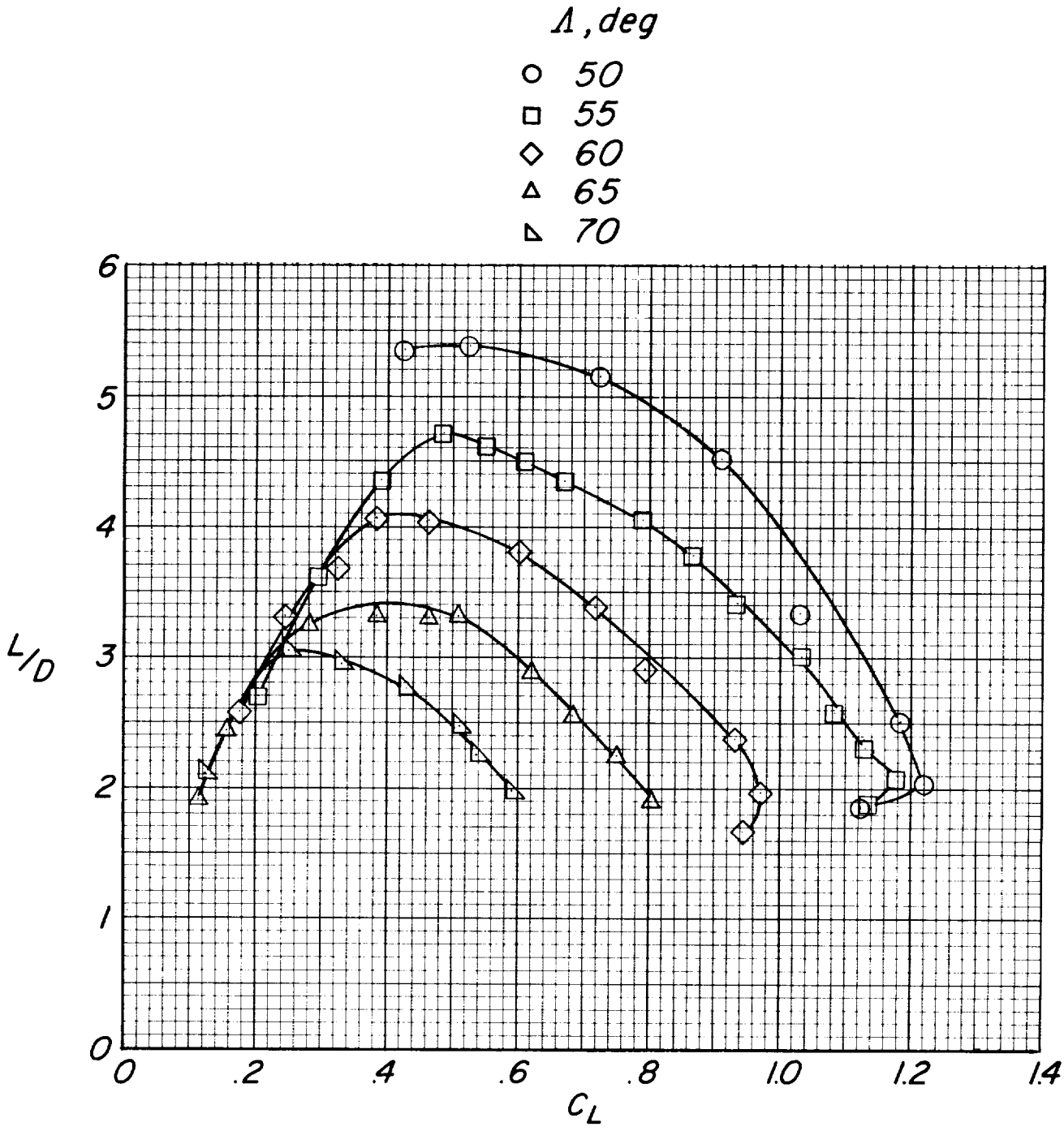

Figure 8.- Continued.

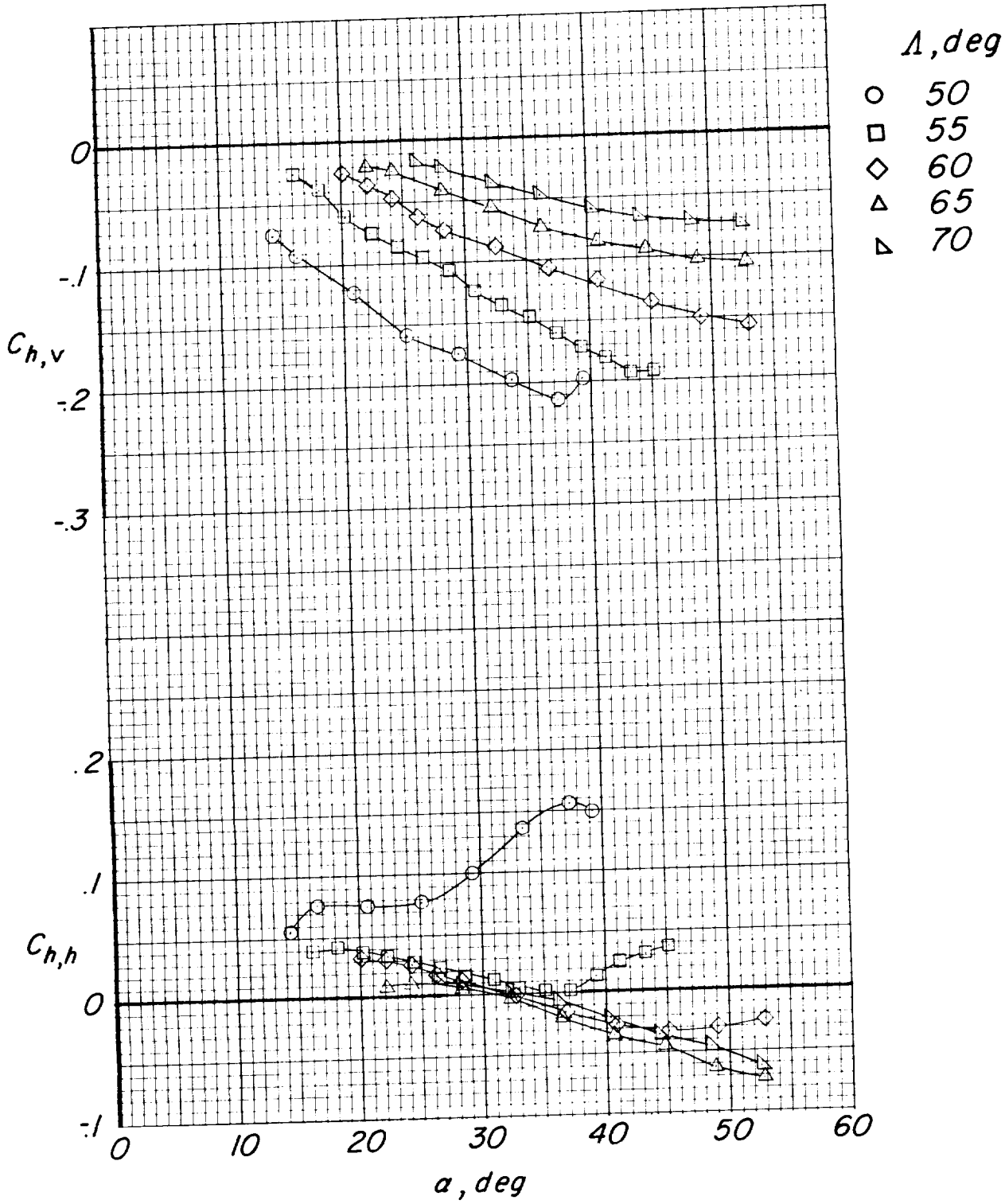

Figure 8.- Concluded.

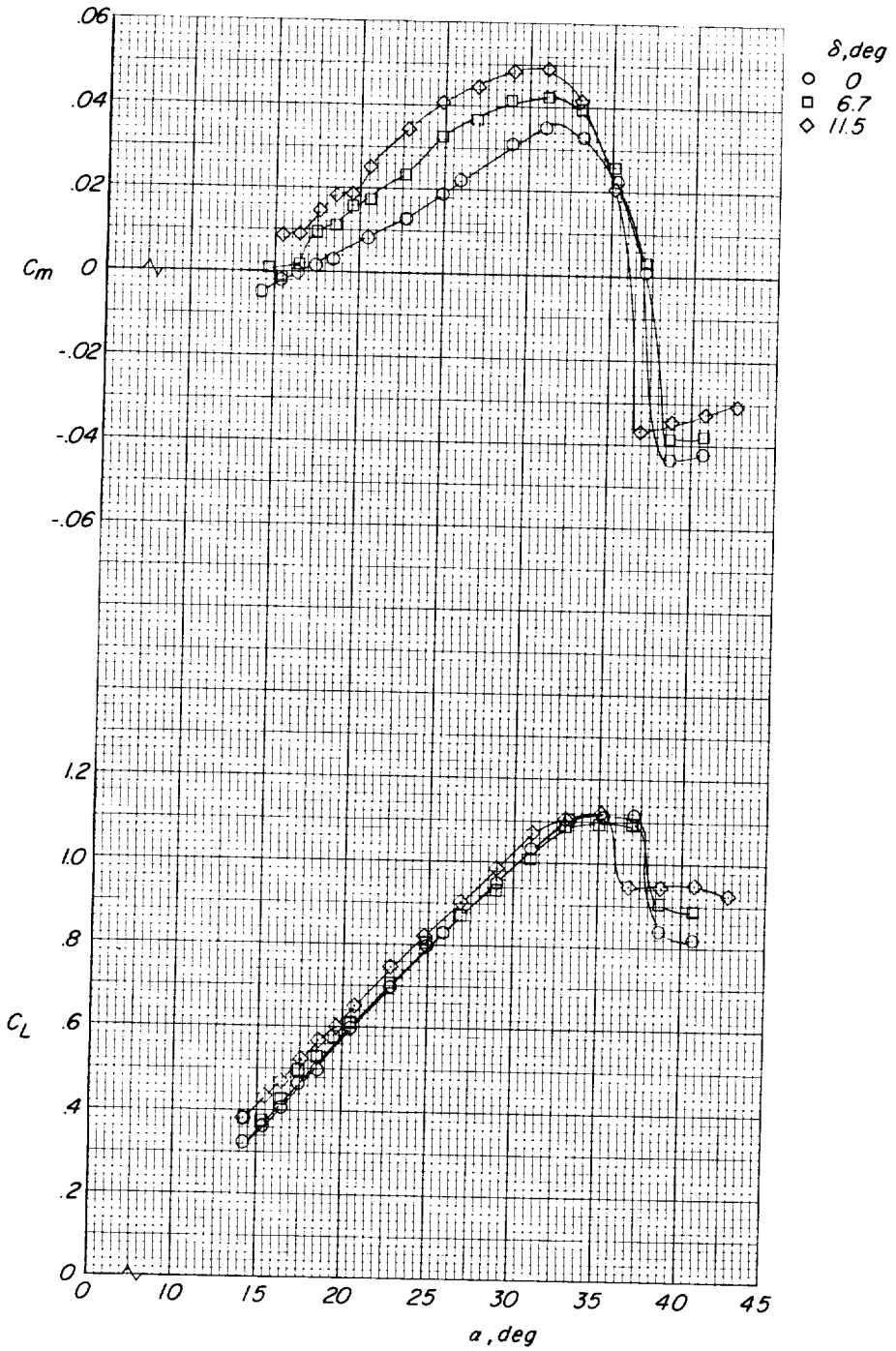

(a) $\Lambda = 50^\circ$.

Figure 9.- Effects of leading-edge deflection angle δ on the longitudinal characteristics of the $\Lambda_O = 45^\circ$ model.

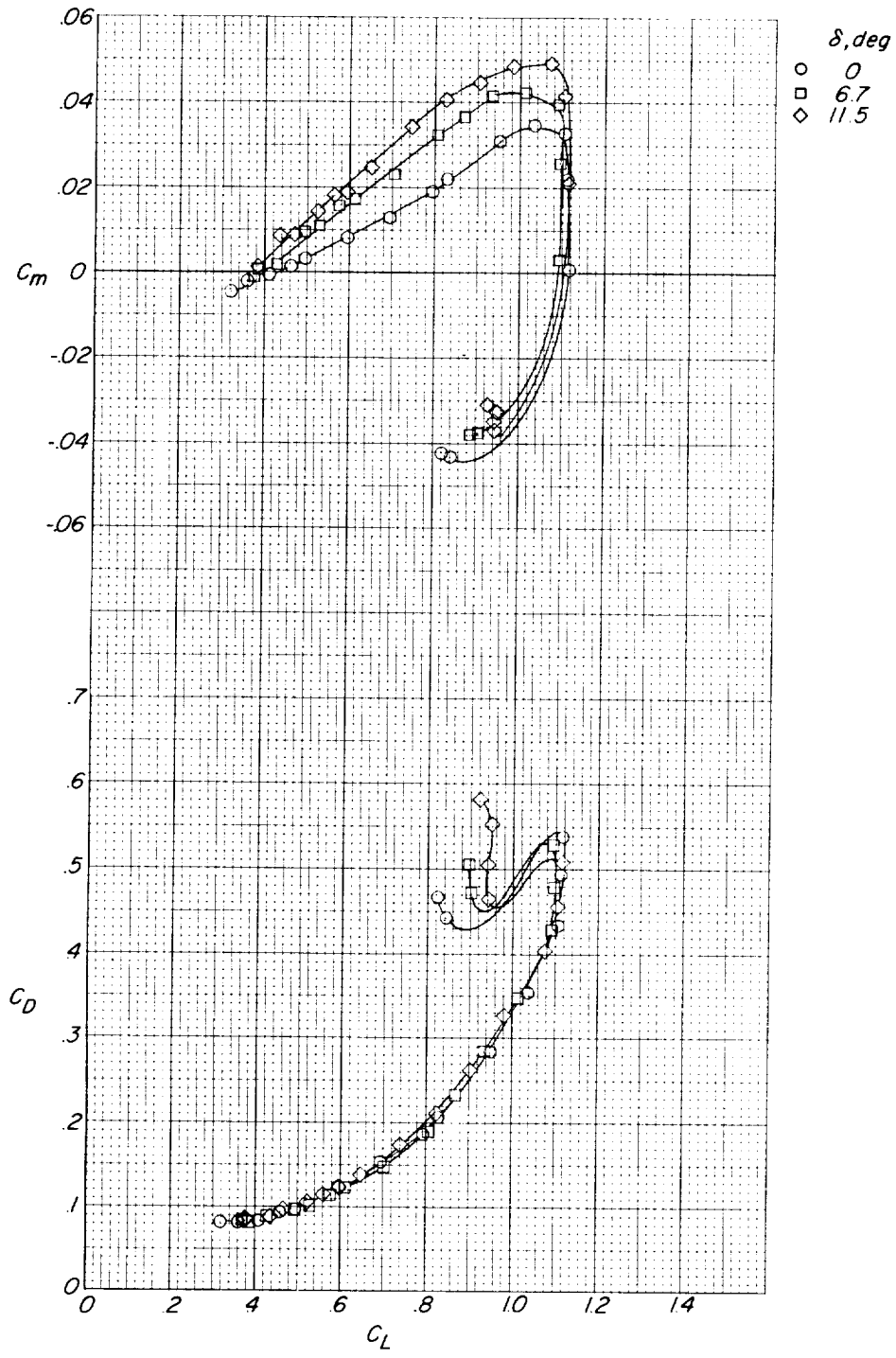

(a) $\Lambda = 50^{\circ}$. Continued.

Figure 9.- Continued.

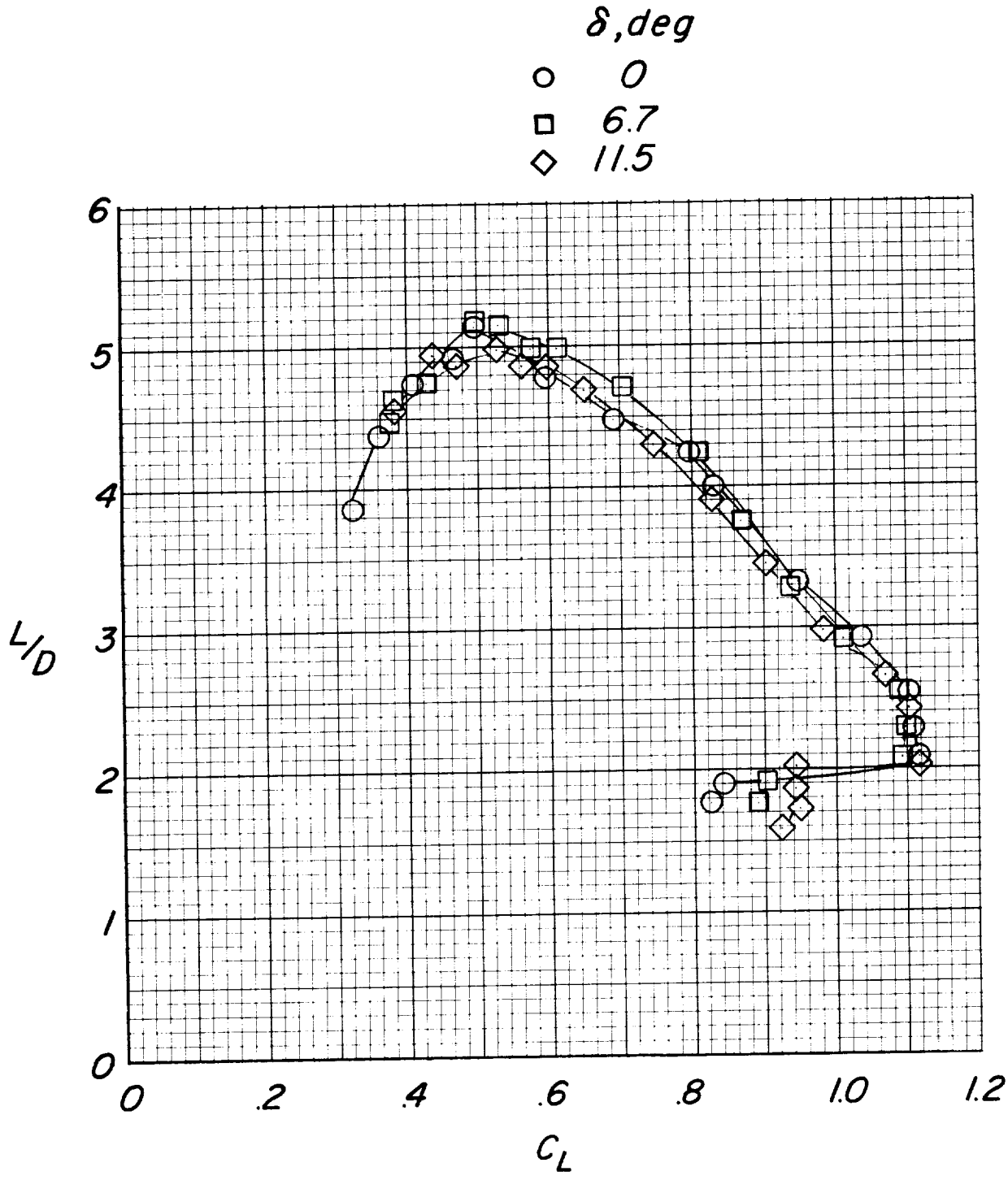

(a) $\Lambda = 50^{\circ}$. Continued.

Figure 9.- Continued.

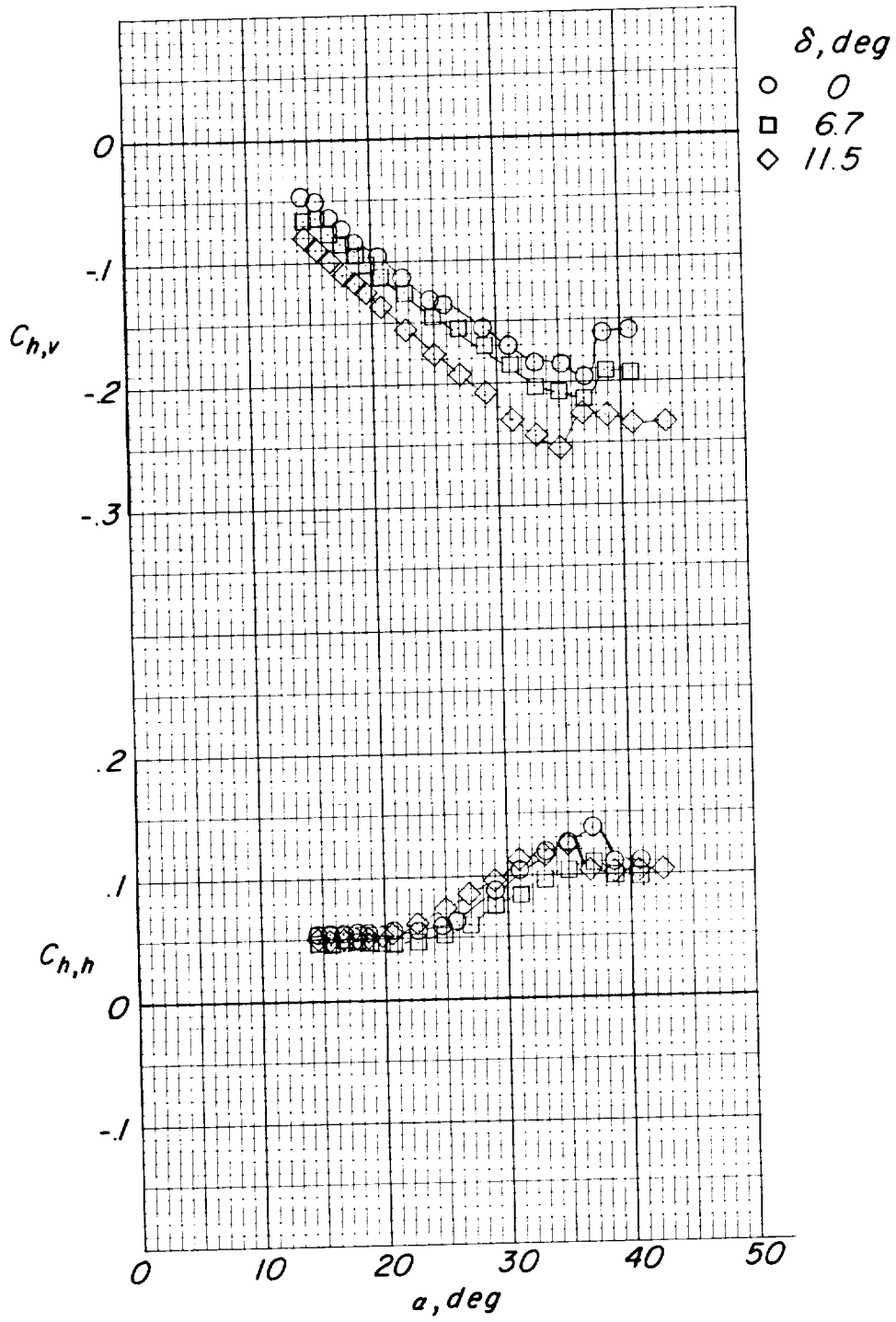

(a) $\Lambda = 50^{\circ}$. Concluded.

Figure 9.- Continued.

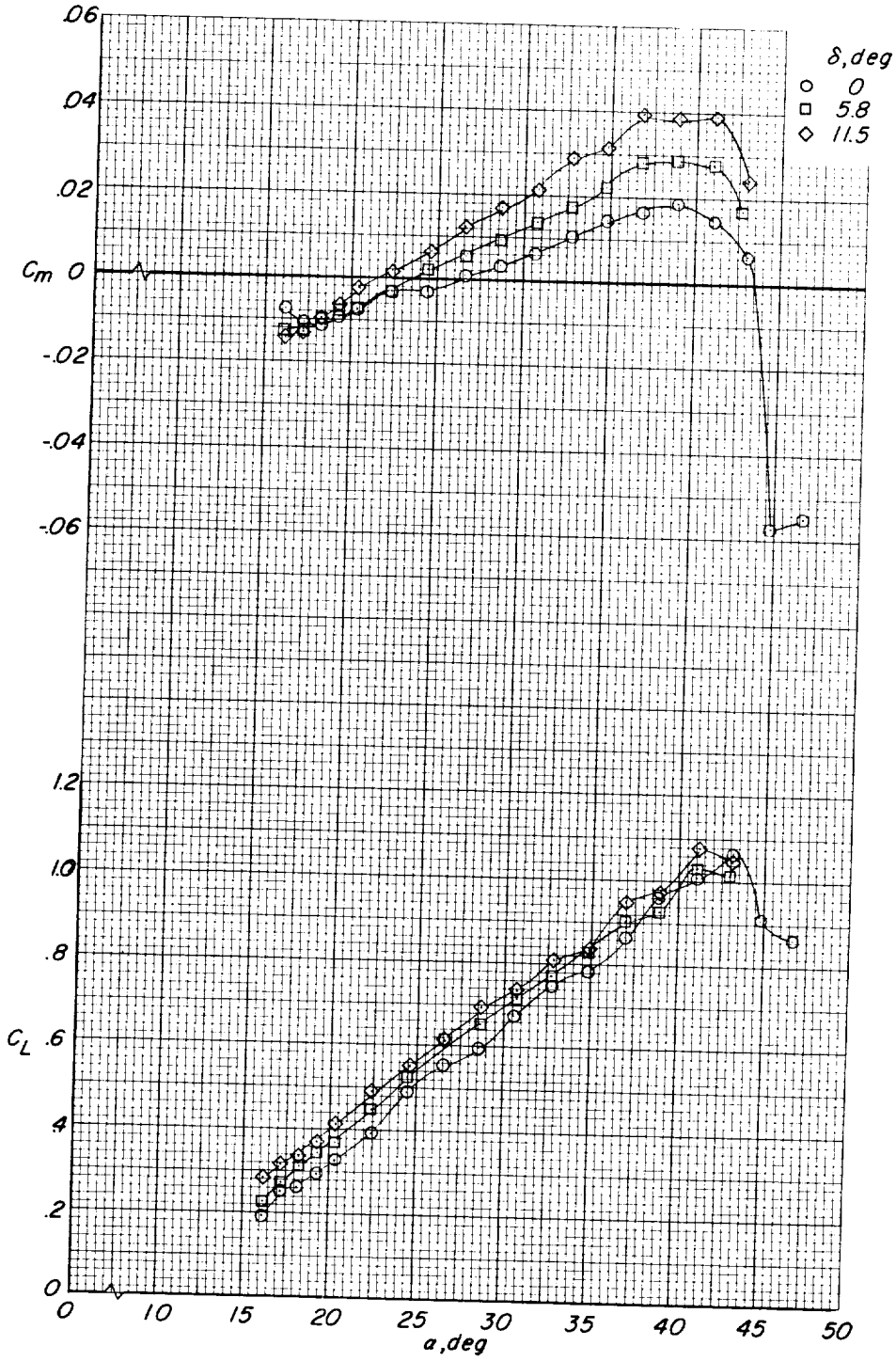

(b) $\Lambda = 55^{\circ}$.

Figure 9.- Continued.

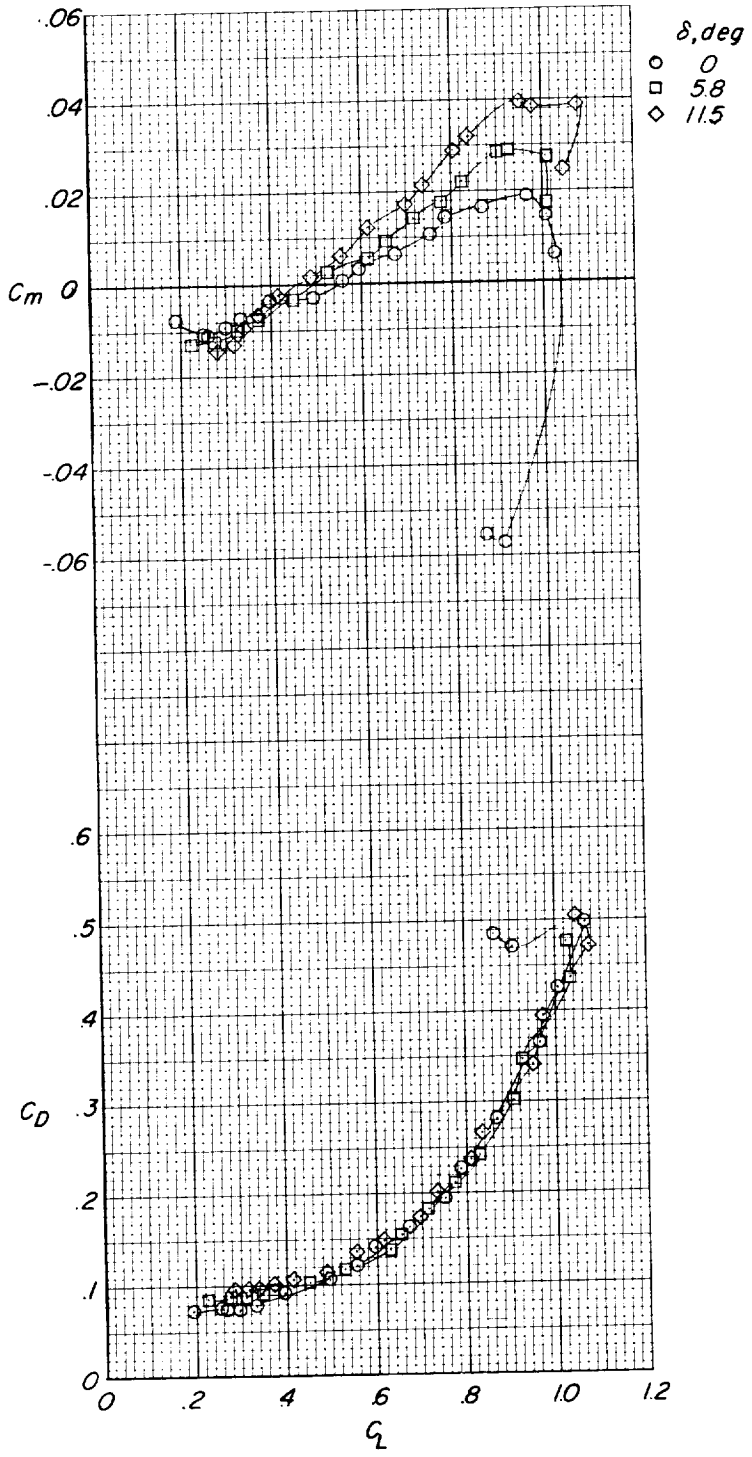

(b) $\Lambda = 55^{\circ}$. Continued.

Figure 9.- Continued.

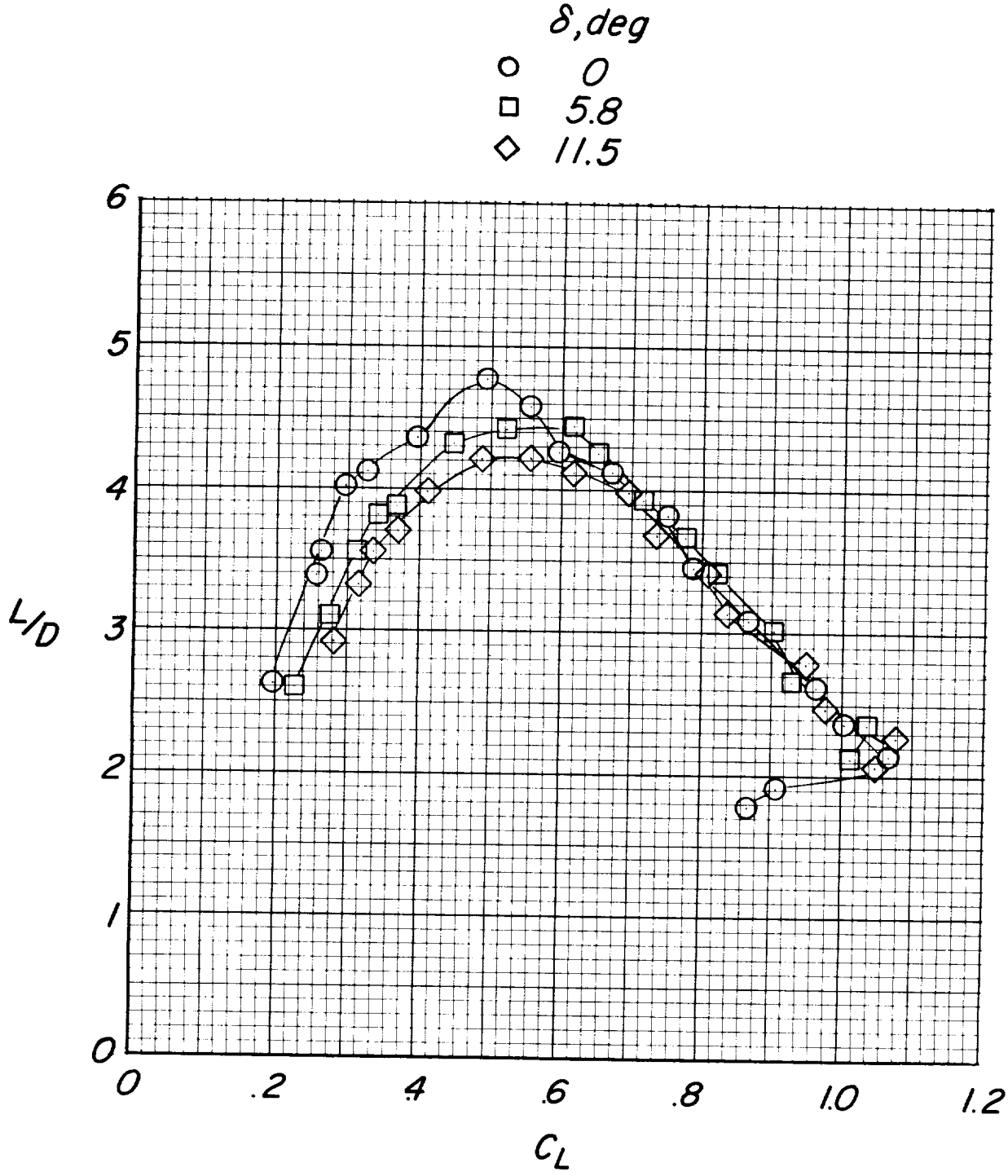

(b) $\Lambda = 55^{\circ}$. Continued.

Figure 9.- Continued.

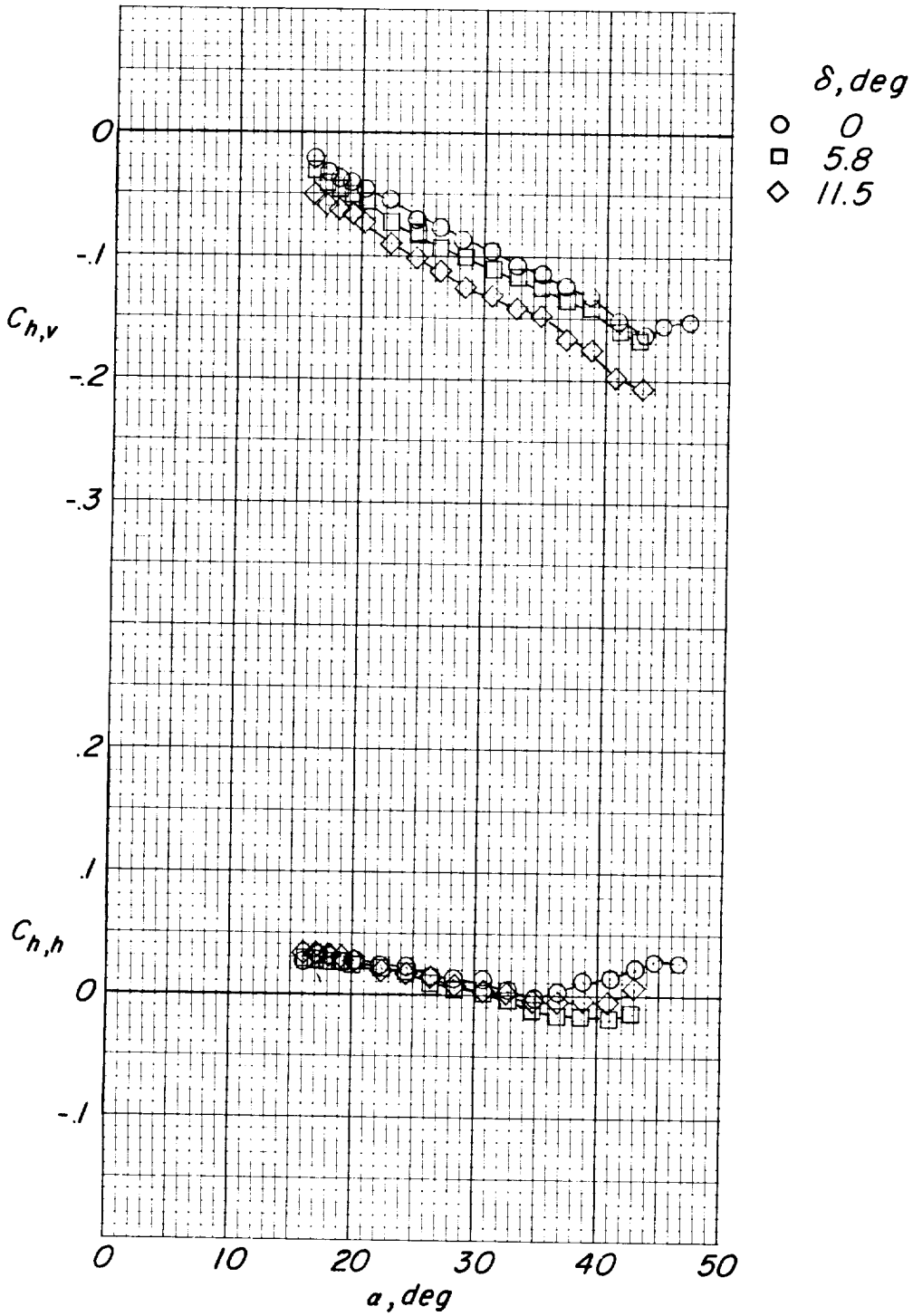

(b) $\Lambda = 55^{\circ}$. Concluded.

Figure 9.- Concluded.

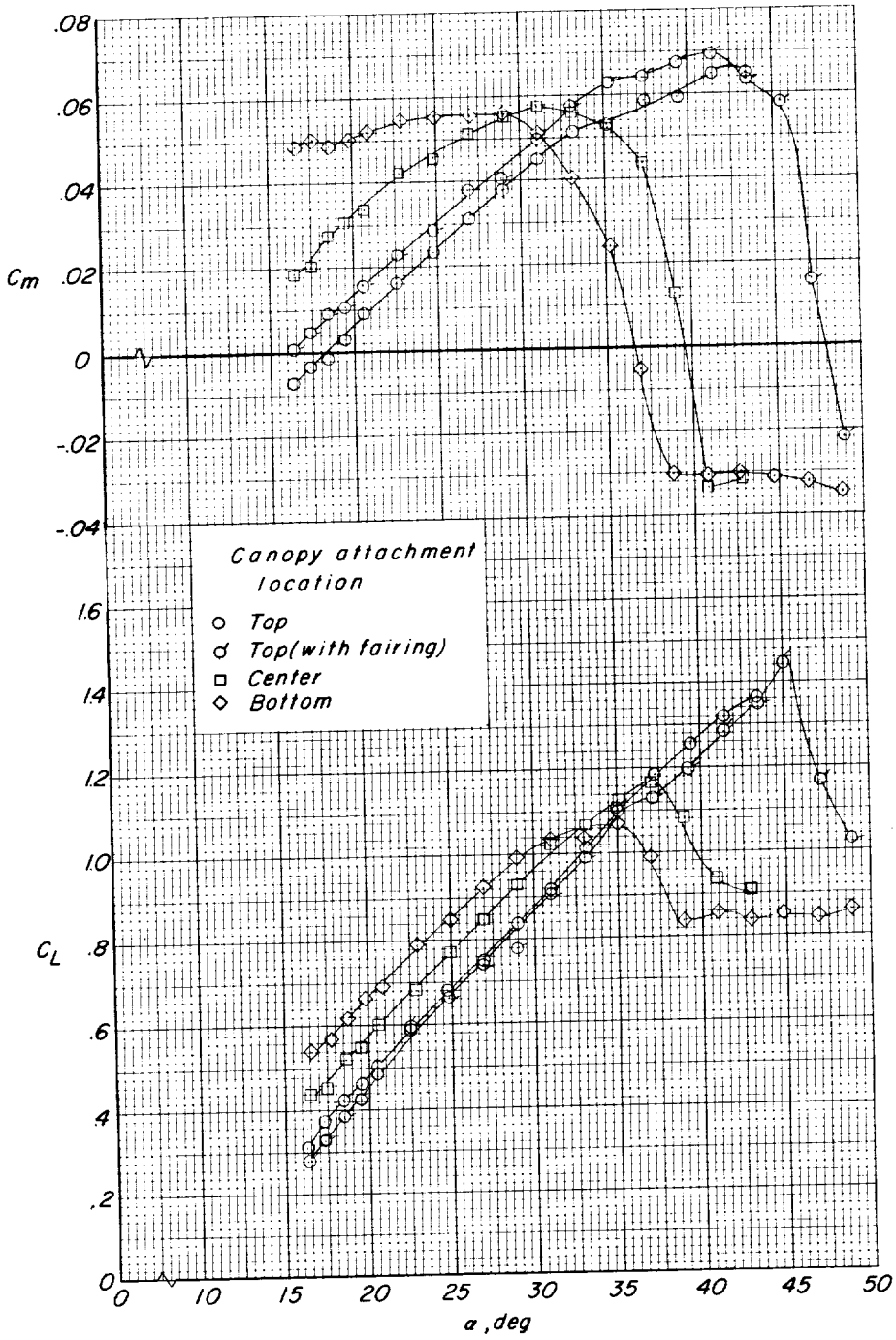

(a) $\Lambda = 50^{\circ}$.

Figure 10.- Effects of canopy attachment location on the longitudinal characteristics of the $\Lambda_o = 45^{\circ}$ model with $0.07l_k$-diameter leading edges and keel.

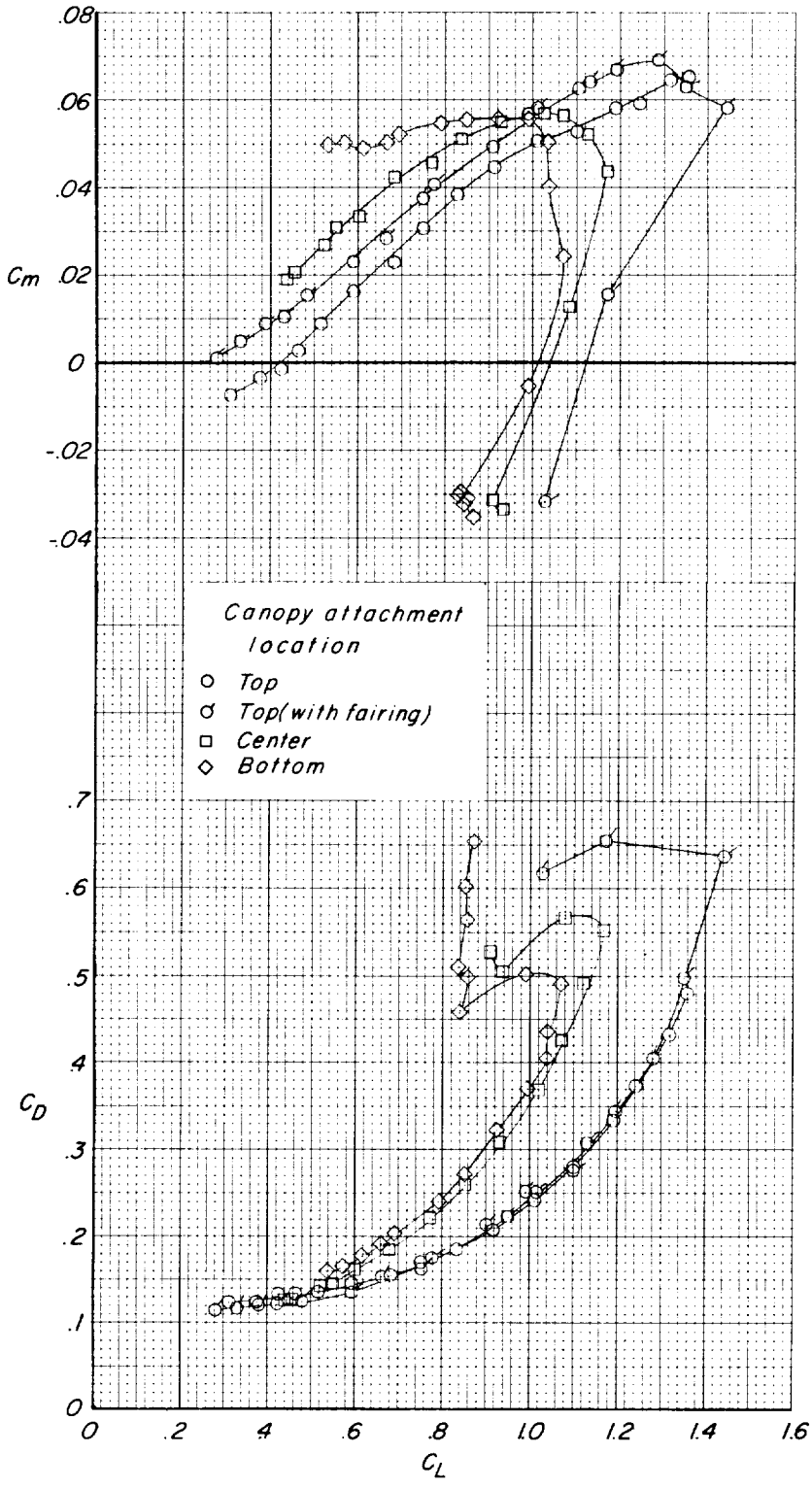

(a) $\Lambda = 50^{\circ}$. Continued.

Figure 10.- Continued.

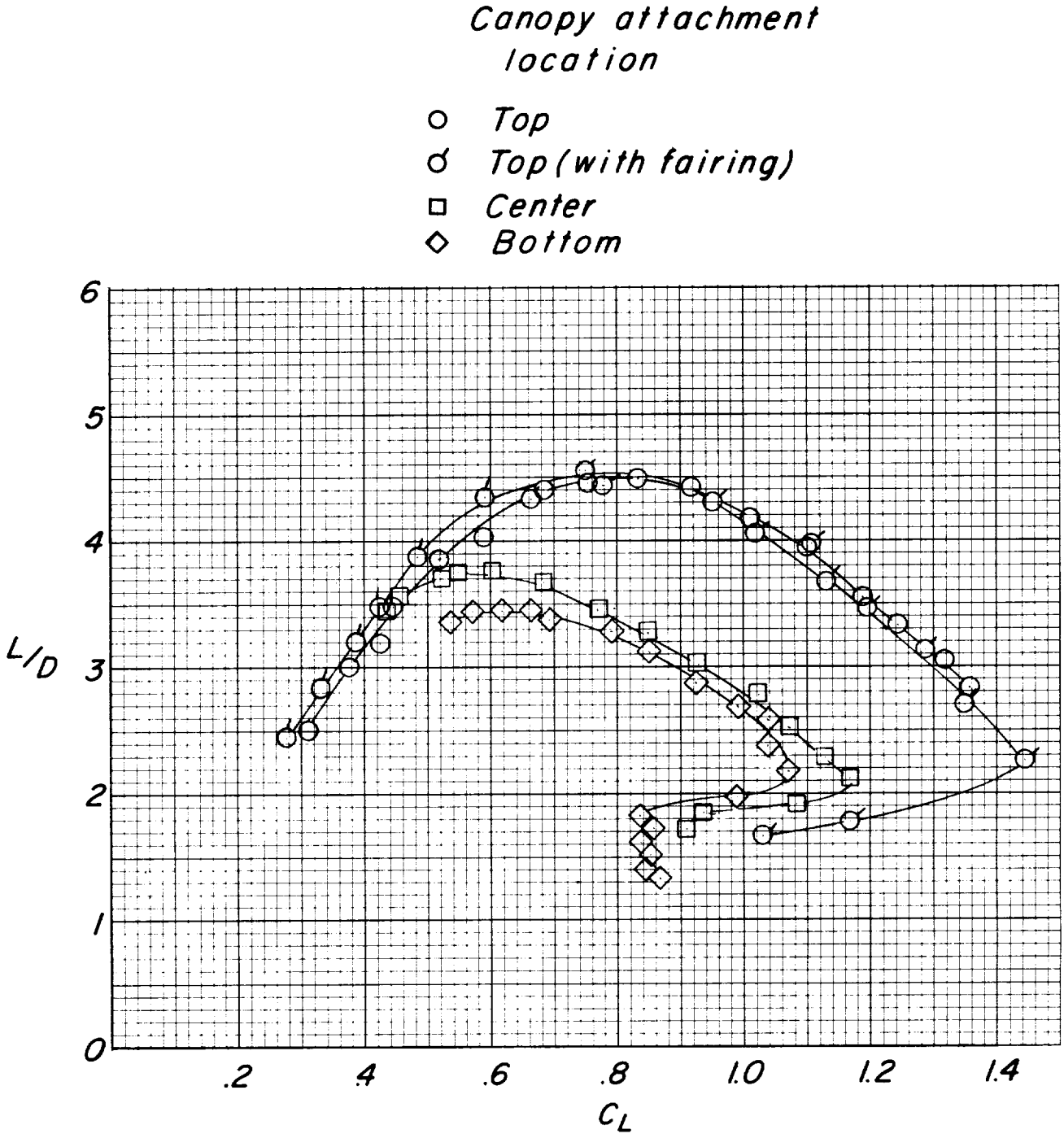

(a) $\Lambda = 50^{\circ}$. Concluded.

Figure 10.- Continued.

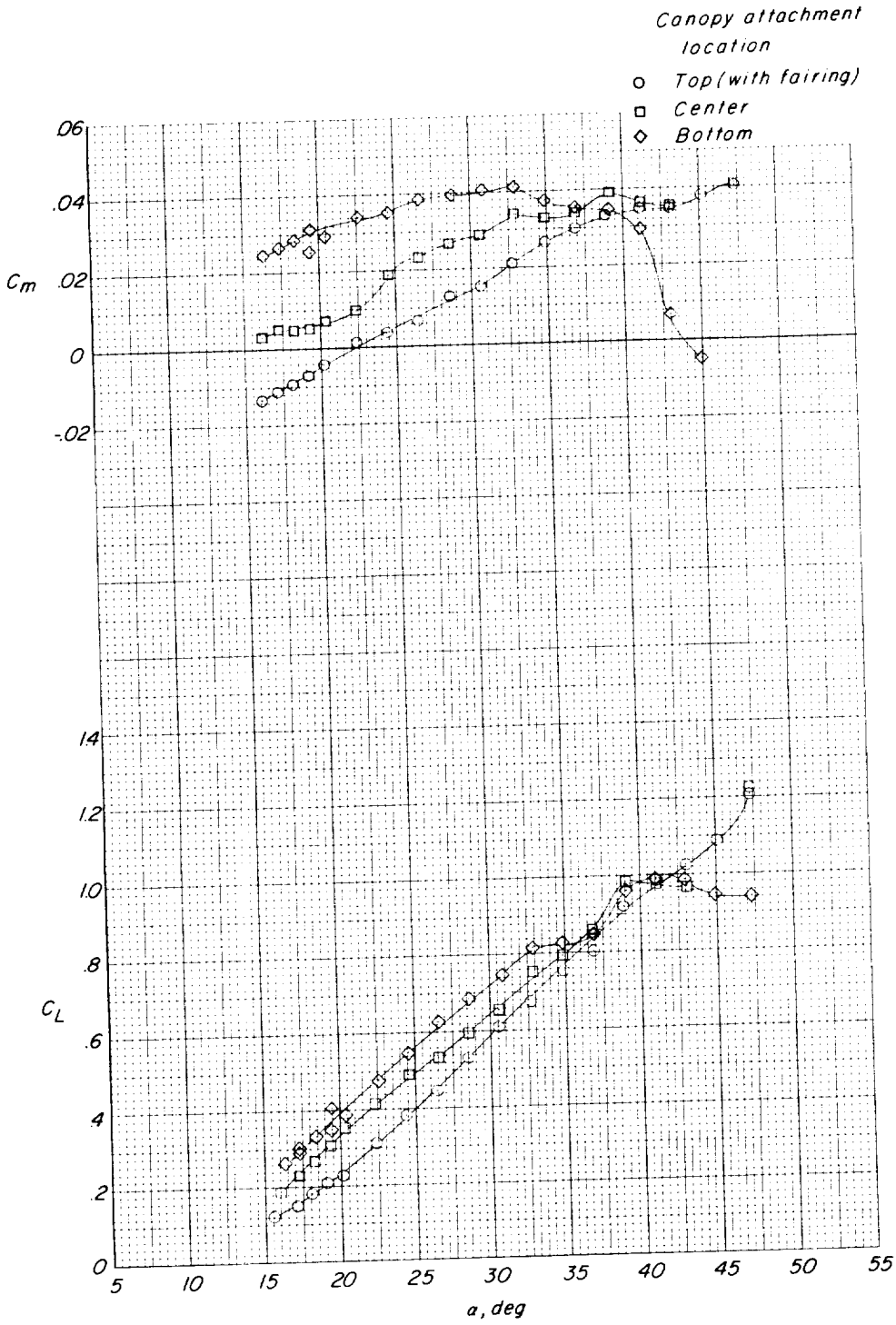

(b) $\Lambda = 55^{\circ}$.

Figure 10.- Continued.

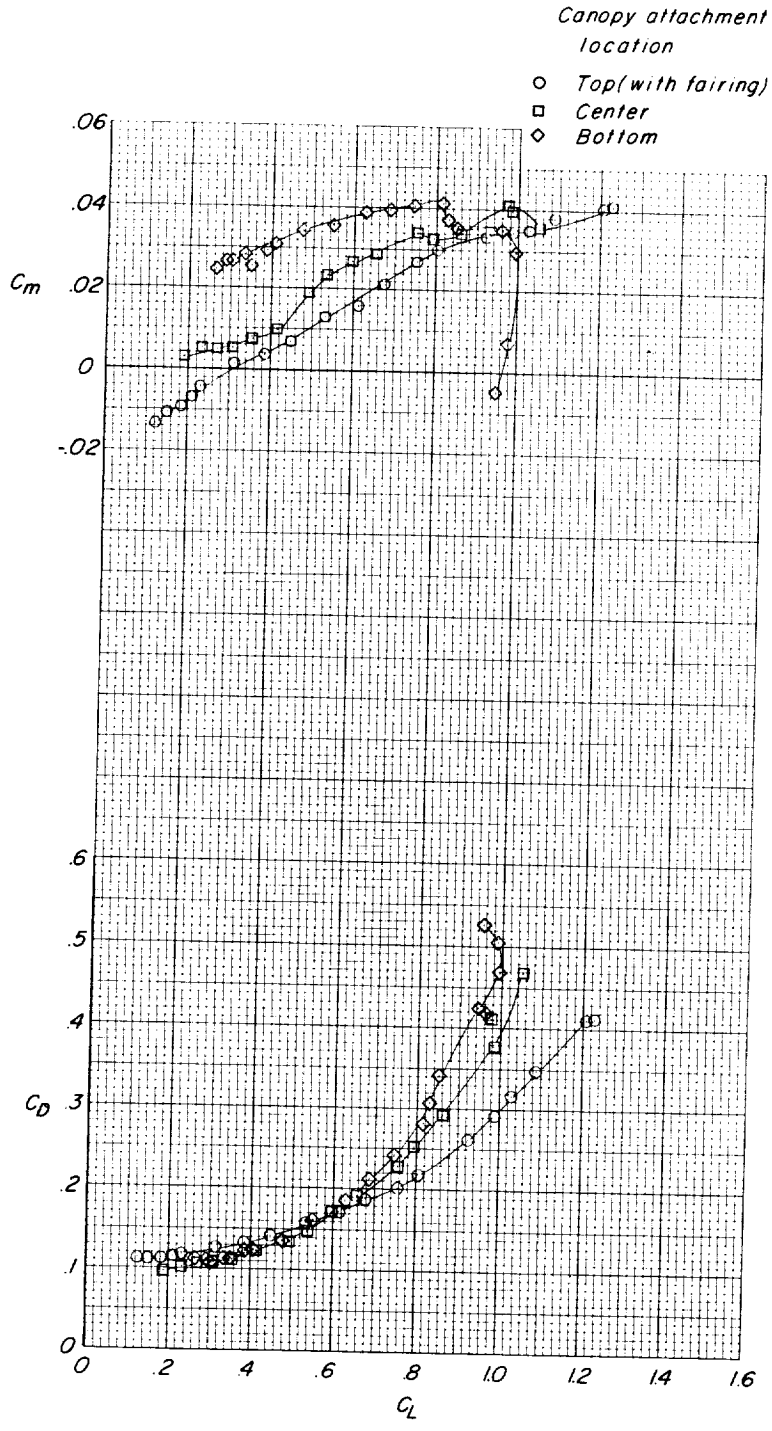

(b) $\Lambda = 55^{\circ}$. Continued.

Figure 10.- Continued.

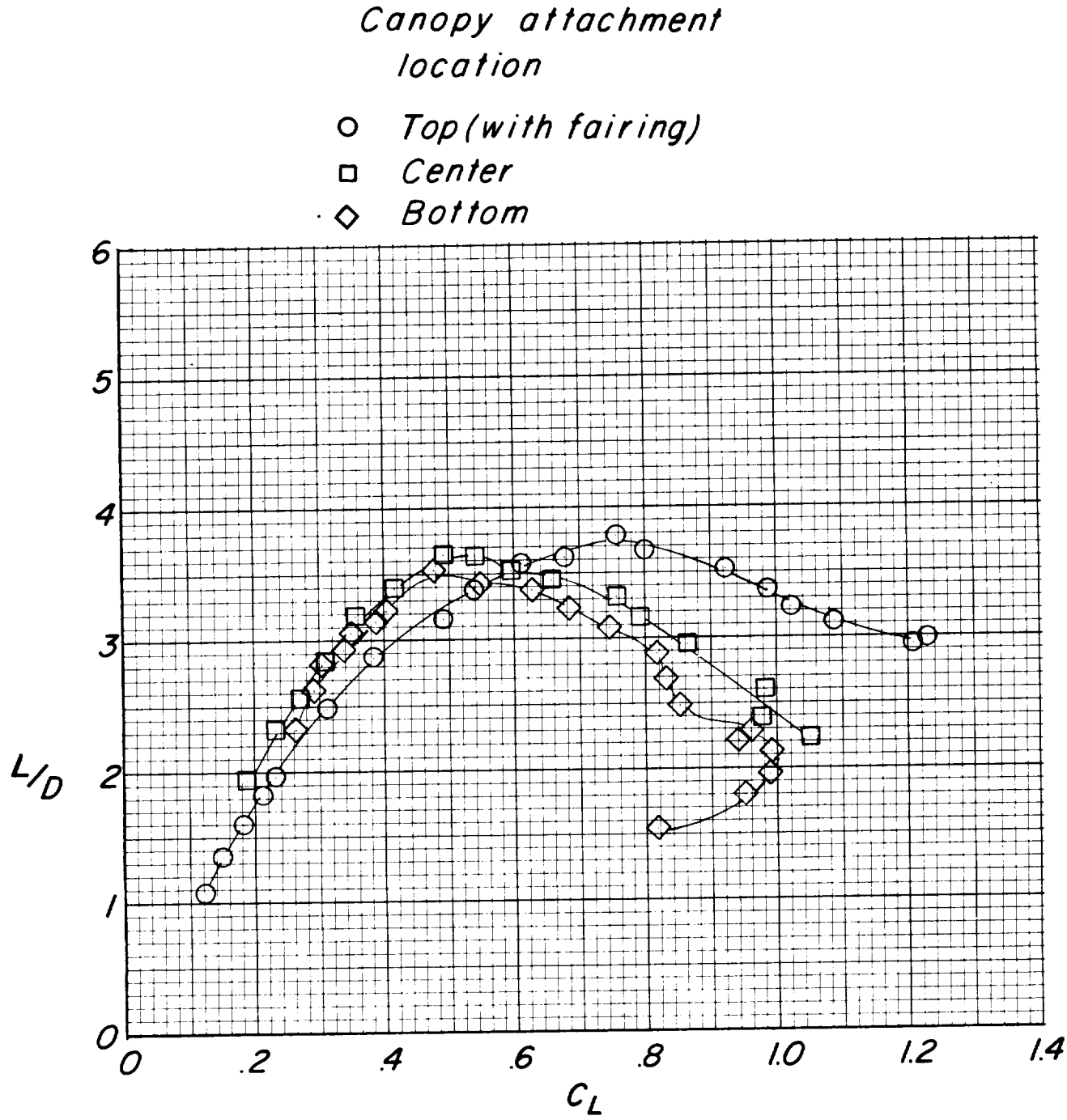

(b) $\Lambda = 55^{\circ}$. Concluded.

Figure 10.- Concluded.

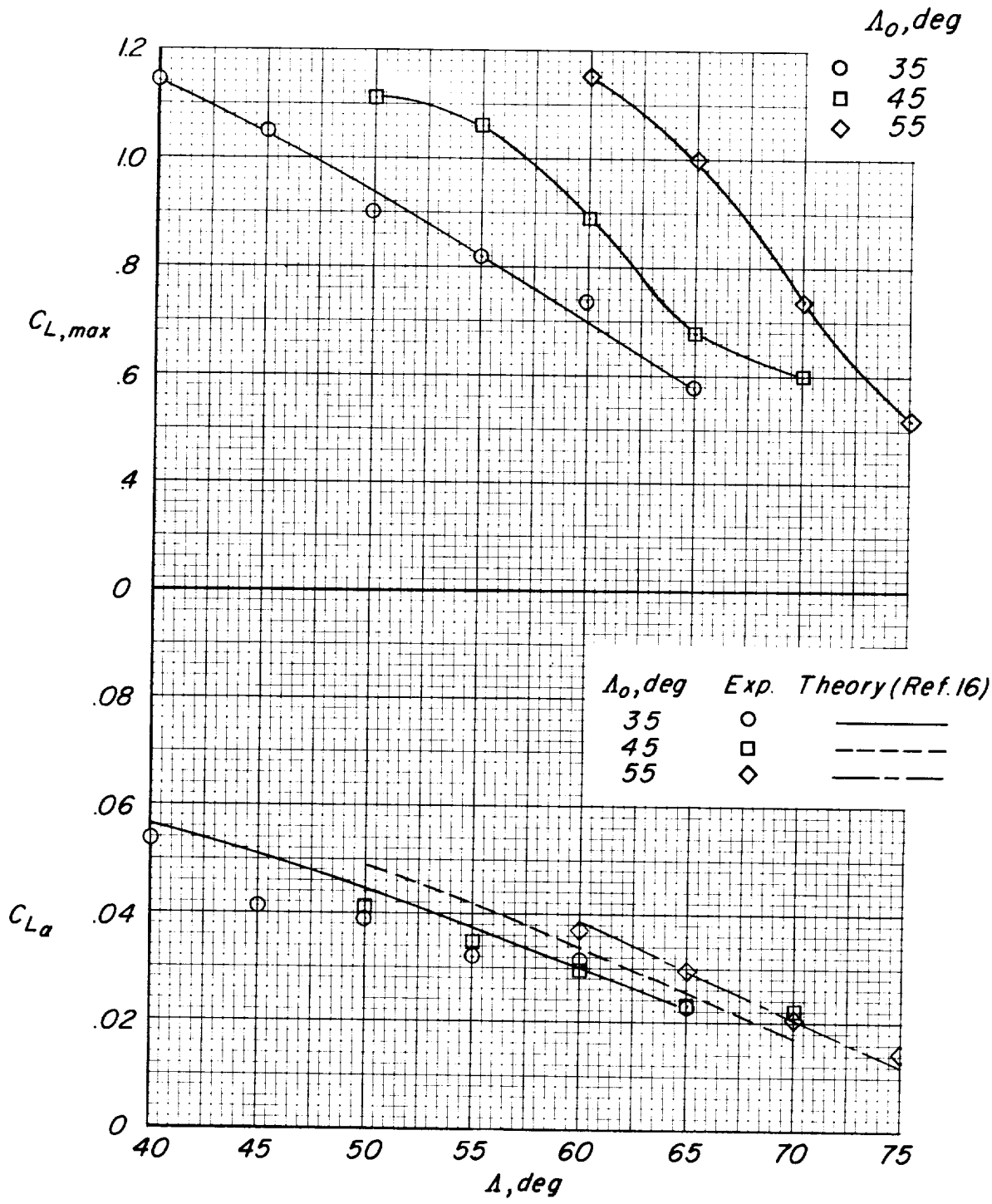

Figure 11.- Variations of lift-curve slope C_{L_α} and maximum lift coefficient $C_{L,max}$ with wing leading-edge sweep for basic models.

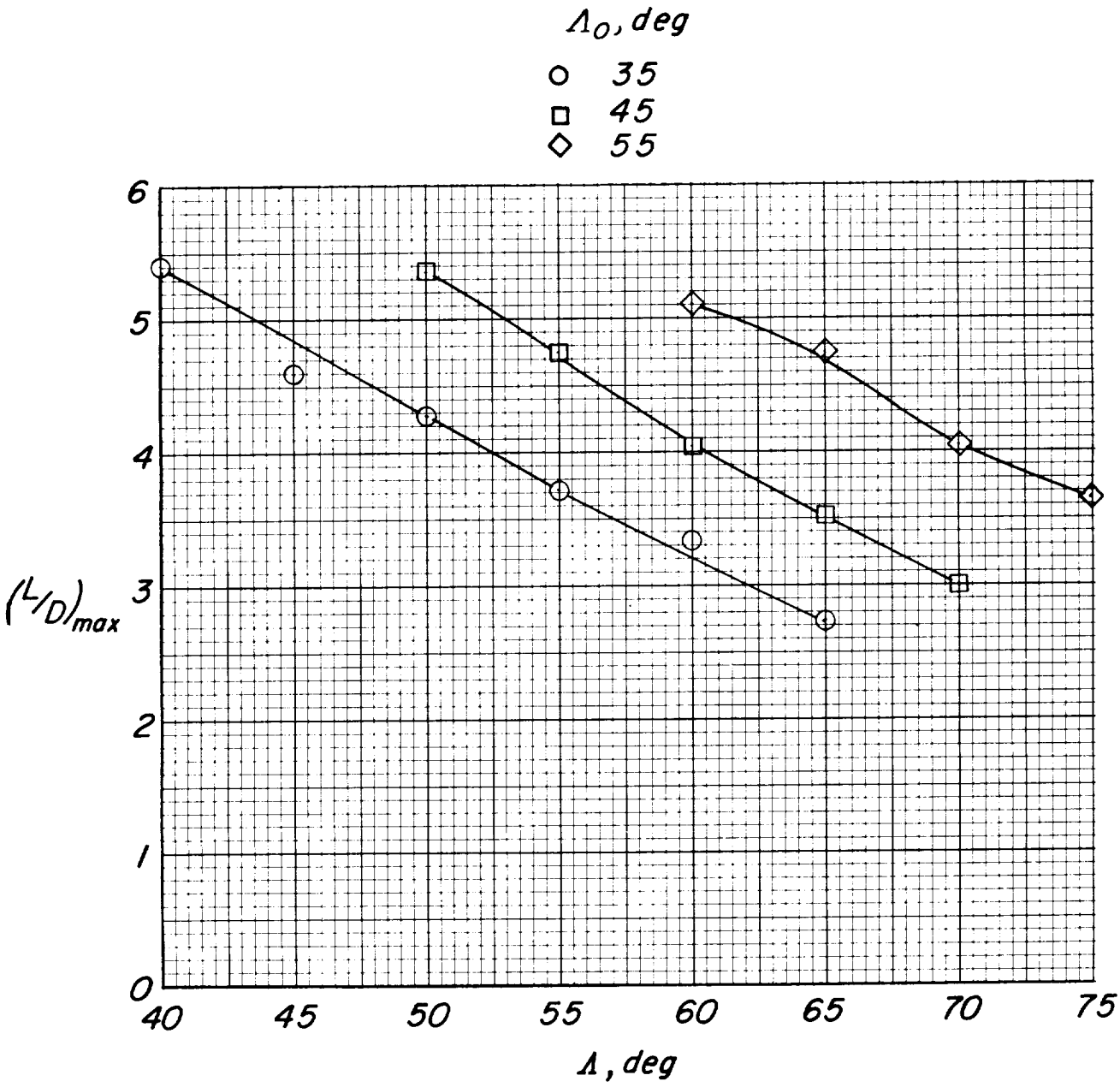

Figure 12.- Variation of maximum lift-drag ratio $(L/D)_{max}$ with wing leading-edge sweep angle for basic models.

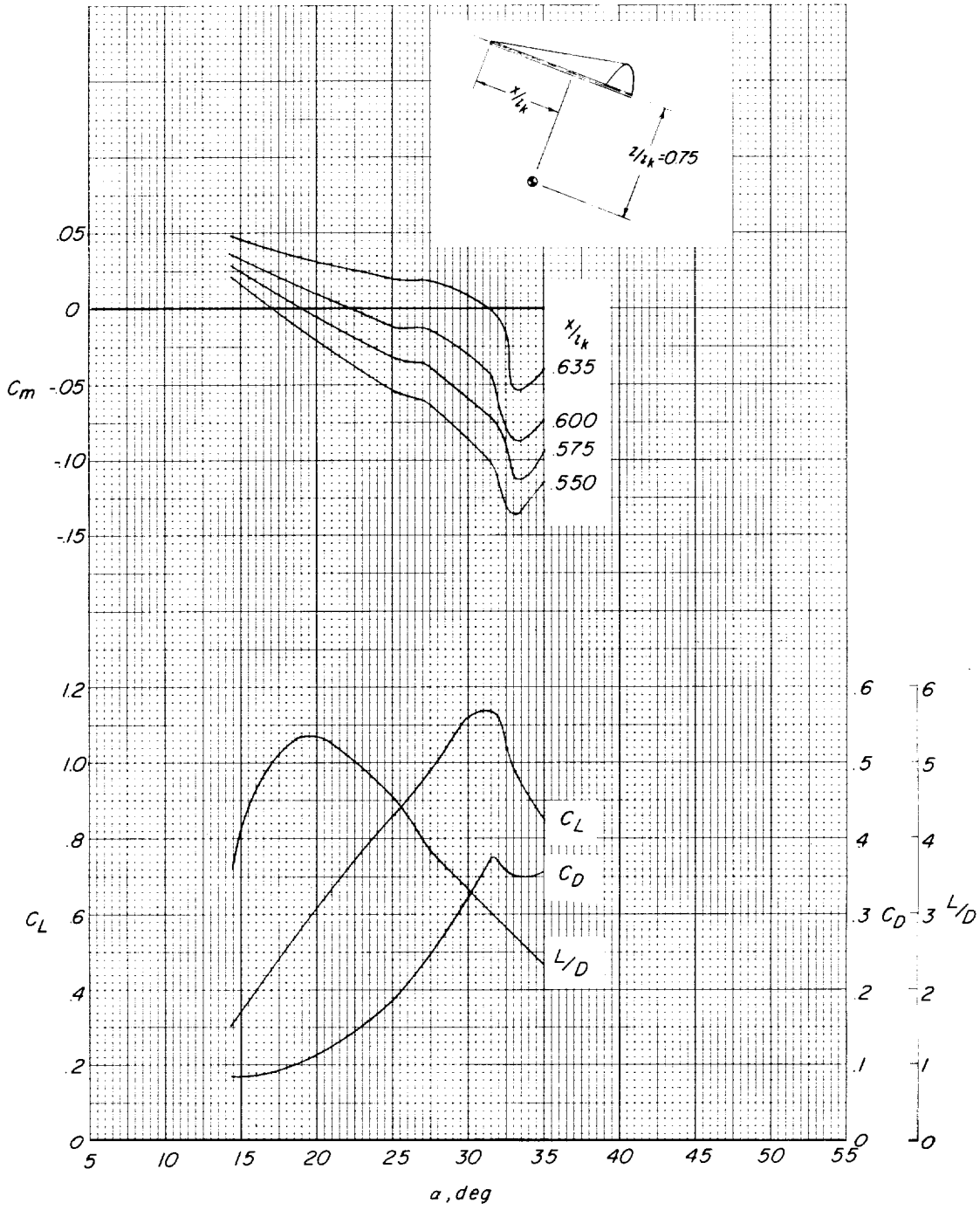

(a) $\Lambda_o = 35^\circ$ model; $\Lambda = 40^\circ$.

Figure 13.- Static longitudinal characteristics of basic parawing models for various longitudinal center-of-gravity locations. Vertical location of center of gravity, $0.75l_k$ below keel.

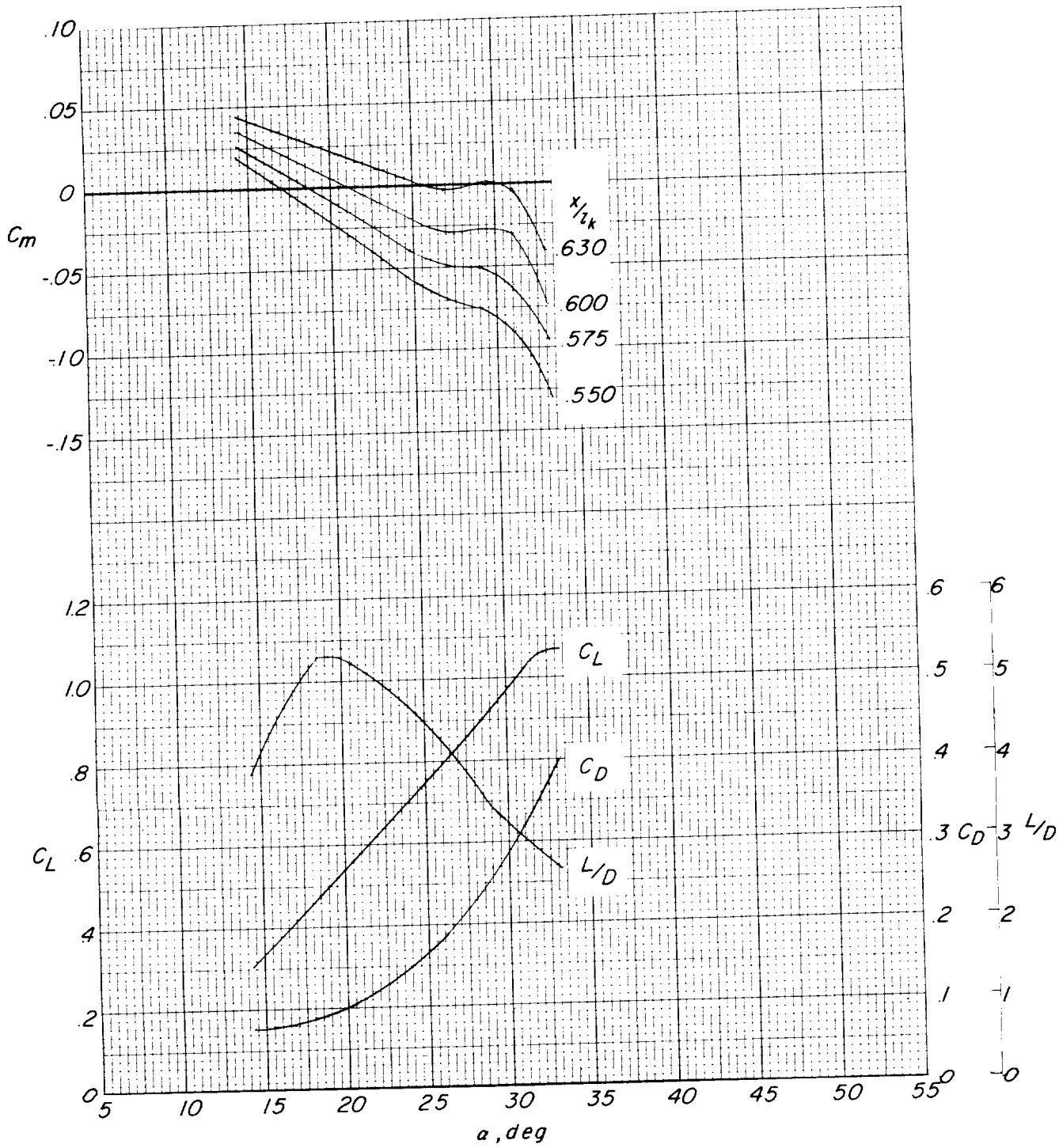

(b) $\Lambda_o = 45^\circ$ model; $\Lambda = 50^\circ$.

Figure 13.- Continued.

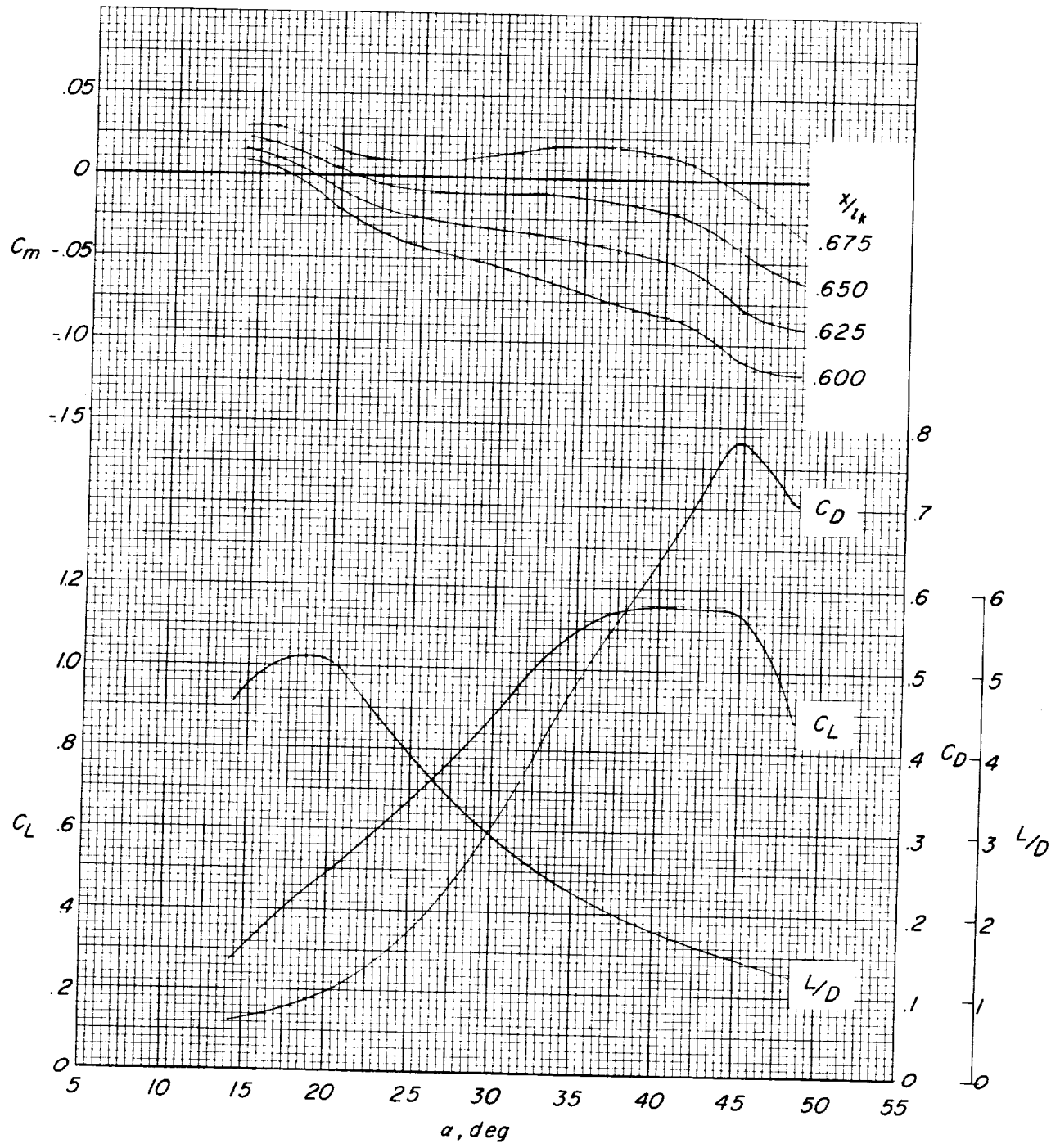

(c) $\Lambda_o = 55^\circ$ model; $\Lambda = 60^\circ$.

Figure 13.- Concluded.

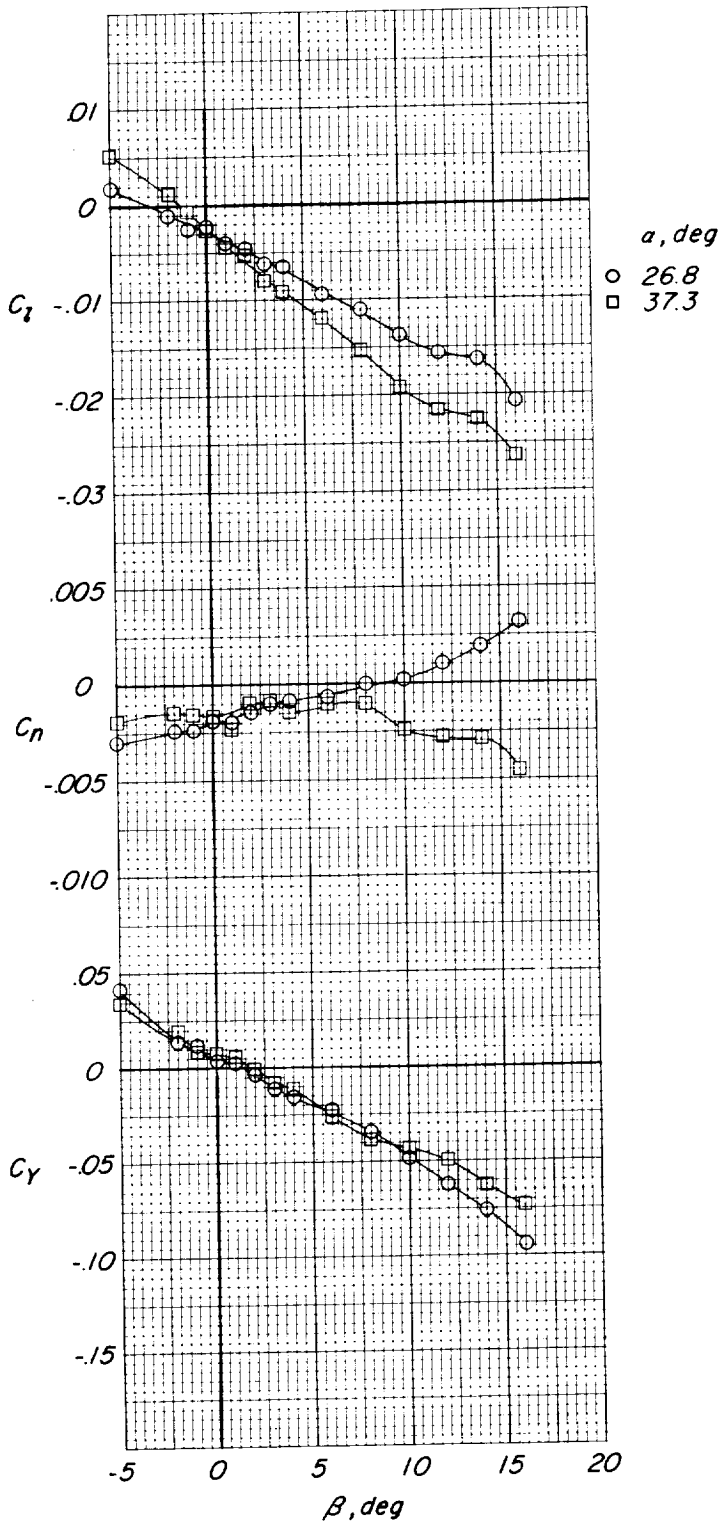

Figure 14.- Static lateral characteristics in sideslip. $\Lambda_o = 35^o$ model; $\Lambda = 45^o$.

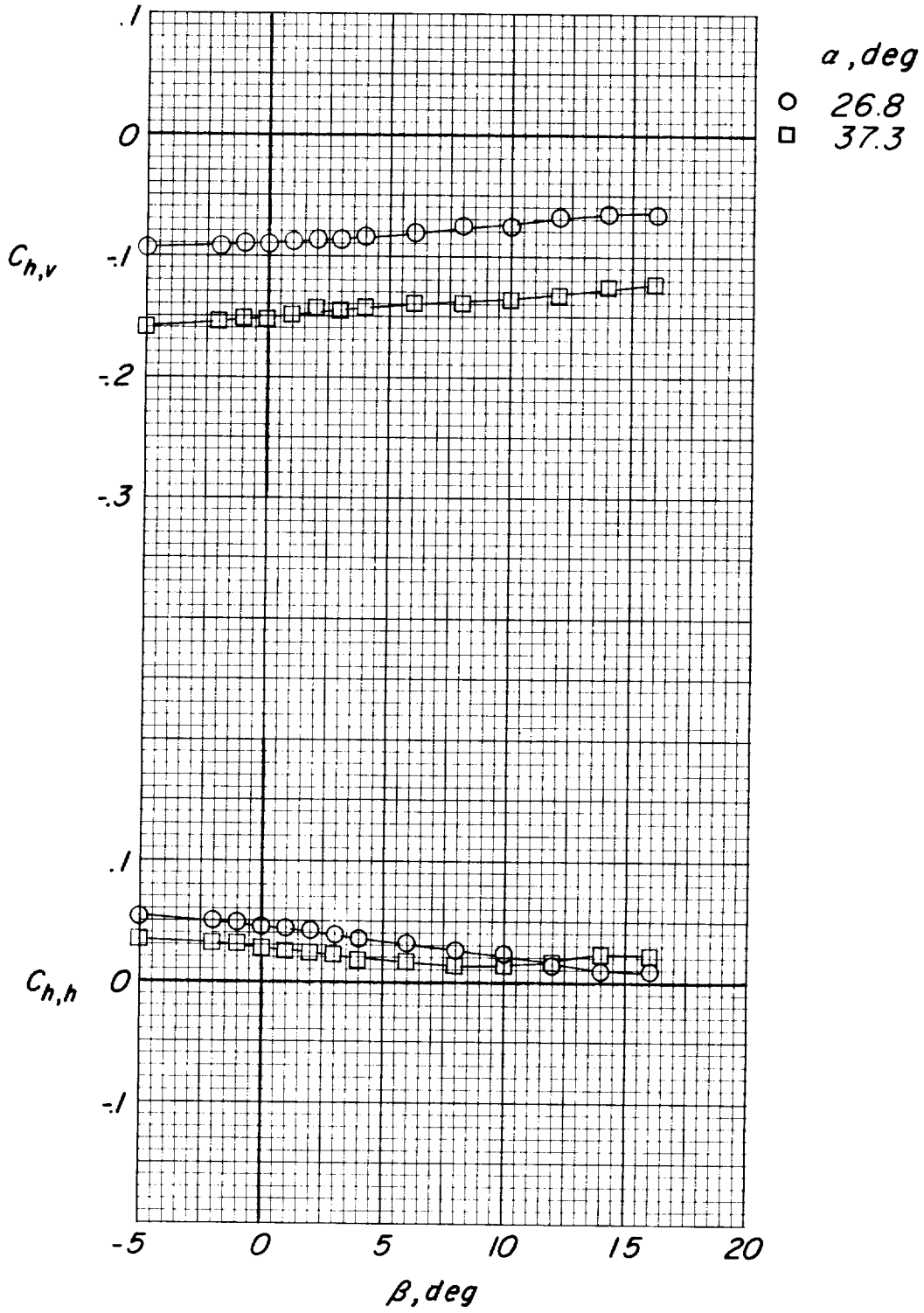

Figure 14.- Concluded.

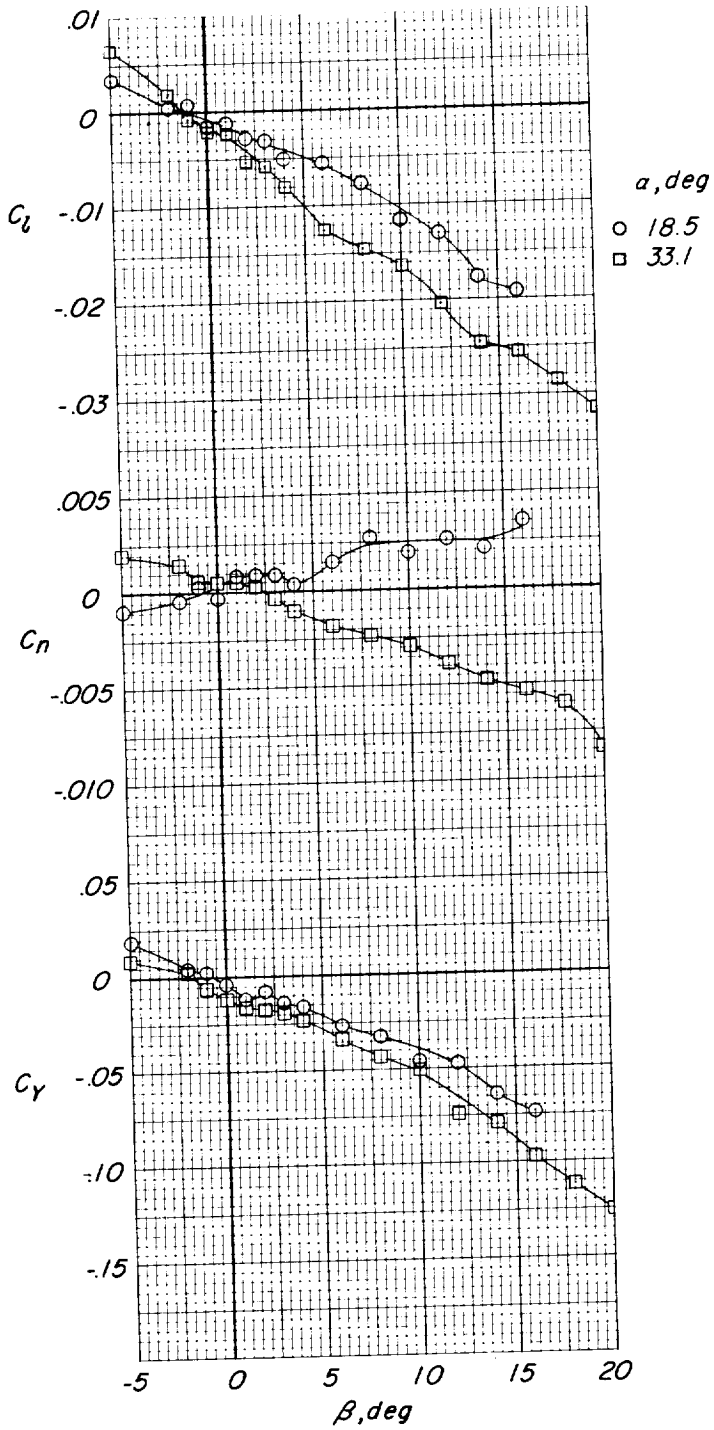

(a) $\Lambda = 50^{\circ}$.

Figure 15.- Static lateral characteristics in sideslip of the $\Lambda_0 = 45^{\circ}$ model for various wing leading-edge sweeps.

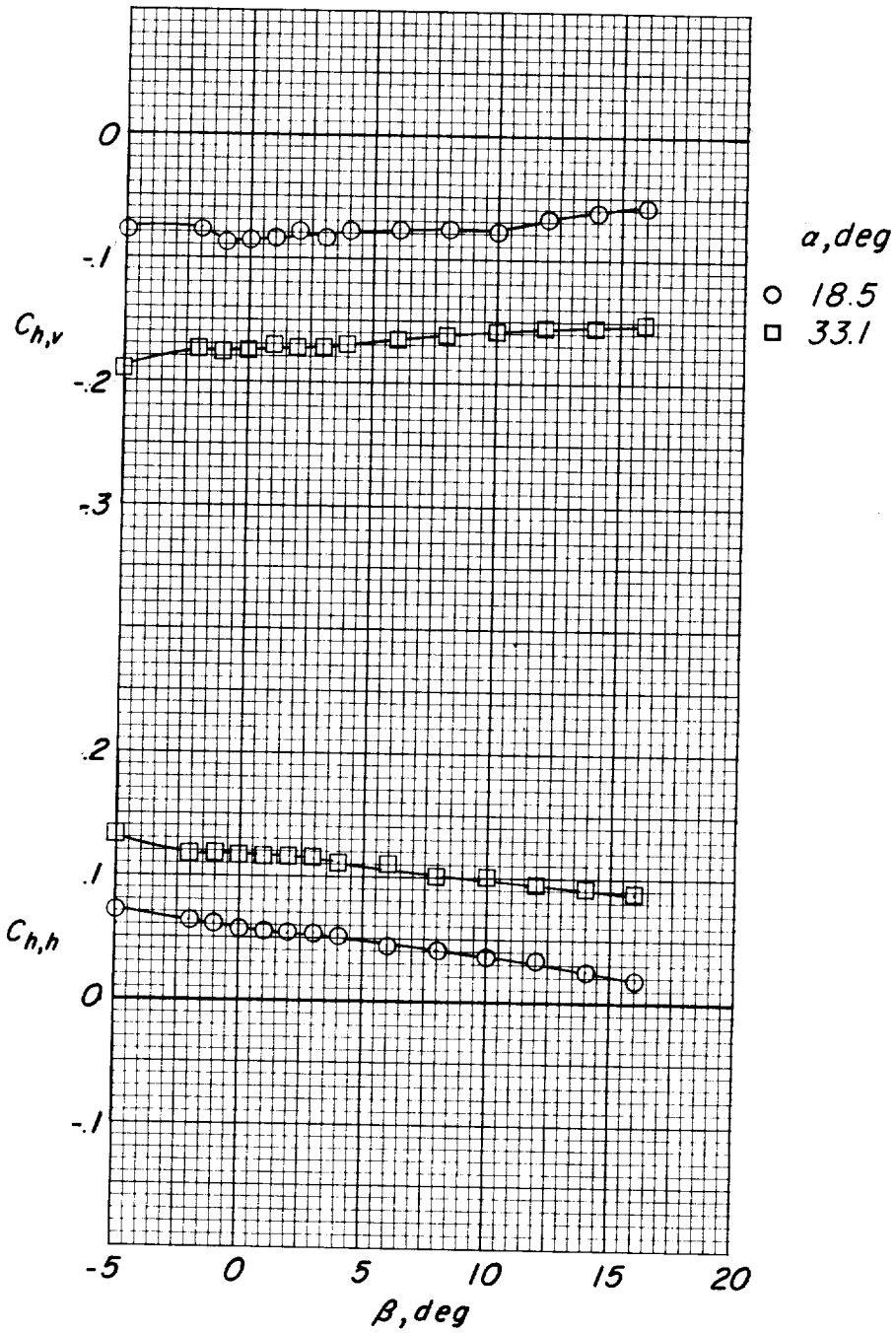

(a) $\Lambda = 50^{\circ}$. Concluded.

Figure 15.- Continued.

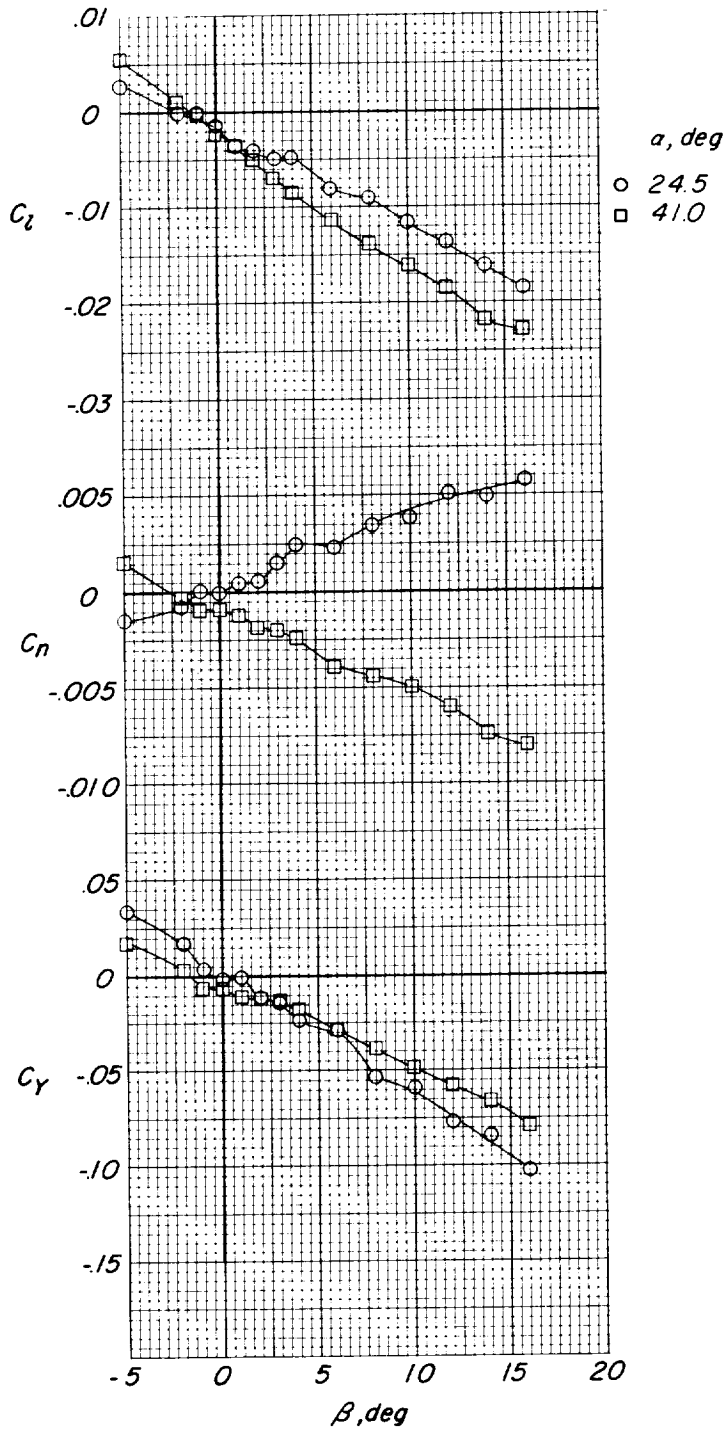

(b) $\Lambda = 55^{\circ}$.

Figure 15.- Continued.

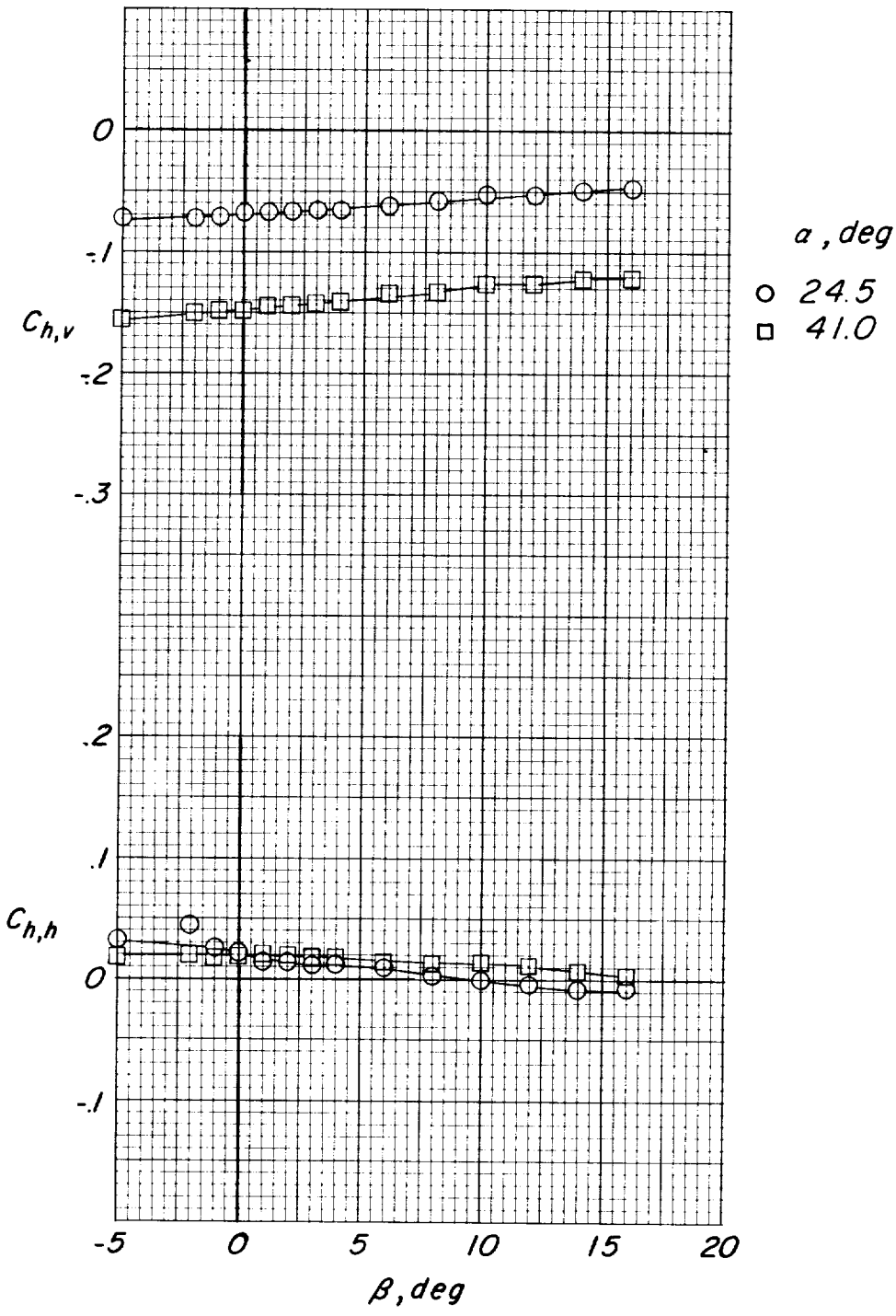

(b) Λ = 55°. Concluded.

Figure 15.- Continued.

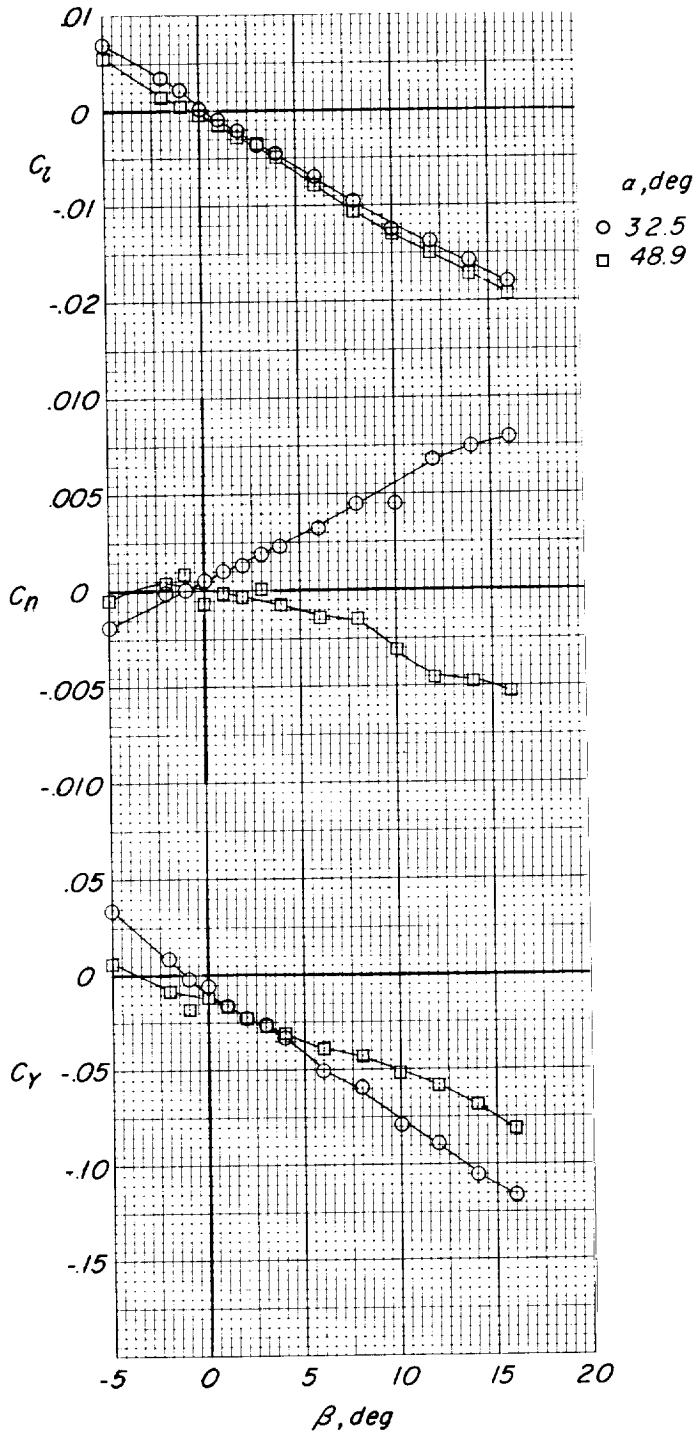

(c) $\Lambda = 60^{\circ}$.

Figure 15.- Continued.

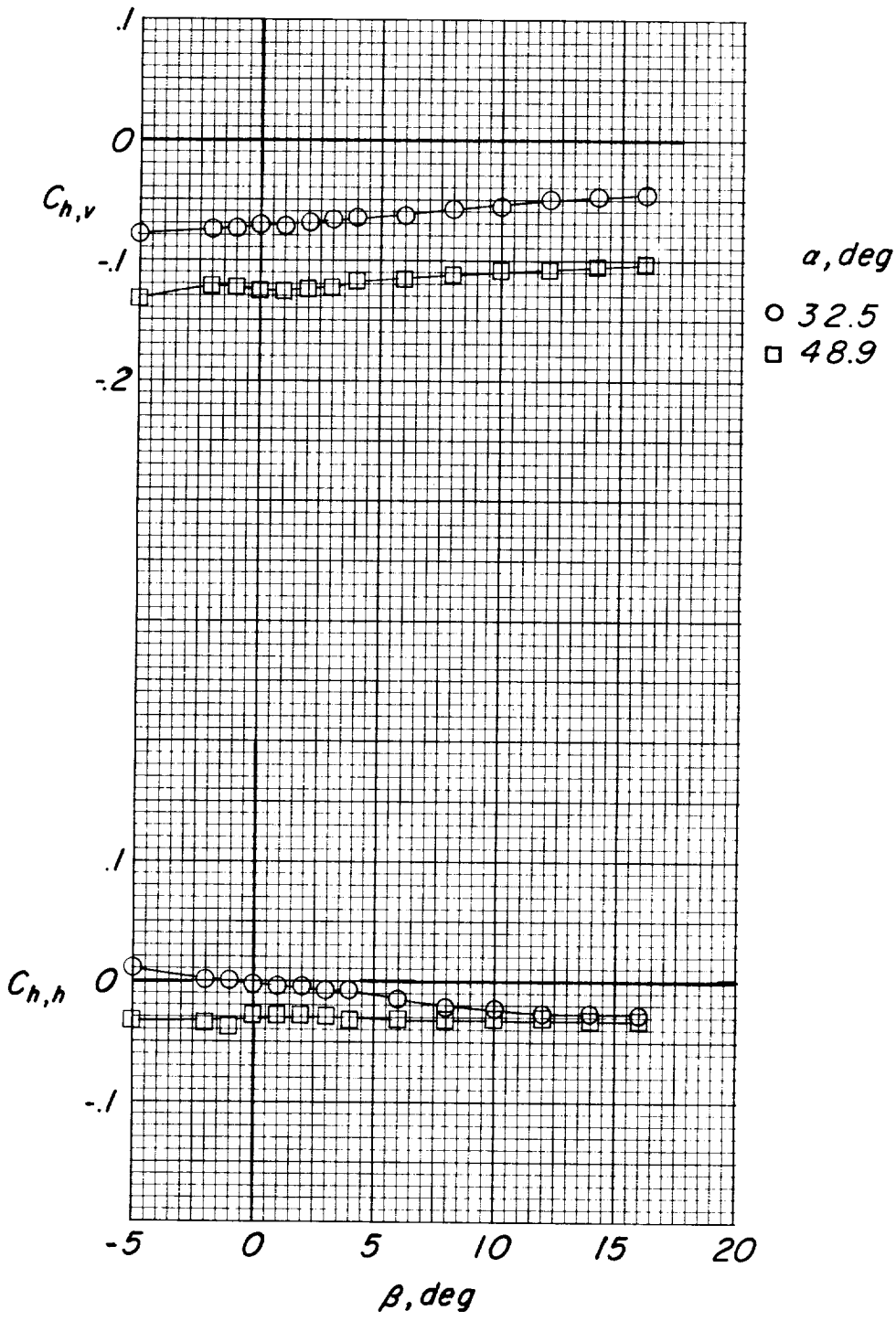

(c) $\Lambda = 60^{\circ}$. Concluded.

Figure 15.- Concluded.

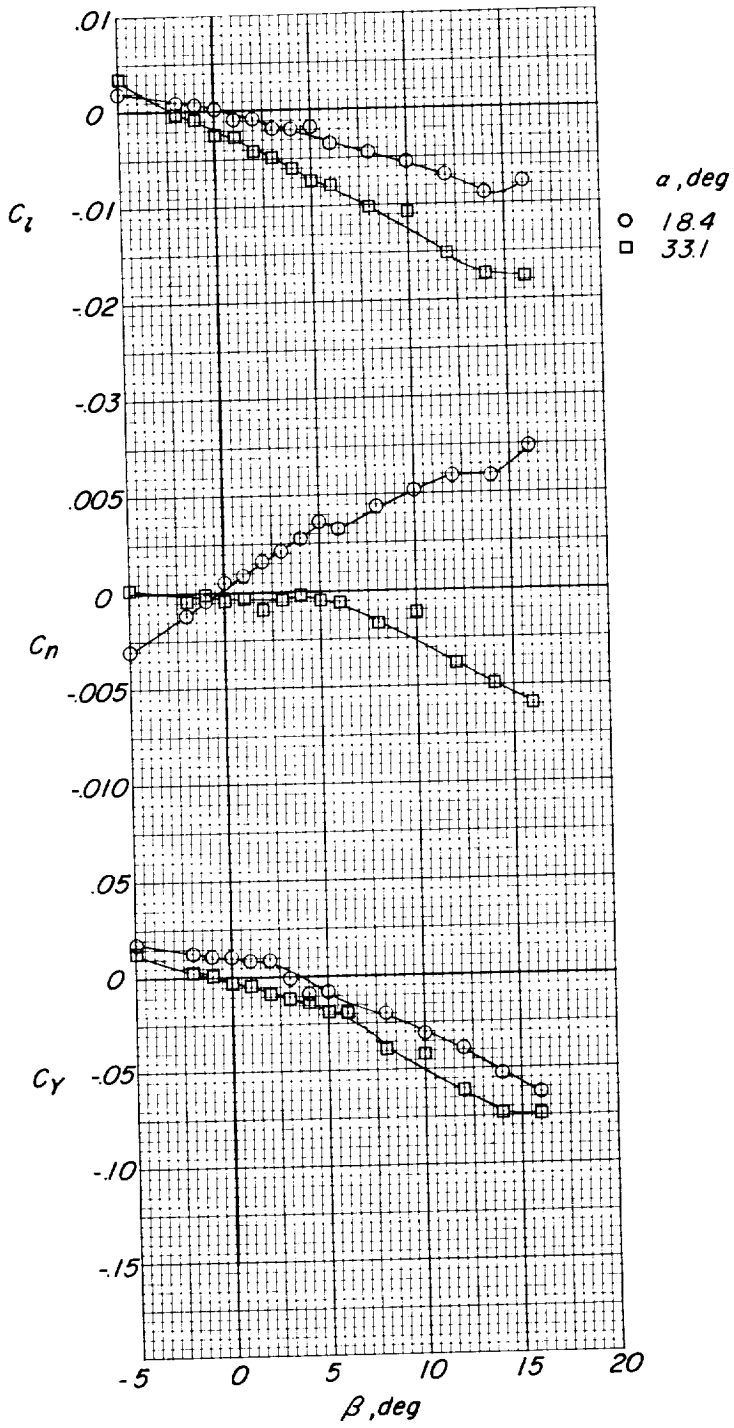

(a) $\Lambda = 50^\circ$; $\delta = 6.7^\circ$.

Figure 16.- Static lateral characteristics in sideslip of the $\Lambda_o = 45^\circ$ model with leading edges deflected below the keel.

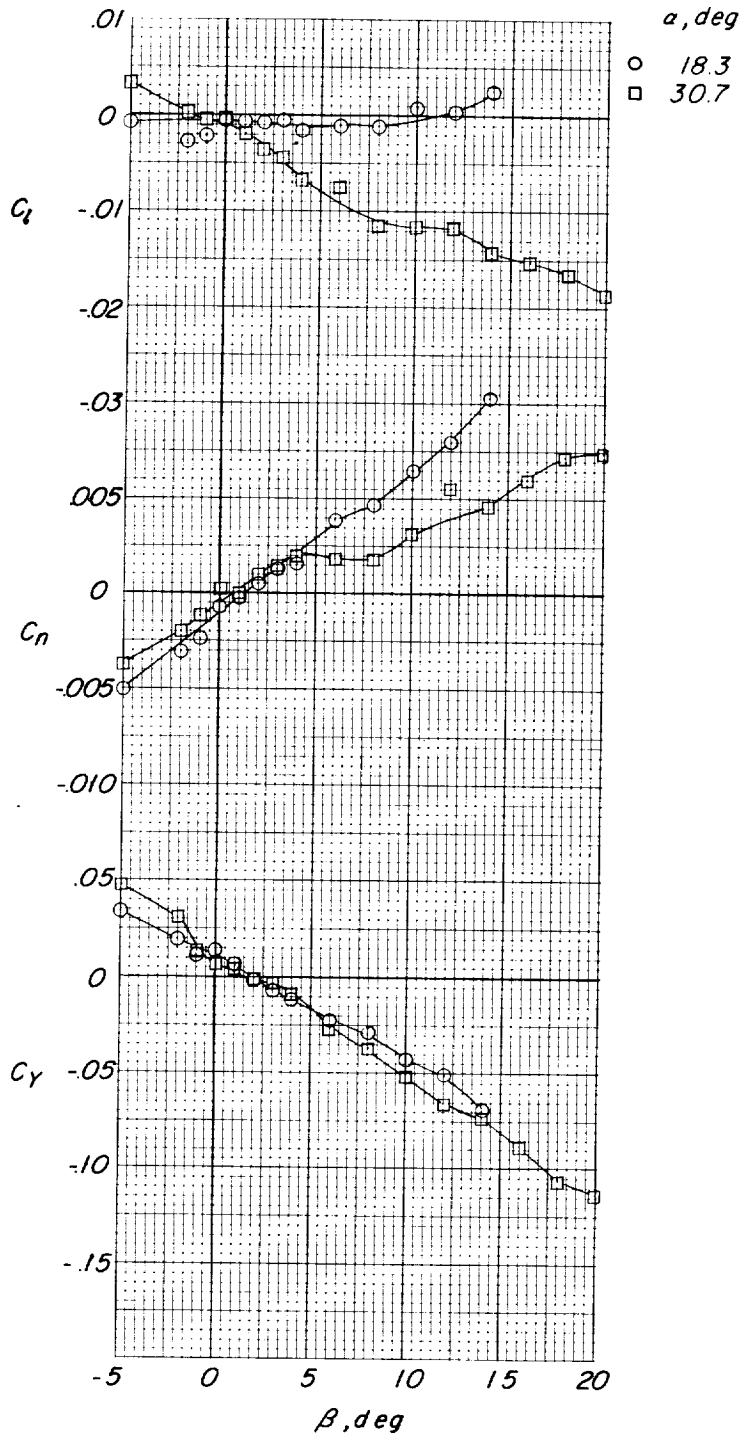

(b) $\Lambda = 55^{\circ}$; $\delta = 5.8^{\circ}$.

Figure 16.- Continued.

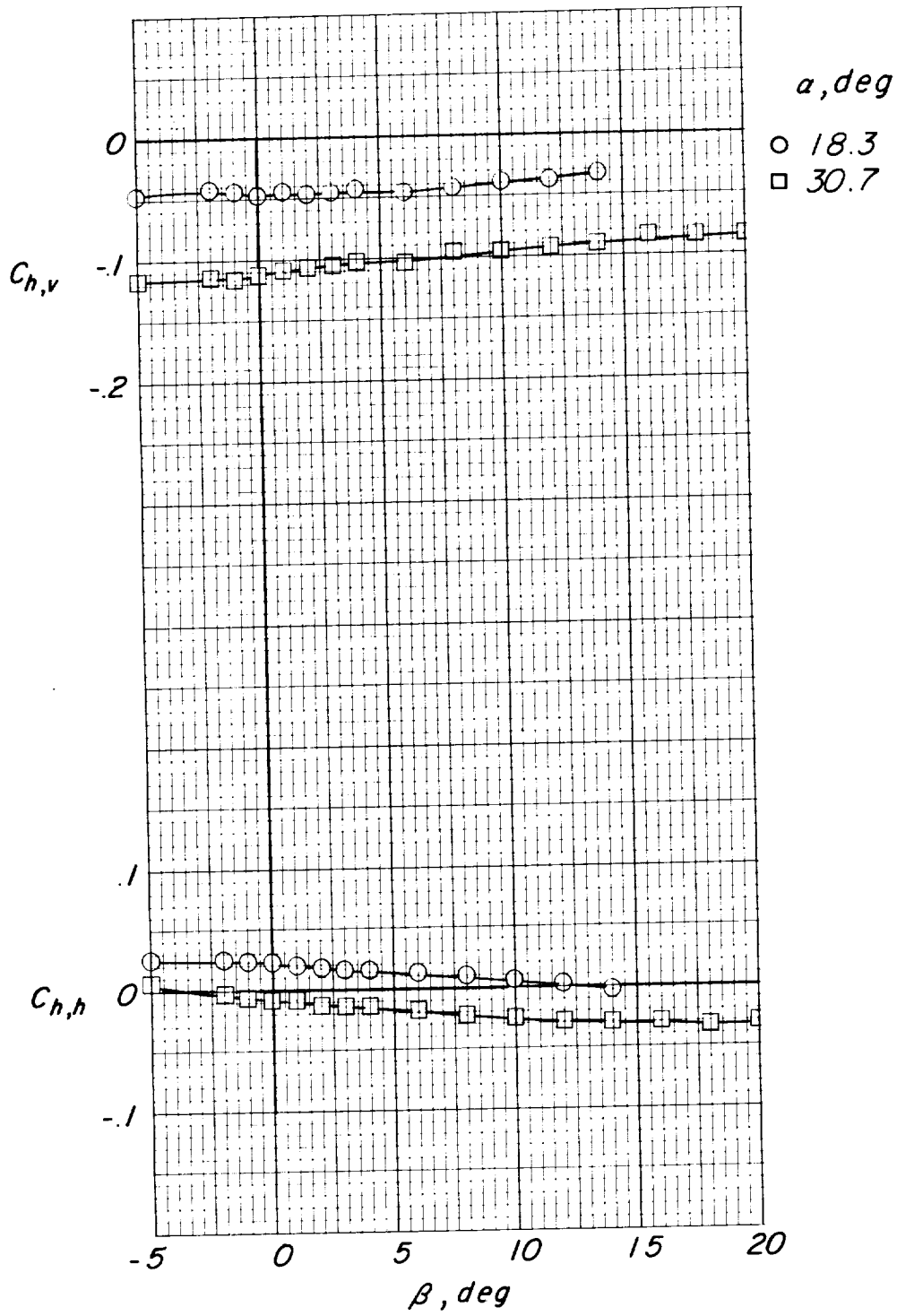

(b) $\Lambda = 55^{\circ}$; $\delta = 5.8^{\circ}$. Concluded.

Figure 16.- Continued.

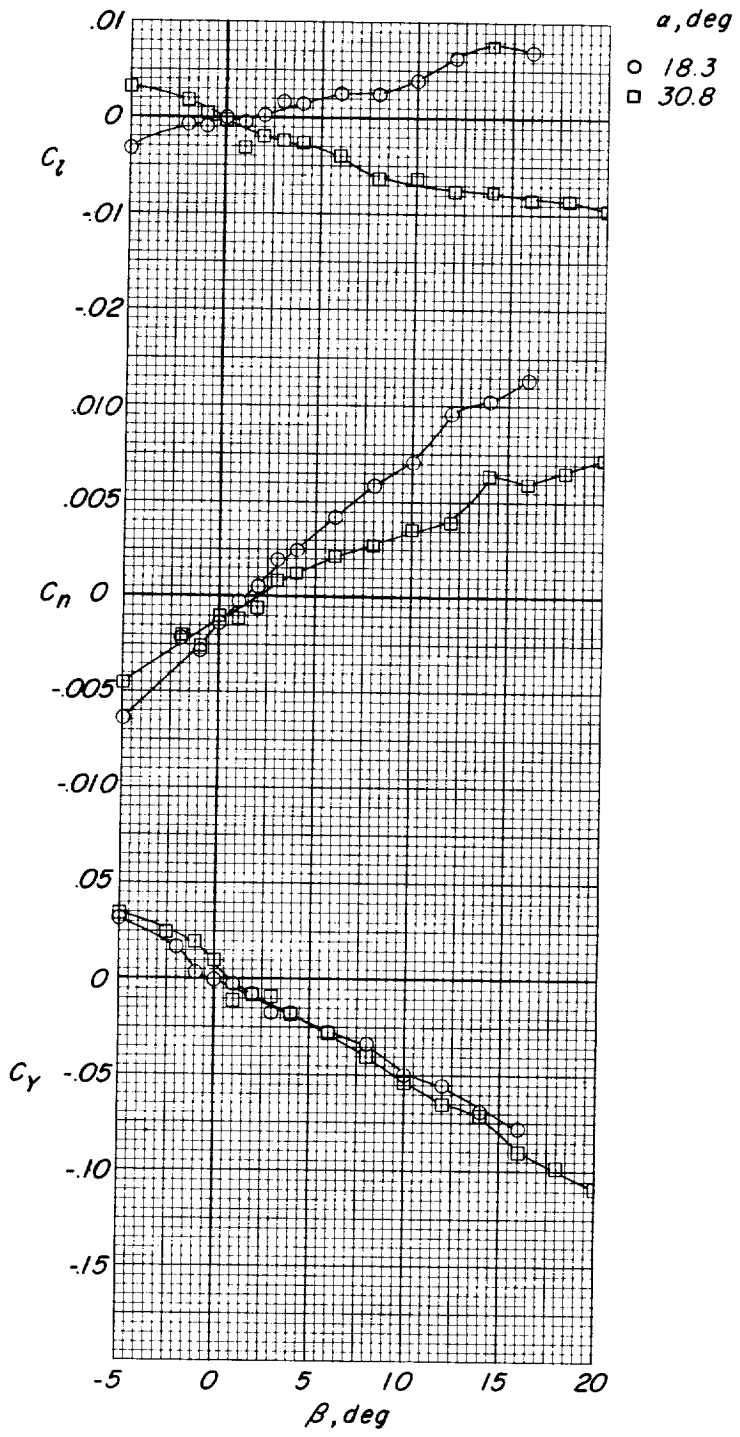

(c) $\Lambda = 55^{\circ}$; $\delta = 11.5^{\circ}$.

Figure 16.- Continued.

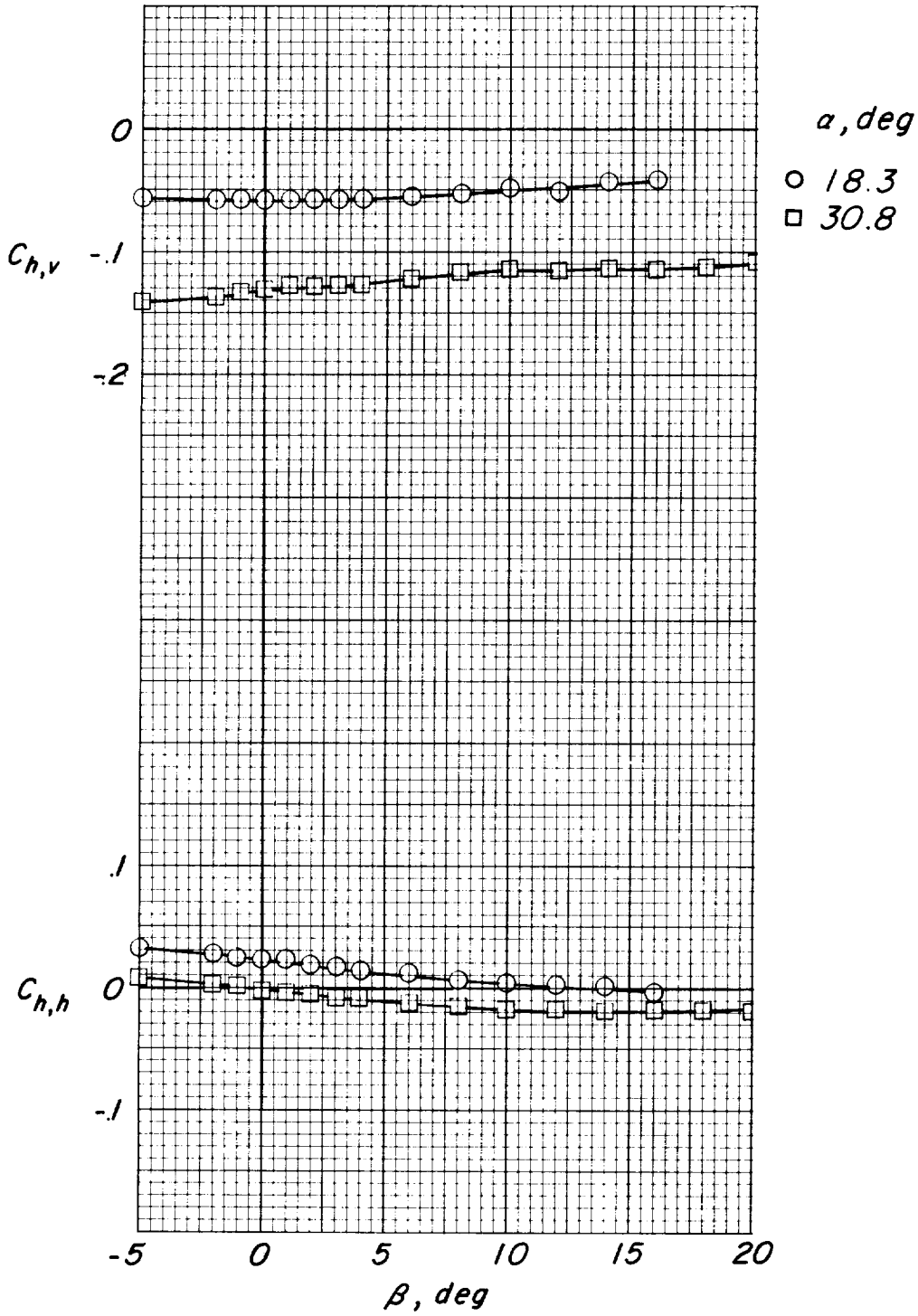

(c) $\Lambda = 55^{\circ}$; $\delta = 11.5^{\circ}$. Concluded.

Figure 16.- Concluded.

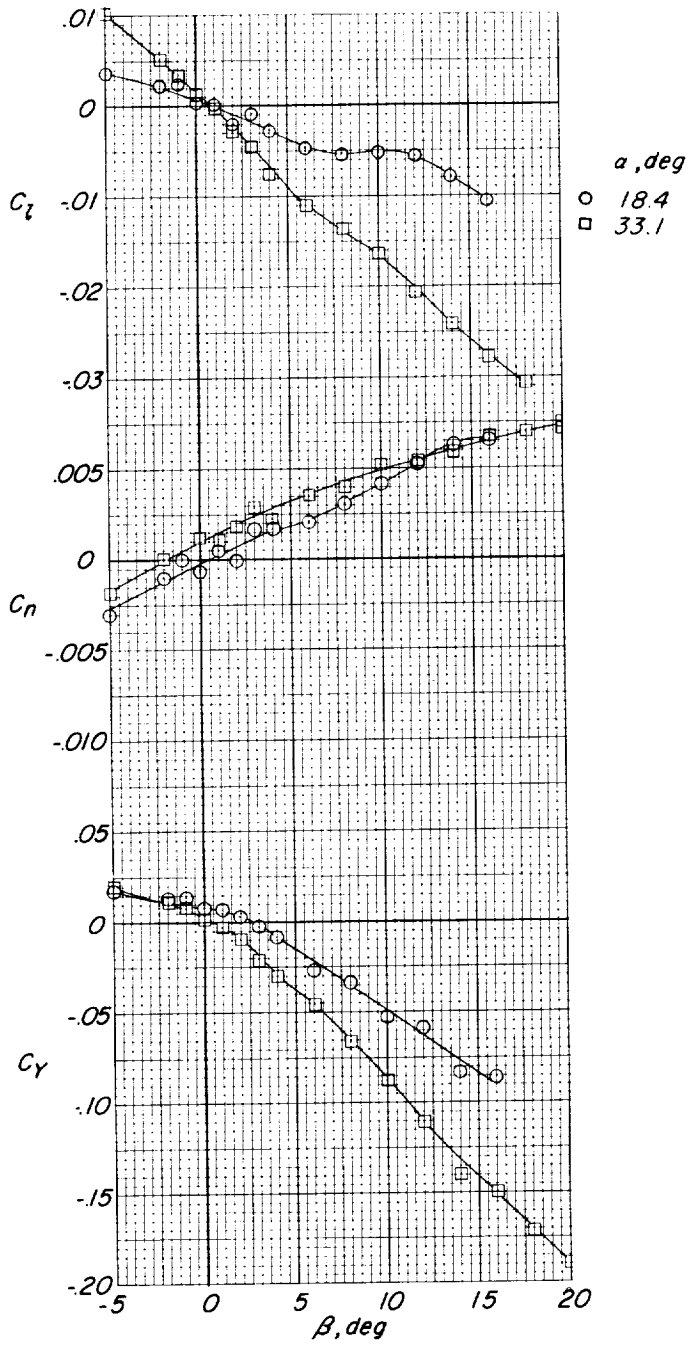

(a) $\Lambda = 50^{\circ}$; canopy attached at top.

Figure 17.- Static lateral characteristics in sideslip of the $\Lambda_0 = 45^{\circ}$ model with $0.07l_k$-diameter leading edges and keel.

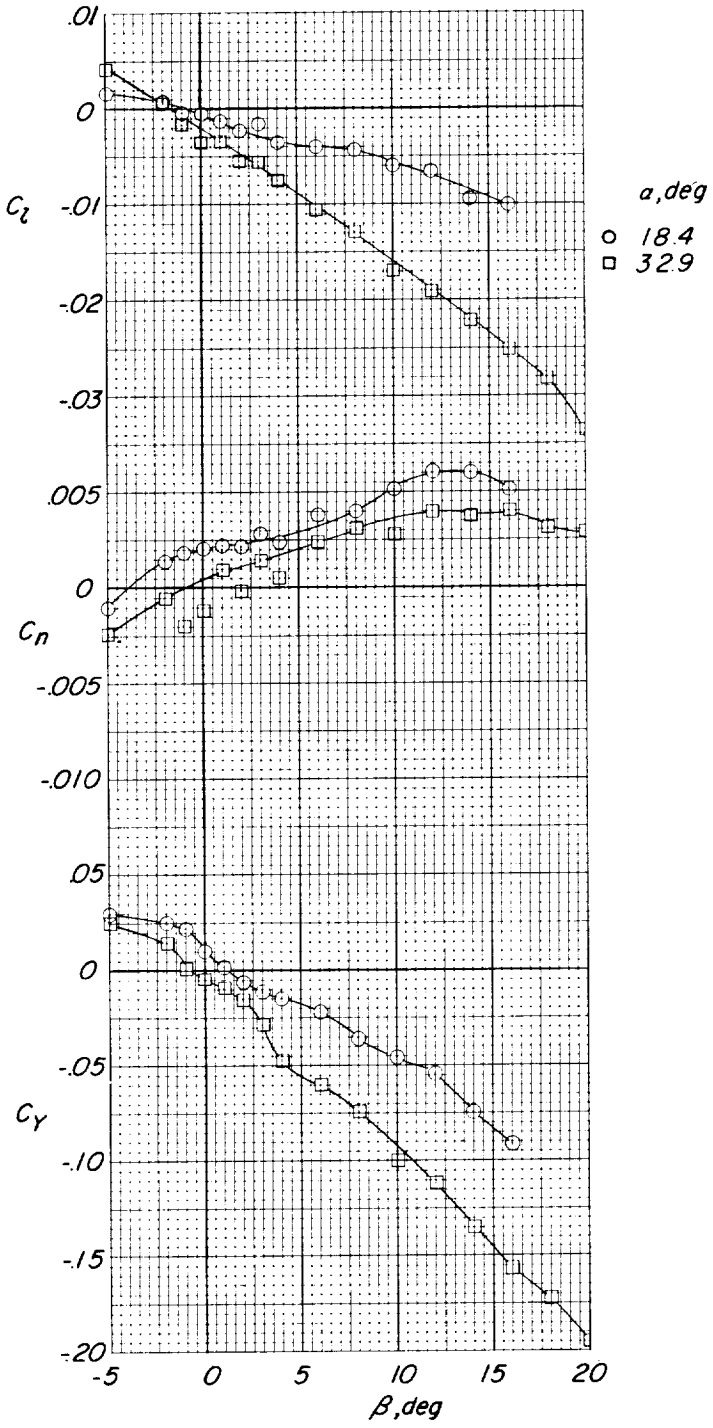

(b) $\Lambda = 55°$; canopy attached at center.

Figure 17.- Continued.

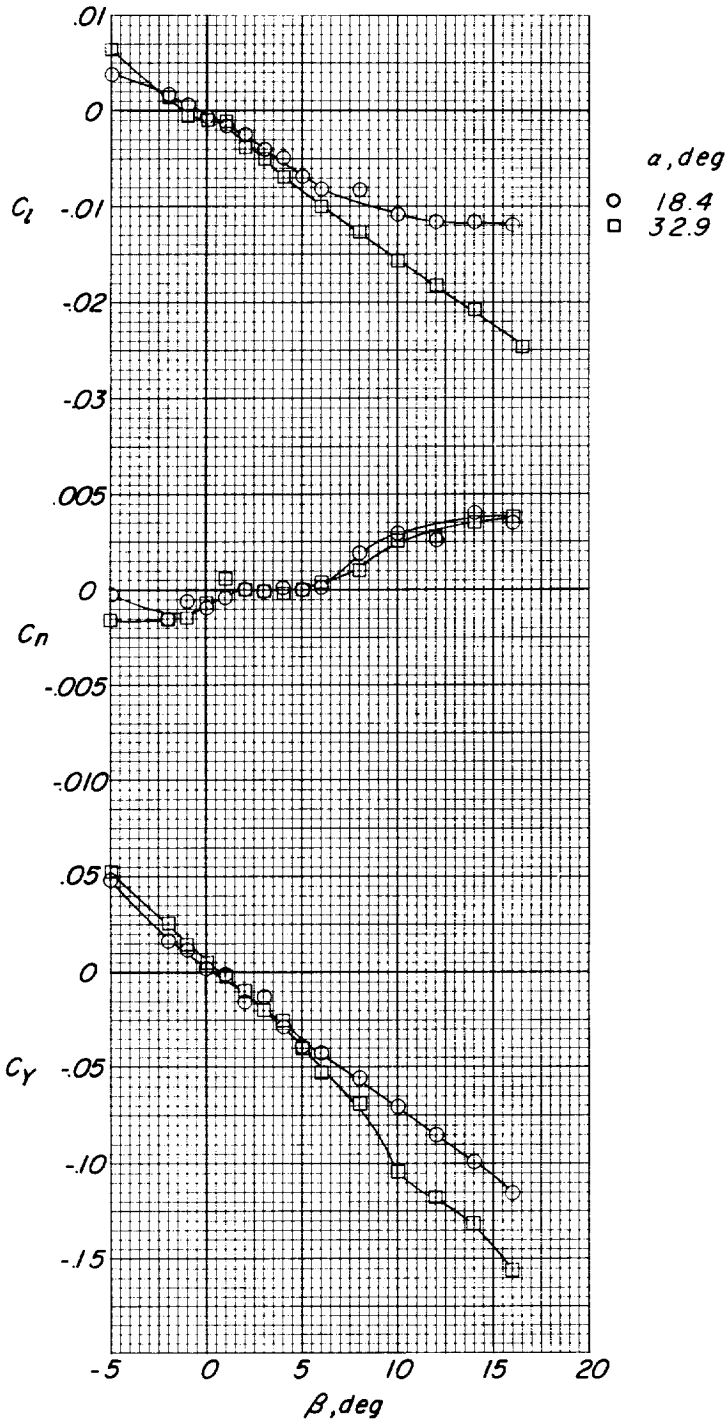

(c) $\Lambda = 55^{\circ}$; canopy attached at bottom.

Figure 17.- Concluded.

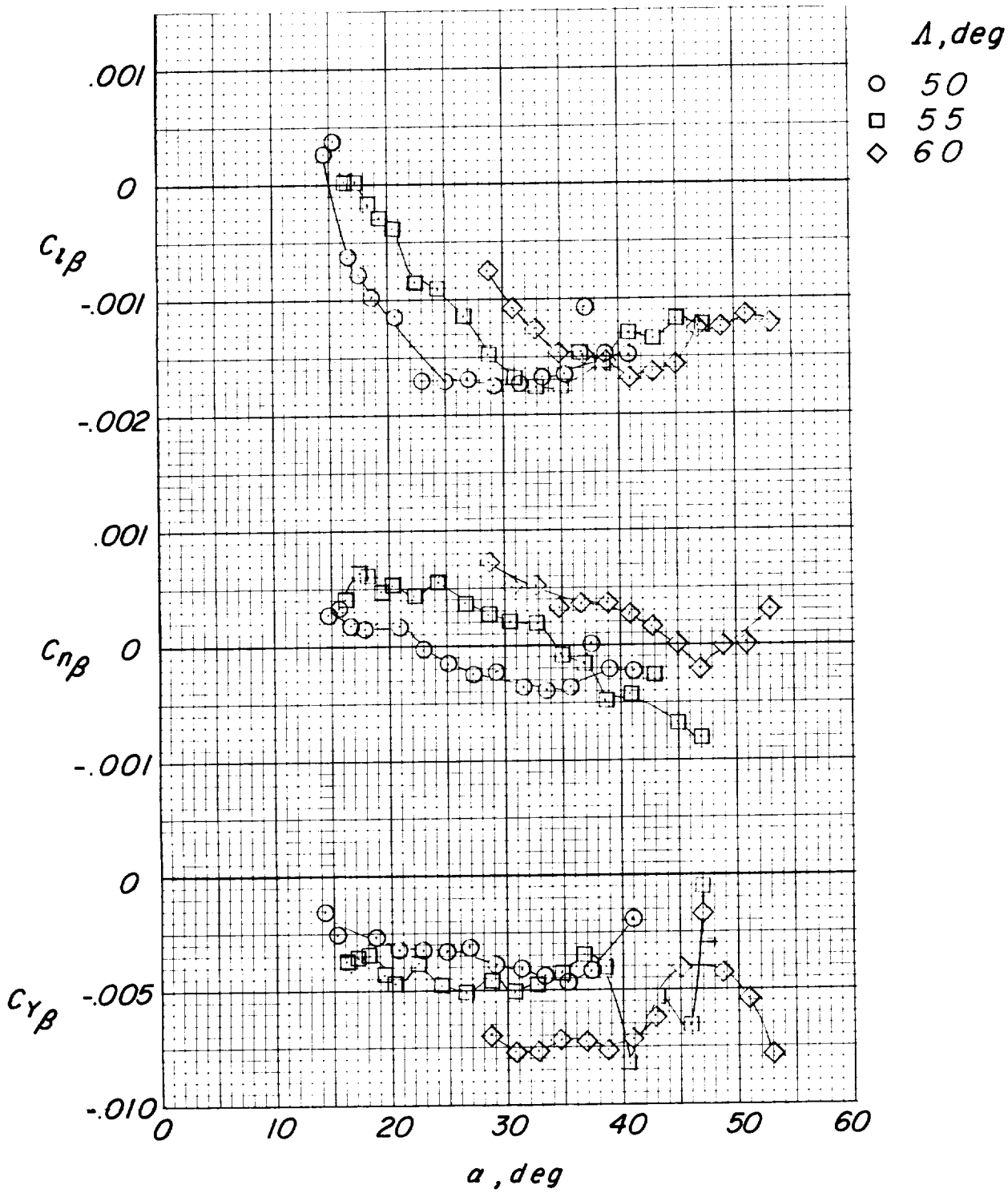

Figure 18.- Effects of changes in wing leading-edge sweep on the static lateral stability parameters for the $\Lambda_0 = 45^\circ$ model.

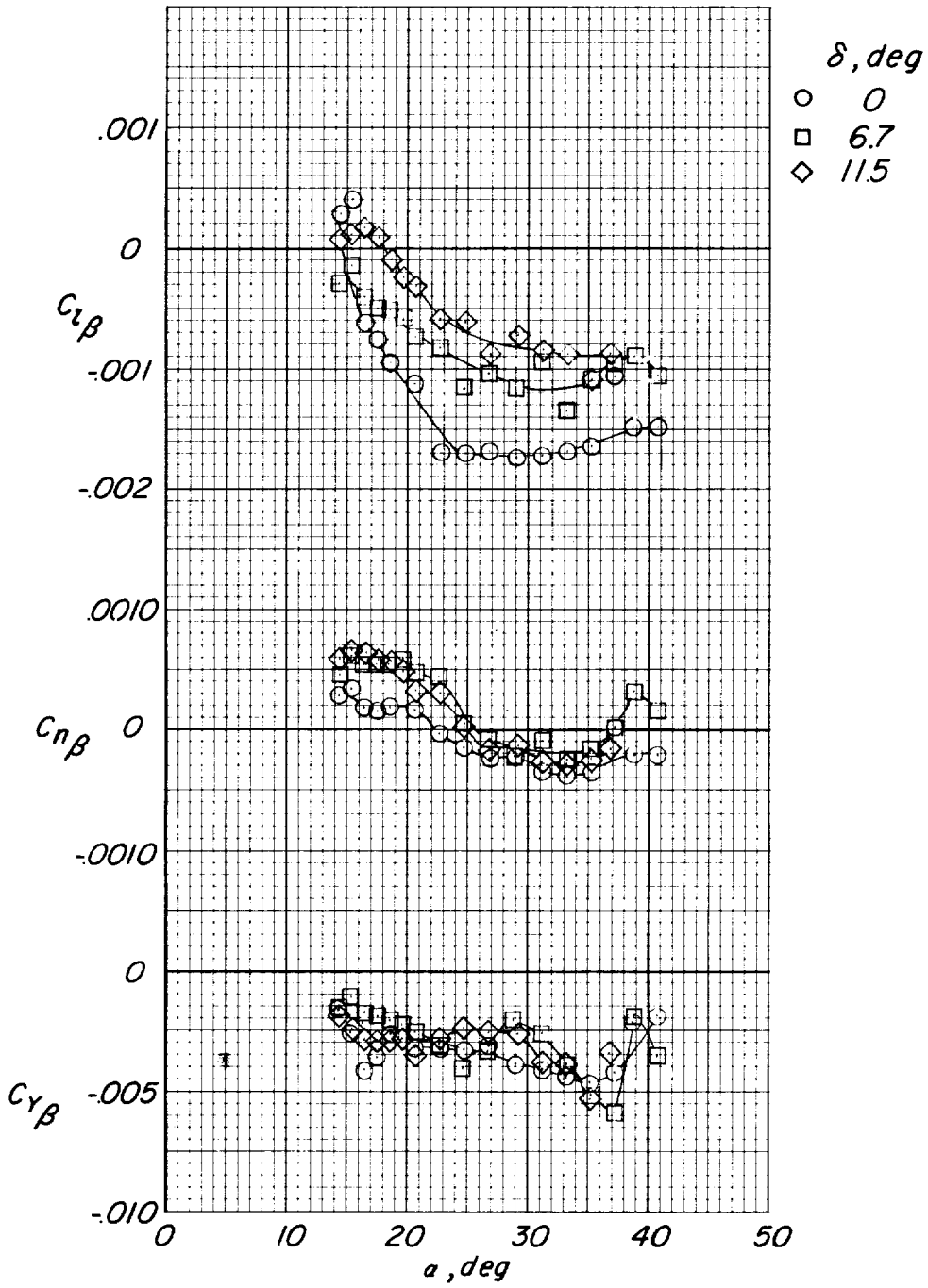

(a) $\Lambda = 50^{\circ}$.

Figure 19.- Effects of leading-edge deflection angle δ on static lateral stability parameters for the $\Lambda_0 = 45^{\circ}$ model.

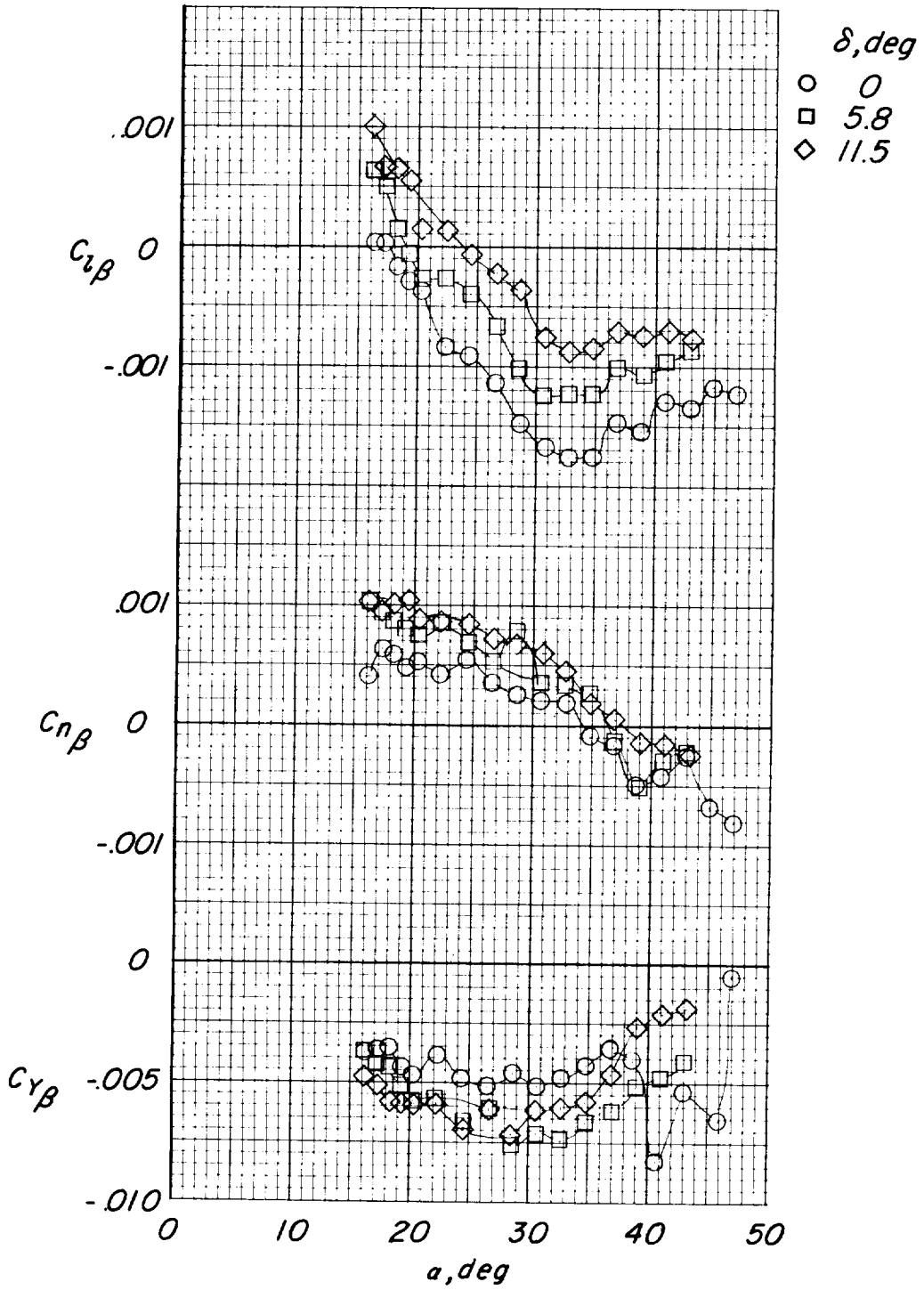

(b) $\Lambda = 55°$.

Figure 19.- Concluded.

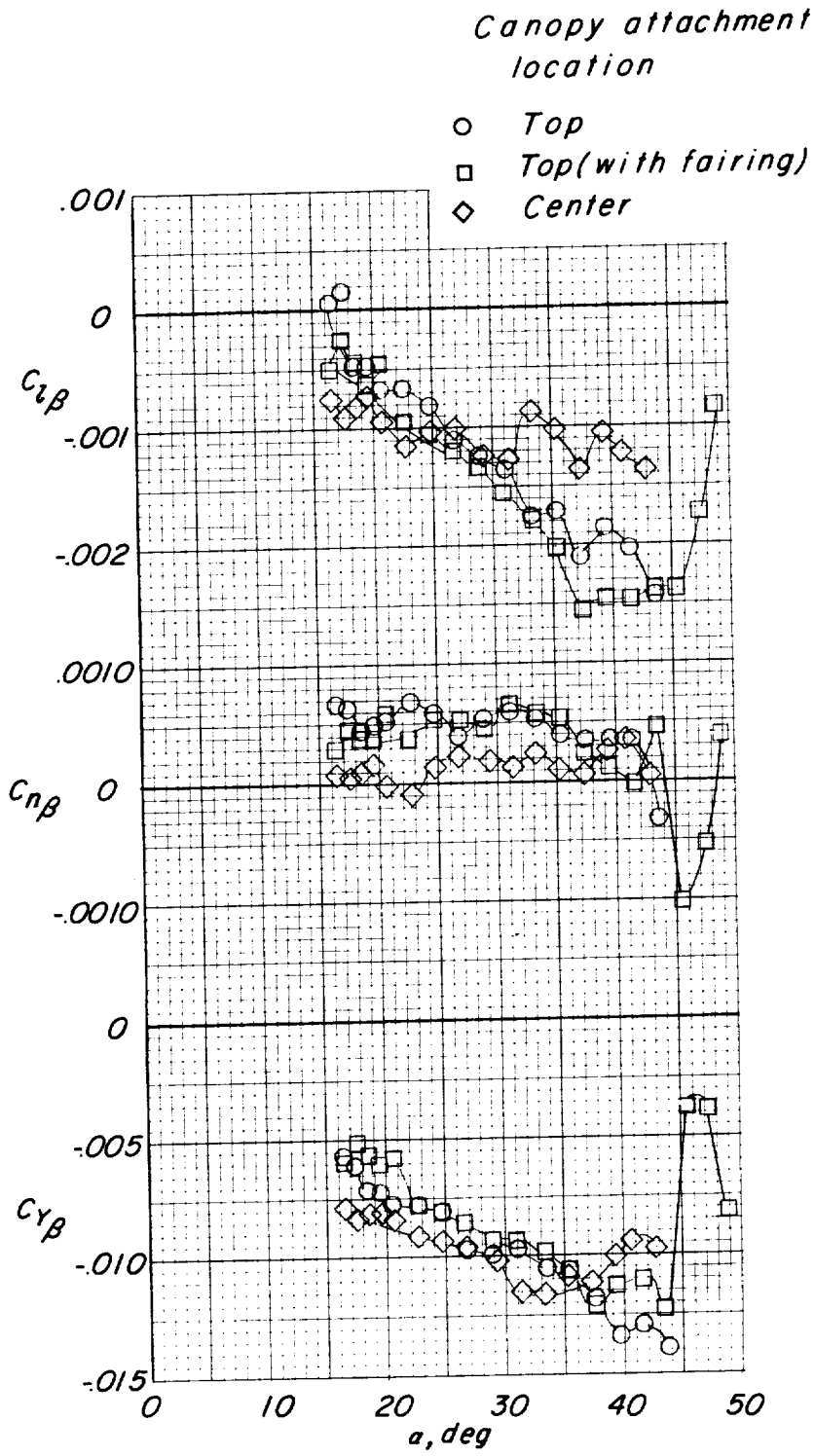

Figure 20.- Effects of canopy attachment location on static lateral stability parameters for the $\Lambda_0 = 45^\circ$ model with $0.07l_k$-diameter leading edges and keel.

NASA-Langley, 1963 L-3271